JKU

**JOHANNES KEPLER
UNIVERSITY LINZ**

ANTHRAQUINONE AND RIBOFLAVIN BASED POLYMERS FOR THE ELECTROCHEMICAL CO$_2$ CAPTURE

Author

Nadine Kleinbruckner

K11702618

Submission

Institute of Physical Chemistry and Linz Institute for Organic Solar Cells (LIOS)

Thesis Supervisor

Univ. Prof. Mag. Dr. DDr. h.c. Niyazi Serdar Sariciftci

Assistant Thesis Supervisor

Priv. Doz.^{in} Dr.^{in} Yolanda Salinas Soler

DI Dr. Dominik Wielend

October 2023
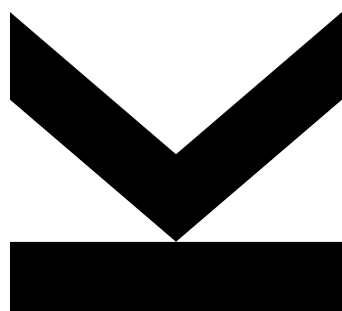
Master's Thesis

to confer the academic degree of

Diplom-Ingenieurin

in the Master's Program

Chemistry and Chemical Technology

Abstract

The rising levels of anthropogenic carbon dioxide in the atmosphere are a significant major cause of global climate change and a threat to public health and the environment. Immediate action is imperative to reduce carbon dioxide emissions and mitigate the long-term consequences of climate change. This involves capturing and storing carbon dioxide preventing the release into the atmosphere. In recent years, there have been emerging proposals for more effective carbon capture methods that involve electrochemical processes as environmentally friendly alternatives.

In this thesis, six different anthraquinone and riboflavin-based polymers synthesized chemically as well as electrochemically are investigated for their ability to capture and release CO_2 electrochemically. Therefore, cyclic voltammetry (CV) measurements are performed in different media, such as aqueous conventional electrolytes with varying pH values as well as ionic liquids. The electrochemical window of the used ionic liquids, EMIM-OTf, EMIM-FSI, and BMPyrr-FSI, was determined using CV experiments.

To quantify the released CO_2, Fourier transform infrared spectroscopy (FTIR) measurements were conducted on three of the investigated polymers, providing prove of the CO_2 capture and release ability of these most promising candidates.

Acknowledgment

First of all, I would like to thank Prof. Niyazi Serdar Sariciftci for giving me the opportunity to work on this interesting topic in my master thesis at the Institute of Physical Chemistry and Linz Institute for Organic Solar Cells.

Moreover, I would like to extend my gratitude to Priv. Doz.^{in} Yolanda Salinas for the wonderful collaboration, and I am thankful to Prof. Oliver Brüggemann for granting me access to their laboratory during my synthesis work.

I would like to express my profound gratitude to Dr. Dominik Wielend, my supervisor, who not only introduced me to this fascinating topic but also ignited my passion for the field of electrochemistry. Despite having completed his own Ph.D. by the time I worked on my master thesis, Dr. Wielend provided unwavering support and guidance. His patience, assistance, and dedication have been truly invaluable, and I am immensely appreciative of his mentorship.

In general, I want to express my deep appreciation to the LIOS team for creating such a friendly and enjoyable working environment, as well as for their generous support. I would like to offer special thanks to Elisabeth Leeb, Katarina Gugujonovic, and Felix Mayr for their support, friendship, and guidance during challenging times. They have truly been remarkable office companions, making even the toughest days more manageable with their advice and encouragement.

I would also like to thank my colleagues Elisabeth Leeb, Magdalena Fidler, and Sarah Schwarz for their great cooperation in diverse laboratories and for making the everyday university brighter with coffee and plenty of laughter.

Table of Content

1. Introduction

The increasing levels of anthropogenic carbon dioxide (CO_2) in the Earth's atmosphere are a major cause of global climate change and pose a threat to public health and the environment. [1–4] The continuous increase in atmospheric CO_2 levels due to the use of carbon-based fuels has led to extensive research in CO_2 utilization chemistry. Up to this point, carbon dioxide has emerged as a predominant contributor to industrial carbon emissions, raising concerns about its role in causing the greenhouse effect and leading to global climate change.[5] Despite some remaining uncertainties, immediate action is needed to reduce CO_2 emissions, which is crucial to reduce the long-term impacts of climate change. While ongoing research and development focus on finding low- or zero-carbon alternatives to fossil fuels, it is imperative to find strategies to stabilize CO_2 levels. This involves capturing and storing carbon preventing the release into the atmosphere. [6]

The aim is to find ways to capture CO_2 from point sources such as power plants or directly from the atmosphere, in order to reduce atmospheric CO_2 concentrations. [7,8] Therefore, two different approaches have been suggested to address the issue of carbon emissions: Carbon Capture and Storage (CCS) and Carbon Capture and Utilization (CCU). The CCU approach aims to make use of captured CO_2 by direct conversion into raw materials in various industrial processes. On the other hand, the CCS approach is focused on storing the collected carbon dioxide rather than utilizing it. The stored CO_2 is injected into appropriate geological formations where it is stored as a gas, liquid, or supercritical fluid, depending on the properties of the trapping medium. [9]

1.1. Carbon Capture and Storage (CCS)

CCS refers to a range of techniques that aim to selectively remove CO_2 from gas streams. The captured CO_2 is then compressed into a supercritical state, transported and stored in geological formations, such as exhausted oil and gas reservoirs. The CO_2 can be directly captured from different power plants, industrial sites, natural gas well and even direct from the atmosphere. [2,10,11] Currently, CCS technologies primarily use liquid sorbents, which act as solvents to dissolve carbon dioxide, or solid sorbents to adsorb the acidic gas. [12]

In conventional technologies the separation of CO_2 in gas stream of different plants relies on thermal amine scrubbing-based methods. [13,14] These methods employ a chemical wet process using aqueous amines to separate CO_2 from natural gas and hydrogen. Different ammonia derivatives are used in the processes in which one or more hydrogen atoms are substituted by an alkyl group, the most common being monoethanolamine (MEA), methyldiethanolamine (MDEA) and diethanolamine (DEA).[15] CO_2 capture processes using amines, so called thermal amine scrubbing, involves directing an exhaust gas stream into a chamber filled with an aqueous amine

solution, resulting in the removal of CO_2. Regarding primary amines, such as MEA, the process is based on chemical absorption to capture CO_2 through a reaction with amine in the form of a carbamate, as shown in **Figure 1**.
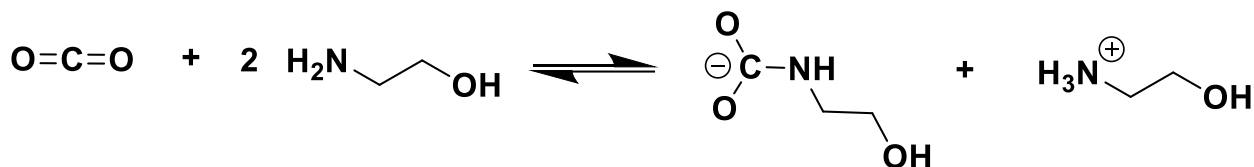
Figure 1. Scheme of reaction of MEA with CO_2 forming a carbamate structure. [16]

In the case of secondary and tertiary amines, they undergo hydrolysis to react with CO_2 in the form of bicarbonate. At high temperatures, the captured CO_2 is released, and the amine solution is recycled. [17] While amine scrubbing remains a proven and dependable technology extensively tested for large-scale CO_2 capture from industrial power plants [13] it does have several drawbacks including high energy consumption during the regeneration process, sorbent degradation and a relatively slow CO_2 adsorption rate. [18–21]

In addition to absorption with amines, other processes for CO_2 capture on an industrial scale are present such as adsorption membrane separation and cryogenic separation, which, however, require high energy consumption. Furthermore, the suitability of these thermal processes for capturing CO_2 from dilute sources, like air and ocean, is often limited by their reliance on the availability of thermal energy leading to a high energy consumption and costs and additionally to the low concentration of CO_2. [22]

1.2. Carbon Capture and Utilization (CCU)

Alongside the CCS approach, CCU is a promising method of reducing the atmospheric CO_2. Unlike CCS, CCU aims not only to decrease the number of emissions released into the atmosphere but also to gain benefits by using CO_2 in various industrial processes by replacing conventional raw material rather than storing it. [23,24] Furthermore, long-term impacts of sequestration are a minor issue with CCU, however despite the considerable benefits provided by CCU over CCS, the conversion of CO_2 and its utilization in chemical reactions poses significant challenges, primarily due to the thermodynamic stability of CO_2. [25]

Serving as a carbon source, CO_2 can be employed as a primary component in the production of fuels and various components. On the other hand, CO_2 can be chemically converted into valuable materials, including methanol, acetic acid, carbonates, and polymers. [24] Producing fuels such as methanol, formic acid, syngas and alkanes is considered as the most important and promising

approach for CO_2 utilization. These synthetic fuels can be further utilized in diverse application like fuel cells and power plant or in the transportation sector. [2] For the process of converting CO_2 into fuels are various different methods available, whereby hydrogenation and dry reforming of methane being the two most prominent ones. However, to achieve high fuel yields substantial heat and catalyst are needed to be applied due to the thermodynamically stable nature of CO_2. [25,26]

Furthermore, formic acid derived from CO_2 utilization has gained significant attention primarily due to the mild reaction conditions during its hydrogenation and the absence of side products. [27]

1.3. Electrochemical carbon capture

In recent years, there have been emerging proposals for more effective carbon capture methods that involve electrochemical processes as environmentally friendly alternative. [12,16,21,28–30] Electrochemical processes are more energy efficient as the captured CO_2 is released without external heat sources or high pressures/vacuum compared to thermal-swing and pressure-swing adsorption processes. [22,29] Additionally, harsh conditions such as high temperatures and pressures are avoided contributing to the stability and life-time of the sorbents. [31] In contrast to temperature swing techniques, electrochemical processes have the advantage of being able to operate consistently at a constant temperature avoiding encountering the efficiency limitations of the Carnot cycle. [32] These electrochemically-mediated carbon capture (ECC) approaches include utilizing electrochemical reactions to regenerate sorbents in existing carbon capture technologies [28,33] or developing chemical complexes that can efficiently and reversibly capture and release carbon dioxide by undergoing changes in their oxidation state. [12,34]

ECC uses redox active organic molecules and can be divided into two main approaches, electrochemical indirect carbon capture (EICC) and electrochemical direct carbon capture (EDCC). [21,29] The fundamental distinction between EDCC and EICC approach lies in the way how the sorbent molecules is involved in the CO_2 capture and release process as illustrated in **Figure 2**.
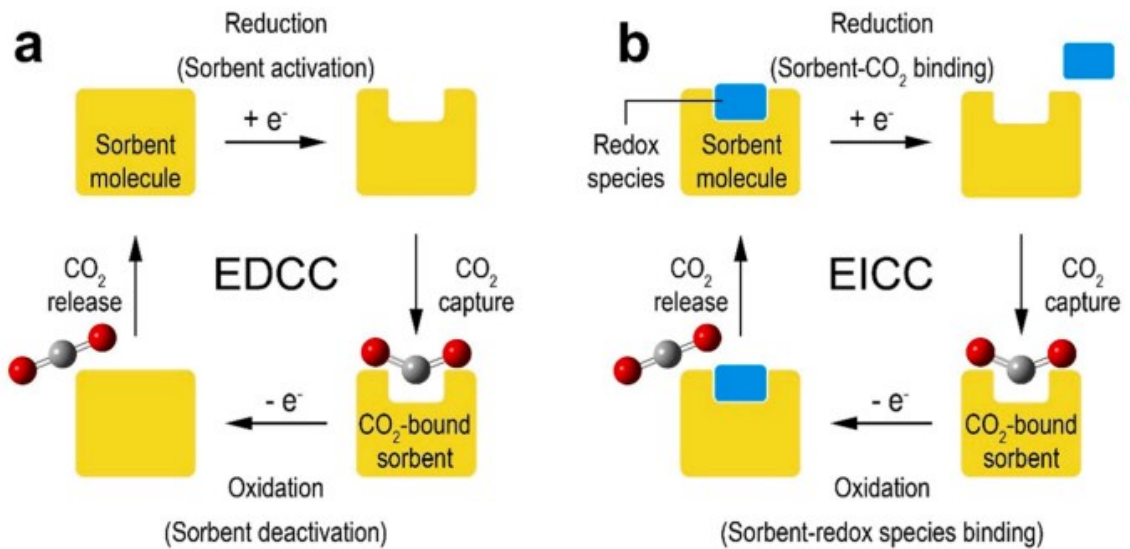
Figure 2. Schematic pathway of **a)** EDCC process, where the sorbent material actively take part in the redox reaction and in the contrast **b)** the EICC process in which an additive redox species engaging in the redox reaction instead of the sorbent material is involved. Reprinted with permission from Choi *et al.* © 2023 Elsevier. [21]

In EDCC, sorbent molecules directly capture CO_2 by undergoing redox reactions altering their CO_2 binding affinities. The sorbent is activated during reduction and deactivated during oxidation. On the other hand, in EICC, sorbent molecules provide constant activated binding sites for CO_2, while a secondary non-CO_2 reactive redox species interact with the sorbent molecules during reduction and oxidation. During reduction, the sorbent binds to CO_2, whereas during oxidation, the sorbent-redox species binding occurs. This interaction controls CO_2 capture/release by competing for binding with sorbents and CO_2 molecules, for example mediated pH swing methods [35,36], electrochemically mediated amine regeneration process [33], and bipolar membrane electrodialysis. [21,37]

1.3.1. Indirect electrochemical carbon capture

Numerous electrochemical methods are based on mediated pH swing methods as EICC method, where CO_2 is captured by changing the working fluid electrochemically between acidic and alkaline pH levels, which affects the thermodynamic equilibrium of CO_2. [12] In acidic solution, CO_2 is predominantly present in its molecular form or carbonic acid (H_2CO_3). The equilibrium distribution gradually shifts from H_2CO_3 towards bicarbonate ions HCO_3^- and further towards carbonate ions CO_3^{2-} with increasing pH. [38]

Furthermore, due to being present in molecular form at lower pH values, CO_2 tends to degas, resulting in lower solubility. This relationship leads to a strong correlation between CO_2 solubility and pH, with higher pH values allowing for greater amounts of CO_2 to be dissolved in an aqueous

solvent. Isothermal electrochemically mediated pH swing methods that utilize proton-storable materials to take advantage of the varying thermodynamic equilibrium speciation of CO_2 at different pH levels have gained significant attention. [12] This approach involves uses of small molecules that perform proton-coupled electron transfer in aqueous solution. Through an electrochemical redox reaction, these molecules can accept or release protons, respectively, resulting in a shift in the solution pH value. If the pH change is significant, it enables a strong absorption of CO_2 at high pH and a subsequent release at low pH. The maximum pH shift that can be achieved depends on factors such as the pKa value of the reduced form of the redox couple, as well as its solubility. [36] In particular, organic molecules undergoing proton-coupled electron transfer and involved in various biological energy conversion processes are investigated in detail in electrochemical pH swing processes for CO_2 capture and release. [12,36,39] Xie *et al.* reported the use of riboflavin 5-monophosphate (FMN) in an alkaline aqueous solution as biological redox proton carrier for CO_2 capture. [40] Furthermore, different quinones derivates have been also investigated. [41] Watkins *et al.* employed quinone, which can undergo a proton-coupled electron transfer creating a pH gradient to develop a functional membrane for capturing CO_2. [42]

1.3.2. Direct electrochemical carbon capture

Apart from indirect methods for CO_2 capture, direct electro-swing of redox-responsive sorbents has emerged as another promising approach for CO_2 captured processes. Organic molecules containing redox centers capable of capturing and releasing CO_2 under different oxidation states are employed in these processes. [12,16,21,29,30] Since 1989, when researchers firstly discovered the electrochemical redox activity and CO_2 capture and release abilities of a quinone derivative 9,10-phenanthrenequinone (PAQ) [43] , numerous research groups have investigated aromatic materials with redox properties and functional groups, such as carbonyls, sulphides and amines. [21] The efficiency of both, the electrochemical reduction of organic molecules and the nucleophilic addition reaction of CO_2, depends significantly on the characteristics of the electrolyte, including the type of electrolyte, the concentration of salts and sorbents, as well as the composition of the air-inlet. [44,45] Significant research efforts are devoted to enhance the energy efficiency and capacity as well as stability of redox-active CO_2 carriers by modifying the electrolyte [44], altering the system configuration [46] and introducing electrolyte additives. [21,47]

Among these redox-responsive sorbents, quinones and derivates containing carbonyl groups have been extensively studied and utilized. [43,48–50] Gurkan *et al.* investigated the CO_2 capture and release abilities of different naphthoquinones in various ionic liquids. This study revealed that a EMIM based ionic liquid resulted in the most promising result as the quinone solubility is enhanced

significantly enabling effective CO_2 separation by preventing back-diffusion from the anodic side when in contact with a cathode. [44]

Simeon *et al.* screened different substituted quinones in homogenous organic solutions for carbon capture. In the absence of CO_2, all quinones showed two separated distinct reduction peaks as illustrated in **Figure 3.**
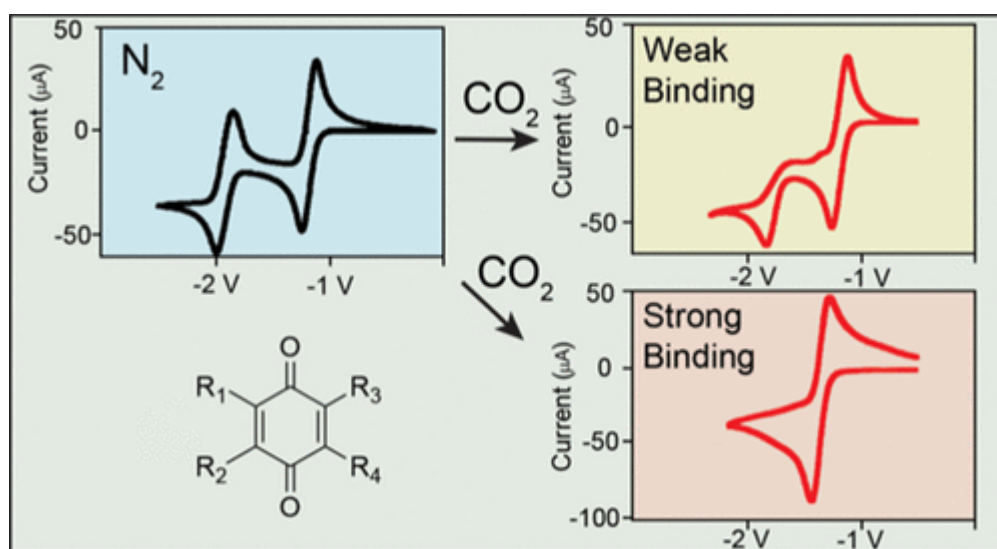
Figure 3. Illustration of CV of quinones with weak or strong binding to CO_2. Reproduced with Permission from Simeon *et al*. © 2022 American Chemical Society. [51]

Quinones with low complexing abilities exhibited a positive shift in their second reduction peak when CO_2 was present, indicating the formation of dianion quinone-CO_2 complexes, while quinones with strong complexing abilities showed the merging of their second reduction peak with the first, suggesting simultaneous transfer of two electrons at that point. Both types of quinones, whether weakly or strongly complexing, experienced oxidation and subsequently the release of CO_2. [51]

Furthermore, Schimanofsky *et al.* has investigated different substituted anthraquinones in homogenous solution showing similar characteristics of weak and strong binding with CO_2 from CV as shown above in **Figure 3**. In addition to previous studies, in-depth UV-Vis spectroelectrochemistry and DFTB calculations were implemented by Schimanofsky *et al.* and an additional case with even smaller binding compared to the one introduced by Simeon *et al.* was observed. [52] An imidazolium-functionalized anthraquinone for electrochemical CO_2 capture was recently reported by Lida *et al.* [53]

Wielend *et. al* reported the use of anthraquinone thin films prepared by evaporation for heterogenous electrochemical CO_2 capture. [54] This quinone compound contain carbonyl groups

that exhibit nucleophilic behaviour under reductive conditions, which enables the capture of CO_2 by forming carbonate-like structures as shown in **Figure 4**.
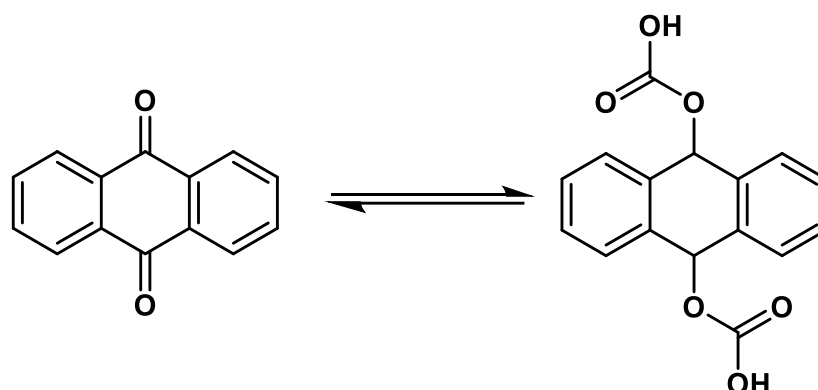
Figure 4. Scheme of anthraquinone capturing electrochemical CO_2 in aqueous electrolyte.

Under saturated CO_2 conditions, the electrochemical response of anthraquinone was found to be notably diminished, resulting upon further reduction in an extremely low observed current during cyclic voltammetry. This observation is in contrast to the studies in homogeneous solution, as illustrated in **Figure 3**. However, after removal of unbound CO_2 from the system and subsequent oxidation, the CO_2 is released from the adducts and the organic reactant is regenerated. This is indicated by the reappearance of the characteristic reversible redox peaks of anthraquinone in the cyclic voltammogram. [7,54]

However, reduced anthraquinone species are easily soluble leading to long-term stability issues, therefore polyanthraquinones are investigated severely for CO_2 capture application to improve the stability of the system. [54,55] Voskian & Hatton reported an electrochemical cell prototype device for CO_2 capture application in high concentration flue gas emission by electro-swing, following the scheme in **Figure 2 a**. The cell consists of polyanthraquinone-carbon nanocomposites combined with poly(vinylferrocene)-carbon nanocomposite in ionic liquids as electrolyte. The design of the cell ensures a maximized surface area exposed to gas, enabling easy stacking of the cells in a parallel passage contactor bed. [31] This prototype was further optimized regarding design and operation at low CO_2 concentration by the same research group for utilization in direct air capture (DAC) of CO_2. [46]

While quinone systems have been extensively studied for electrochemical carbon capture their applicability in direct air capture is restricted due to their sensitivity towards oxygen. These quinone-based systems tend to degrade or other chemical reactions occur when exposed to input streams containing oxygen. This is primarily because the reduced nucleophiles within the system react with oxygen molecules, generating superoxide. Furthermore, many quinones and derivates

are reported simultaneously for hydrogen peroxide production by reduction of oxygen. [56] This results into competitive reactions leading to unproductive carrier molecules for carbon capture and therefore restrict the use in direct air capture. [47]

Besides anthraquinone thin films, our institute investigated thin films of organic pigments specifically quinacridone as well as a derivative of naphthalene bisimide (NBIT) illustrated in **Figure 5** for the use of heterogeneous electrochemical capture and release of CO_2. [55,57]
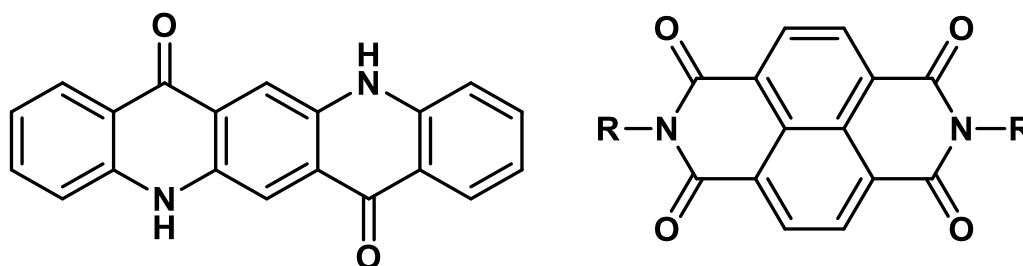
Figure 5. Structure of quinacridone (left) and NBIT (right).

This organic semiconductor NBIT was specifically designed to enable a reversible reduction involving one electron and a quasi-reversible reduction under aqueous conditions, all while maintaining its structural integrity without dissolution or degradation. [57]

1.4. Organic redox active sorbent materials

Organic molecules containing redox centers undergoing reversible redox reaction are used as redox active sorbent materials in electrochemical processes. Numerous research groups have explored aromatic compounds possessing redox characteristics, along with functional groups like carbonyls, sulphides, and amines. Among these responsive sorbents with redox properties, quinones and their derivatives, which incorporate carbonyl groups, have been subject to extensive investigation and utilization. [16,21,29]

However, homogeneous catalytic systems encounter challenges related to their stability and the complexities of catalyst recovery. Furthermore, a majority of catalysts exhibit restricted solubility, which limits their effectiveness. Therefore, immobilizing the redox active units for heterogenous catalysis can improve the stability of the electrochemical system and overall performance.[58]

To address this challenge, various strategies have been investigated over the past few decades. One possibility without involving chemical reaction is the blending of redox-active molecules with carbon materials to enhance overall conductivity, either as composites [59] or through a more targeted method involving the non-covalent binding of redox active units to carbon nanotubes. [60,61] Another approach involves immobilizing redox active units in a polymer chain. For this, conductive

polymer can be used, such as polyacetylene, polythiophenes (Pth), polypyrrole (PPy), poly(3,4-ethylenedioxythiophene) (PEDOT) polyaninline (PANI) being the most prominent ones.

Conductive polymers demonstrate to have a high electrical conductivity due to their extensively conjugated electronic structure along the polymer backbone. [62] The origin of these conductive polymers can be traced back to the pioneering research in the 1970s on doping the polymer polyacetylene conducted by Alan Heeger, Alan MacDiarmid, and Hideki Shirakawa. [63,64] In recognition of their contributions to the investigation of conductive polymers, they received the Nobel Prize in Chemistry in the year 2000.

Conductive polymers can be directly electro polymerized onto the electrode such as polythiophenes, polypyrrol and polyaniline having the advantage that they are typically insoluble after polymerization. In addition to utilizing conductive polymers, there is a well-documented approach involving the attachment of redox-active components to non-conductive polymer chains, which are often used in battery applications. [58,65,66]

1.4.1. Anthraquinone and derivates

Anthraquinones represent a significant subgroup within the quinone class and are characterized by a core structure of 9,10-dioxoanthracene. Anthraquinone and its derivates have been already reported for the electrochemical CO_2 capture in different media. [44,51,52] However, reduced anthraquinone species are easily soluble in various solvents leading to long-term stability issues in energy storage applications. [54] To overcome this problem, anthraquinones, especially with an amine as a functional group like 1-Aminoanthraquinone (1-AAQ) and 1,5-Diaminoanthraquinone (1,5-DAAQ) can be directly polymerized onto the electrode to immobilize the redox active units while enhancing the stability.

Poly(1-aminoanthraquinone) (PAAQ) was first prepared through anodic electrochemical polymerization in acetonitrile on glassy carbon electrodes by Ismail *et al.* and later in 6 M H_2SO_4 by the same group. The electropolymerization of AAQ proceeds *via* the formation of C-N couplings as can be seen in **Figure 6**, similar to the well-studied conductive polymer polyaniline. [67–69]
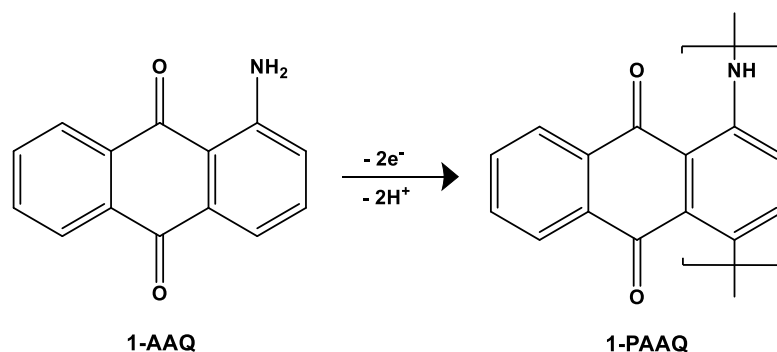
Figure 6. Structure of 1-AAQ and 1-PAAQ.

Poly(1,5-diaminoanthraquinone) (P15DAAQ) was first reported by Naoi *et al*. [70] The formation of the polymer occurs by a sequence of coupling reactions involving radical cations and followed by an electron transfer of an electrochemical reaction, subsequent chemical reaction and again an electrochemical reaction. Both amino groups are oxidized and are involved in bonding mainly in the 1,4,5 and 8 positions creating a ladder like structure. The proposed mechanism of the oxidative electropolymerization following a four-electron process is presented in **Figure 7**. [71]
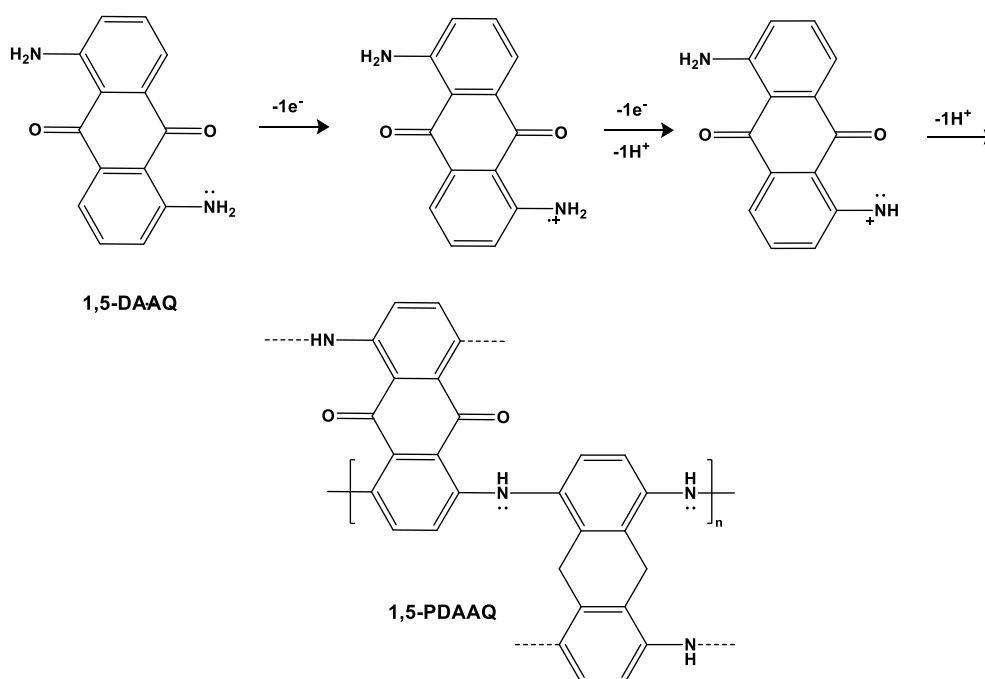
Figure 7. Proposed mechanism for the oxidative electropolymerization of 1,5-DAAQ.[71]

Furthermore, PAAQ, as well as P15DAAQ, are reported for several different applications such as batteries [72], biosensors [73], and supercapacitors. [70] Wielend *et al.* investigated oxygen reduction reaction (ORR) to hydrogen peroxide using different anthraquinone-based polymers. [58]

1.4.2. Riboflavin and derivates

Riboflavin, also known as vitamin B2, is a yellow, water-soluble pigment that was first isolated from milk in the 1870s. Its chemical structure comprises a heterocyclic isoalloxazine and ribitol side chain, as illustrated in **Figure 8**.
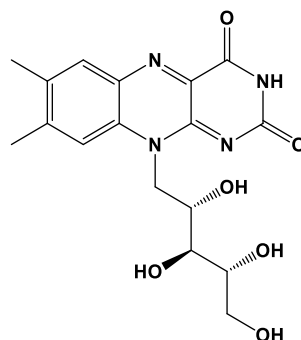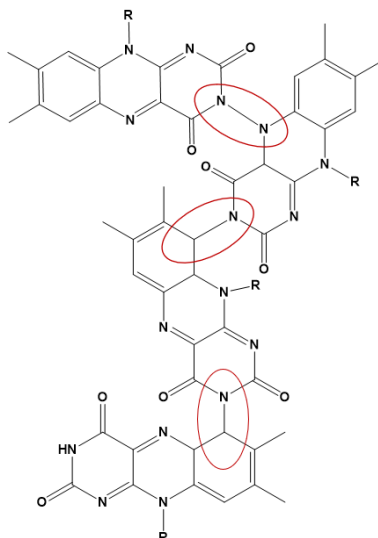

Figure 8. Structure of riboflavin.

Riboflavin plays a crucial role as a precursor to the coenzymes flavin monophosphate (FMN) and flavin adenine dinucleotide (FAD) in biological systems. [74] These coenzymes FMN and FAD are essential components of the active sites of flavoenzymes, which are involved in various biological processes such as dehydrogenation reactions, dioxide activation as well as electron transfer reaction. [75] Due to its aromatic nature, functionality, and redox properties, riboflavin exhibits an electroactive behaviour, making it suitable for use in various electrochemical applications, including electrochemical sensors [76,77] and as redox mediator. [78] Furthermore, FMN has been reported as redox proton carrier for CO_2 capture by Xie *et al.* [40]

Riboflavin can be adsorbed physically from saturated solutions onto different electrodes such as carbon-based electrodes [79] and platin electrodes [80] or is incorporated in carbon nanomaterials [61] for different applications and to study the electrochemical behaviour. Wang *et al.* used a riboflavin-anthraquinone hybrid molecule and incorporated the substance in carbon black as an organic catalyst for oxygen reduction to H_2O_2. [81] Furthermore, riboflavin was reported by Leeb *et al.* from our institute as an electrocatalyst for oxygen reduction reaction in homogeneous solution at various pH values. [82]

As heterogenized structures are preferred, the oxidative electropolymerization of riboflavin was firstly reported by Ivanova and Karyakin, who performed the electropolymerization of different flavins on glassy carbon electrodes. [83] Additionally, Radzevi *et al.* investigated the electropolymerization of riboflavin in different aqueous media by cyclic voltammetry to receive an optimized stable electroactive polymerized riboflavin film. [84] A possible structure of the electropolymerized polyriboflavin (PRF) according to Radzevi *et al.* is depicted in **Figure 9** showing possible N-C as well as N-N bonds between the monomer molecules. However, the N-N

interaction is less likely than the C-N bonds which were confirmed by Raman as well as IR-spectroscopy in literature. [84]

Figure 9. Proposed structure for polyriboflavin. R = ribitol side chain. [84]

As reported for the monomer also PRF is utilized as a biosensor for various biological molecules [85,86]

1.5. Ionic liquids
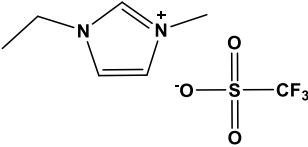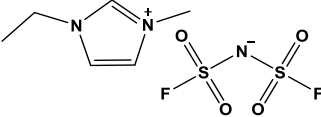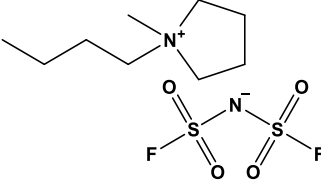
Ionic liquids (ILs) are generally described as substances consisting entirely of ions mainly organic, which have a melting point that is lower than 100°C. [87,88] This characteristic is due to the presence of hydrogen and van der Waals bonds, as well as the symmetry of the ions within the liquid. [89] They are unique liquids with outstanding properties, such as low volatility, negligible vapor pressure, high thermal stability, high electric conductivity and designability. [90] Therefore, they are used as solvents, electrolytes and reaction media in numerous chemical processes. Due to their exceptional properties and stabilization of reaction intermediates, ionic liquids have attracted significant attention in various fields, including electrochemistry, catalysis, and materials science and are considered suitable substitutes for volatile organic solvents. [91,92] The electrochemical stability of aqueous electrolytes is restricted by the occurrence of water splitting at 1.23 V. [93] Similarly, traditional non-aqueous electrolytes such as acetonitrile-based with tetraethylammonium or triethylmethylammonium tetrafluoroborate salts also have limited potential windows due to the decomposition of the solvent. [94] Therefore, ILs have gained importance especially in the field of electrochemistry, since they offer a wider electrochemical window and no solvent evaporation loss compared to conventional electrolytes in particular aqueous solutions. [91]

The electrochemical window of a solvent is a crucial factor in designing electrochemical applications. It refers to the voltage range within which the solvent can operate without undergoing reduction or oxidation. [95]

Furthermore, ionic liquids have been demonstrated to have greater solubility for carbon dioxide compared to traditional organic solvents at various temperature and pressure ranges. Carbon capture in ionic liquids is achieved by either chemical or physical absorption, however, the specific mechanism of absorption depends on the functional groups being present in the particular ionic liquid. [96,97] In terms of physisorption, the interactions between CO_2 and the anion, as well as those between the cation and the anion are important factors in CO_2 solubility. Whereby, concerning chemisorption, the reactivity with CO_2 can be adjusted by the basicity of the anion, while the stability of the ionic liquid can be improved by tuning the cation. [98] In general, the employed anion in the IL has a significant impact on the solubility of CO_2. In addition, increasing the cation alkyl chain length is reported to enhance the solubility of CO_2 even further. [99] This is primarily attributed to van der Waals forces, with a greater hydrophobicity of the cation leading to stronger attraction between the cation and CO_2. This also applies regarding the anion as a more hydrophobic anion prevents the IL moiety attacking water molecules resulting in the formation of a strong bond with the molecule. Specifically, longer alkyl chains and the use of fluorinated anions have been observed to be more likely to improve CO_2 capture process. [100] The relationship between the properties high conductivity and low viscosity are crucial characteristics of ionic liquids for the application in carbon capture. [100,101] In many carbon capture processes, high viscosity is an inhibiting element and it is preferred to keep it to a minimum in most processes. This is due to a high viscosity can lead to the formation of solids or gels due to the formation of hydrogen bonds, which has a negative impact on the mass transfer of CO_2. [102]

Ionic liquids are reported as suitable electrolytes for carbon capture due to their wide electrochemical range, remarkable CO_2 solubility, and no losses from evaporation. [44] Therefore in this thesis, ionic liquids are utilized with the mentioned polymer to investigate an improvement of the capture ability of the used polymers. The Ionic liquids used in this thesis as well as their physical properties are depicted in **Table 1**.

Table 1. Ionic Liquids used as well as their structure and viscosity.

Ionic Liquid	Abb.	Structure	η / mPa s
1-Ethyl-3-methylimidazolium trifluoromethanesulfonate	EMIM-OTf		43[103]
1-Ethyl-3-methylimidazolium bis(fluorosulfonyl)imide	EMIM-FSI		22[104]
1-Butyl-1-methylpyrrolidinium bis(fluorosulfonyl)imide	BMPyrr-FSI		53[105]

The IL presented in **Table 1** are considered as room temperature ionic liquids (RTIL) being in a liquid state at room temperature as indicated by their name. Imidazolium-based ionic liquids, such as 1-ethyl-3-methylimidazolium (EMIM), are extensively studied due to low viscosity, low cost and ease of synthesis allowing the customization of imidazolium-based ILs to suit specific applications. These ILs have shown great promise in electrochemical applications, such as energy storage and conversion, due to their remarkable stability under oxidative and reductive conditions as well as efficient mass transfer capabilities. [106] In particular, Pardal *et al.* has reported the use of an electrolyte consisting of a mixture of water and EMIM-OTf to achieve efficient electrochemical reduction of CO_2 to syngas under high pressure. [107]

1.6. Objective

In this master thesis six different anthraquinone and riboflavin-based polymers presented in **Figure 10** are investigated for the electrochemical carbon capture in different media, such as aqueous conventional electrolyte as well as ionic liquids.
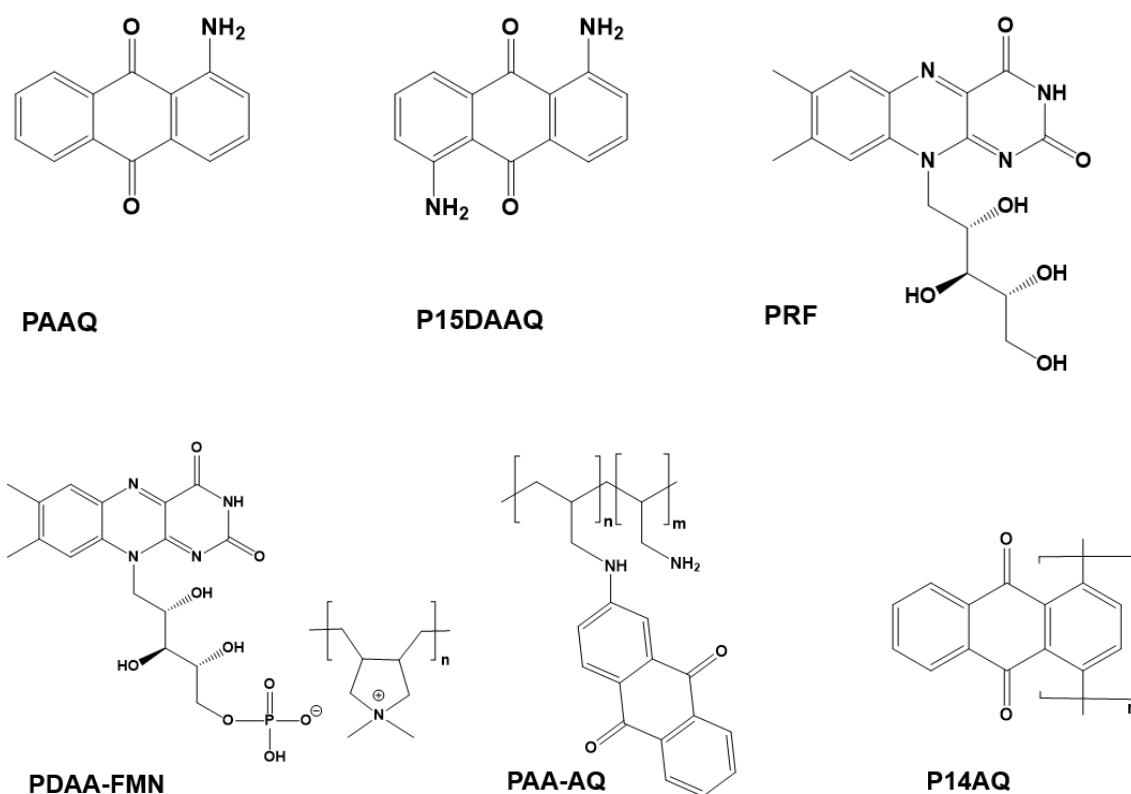
Figure 10. Used Polymers.

Poly-1-Aminoanthraquinone (PAAQ), poly-1,5-diaminoanthraquinone (P15DAAQ) and polyriboflavin (PRF) are electrochemically synthesized, while poly(allyamine anthraquinone), (PAA-AQ), polyanthraquinone (P14AQ) and poly(diallyldimethyl ammonium flavin mono nucleotid) (PDAA-FMN) are chemically prepared. The used polymers are characterized by Scanning electron microscopy (SEM), Fourier transform infrared spectroscopy (FTIR), Raman spectroscopy and contact angle measurements. In addition, with the most promising polymers also quantification of released CO_2 via FTIR and potentiodynamic electro-swing experiments were performed.

2. Experimental

1-Aminoantraquinone (1-AAQ) and 1,5-Diaminoanthraquinone (1,5-DAAQ) were purified by train sublimation performed twice by Dr. Mihai Irimia-Vladu. All other chemicals were used as received without further purification. Electrochemical measurements were performed either with an IPS Jaissle Potentiostat / Galvanostat PGU 10 V - 100 mA, a Jaissle Potentiostat / Galvanostat 1030 PC or Ivium.Vertex One. All potentials mentioned are recalculated and stated versus the standard hydrogen electrode (SHE).

2.1. Electrode preparation

2.1.1. Glassy Carbon (GC)

The glassy carbon electrode was polished with different alumina pastes, with decreasing particle sizes (1 µm, 0.3 µm, 0.05 µm). In order to remove residual aluminum particles, the GC was polished with toothpaste as the last step. After each polishing step, the electrode was sonicated for approximately 15 min in 18 MΩ water followed by isopropanol (IPA) for an additional 15 min. The polished GC was connected to a copper wire using silver paste and fixed with Teflon tape. The electrode was activated in 0.5 M H_2SO_4 in a one-compartment cell like in **Figure 11** using the electrochemical parameters depicted in **Table 2**. As the reference electrode an Ag/AgCl (3 M KCl) electrode and for the counter electrode a Pt electrode was used.

Table 2. Electrochemical parameter for the activation.

1st Potential / V	2nd Potential / V	Scanrate / mV s^{-1}	Current Range / mA	Nr. of Cycles
1.65	-0.85	50	100	30

2.1.2. Carbon Paper (CP)

The Carbon Paper (Alfa Aesar, Toray Carbon Paper, TGP-H-60) was cut into 1x3 cm rectangles and used without further activation. The CP was contacted to a copper wire by a silver crocodile clip fixed with Teflon tape.

2.1.3. Cr-Au electrodes

For FTIR and Raman-spectroscopy measurements of the electropolymerized polymer films, Cr-Au electrodes on glass substrates were prepared. Therefore, glass substrates were cut into 0.7 cm times 6 cm rectangles. The glass substrates were cleaned by sonication for 15 min in acetone, 15 min in 2% Hellmanex solution, and 15 min in deionized water followed by IPA for additional 15 min. Further treatment was performed in a Plasma ETCH P25 plasma oven under O_2 at 100 W for

2 min. In a thermal metal evaporation chamber, 5 nm of chromium with a current of 1.5 A and a rate of 0.04 nm s^{-1} were deposited onto the glass substrate, followed by gold with a current of 3 A at approximately 10^{-6} mbar until a film thickness of 100 nm was reached.

2.2. Electropolymerization

Electropolymerizations of 1-AAQ and 1,5-DAAQ were performed on GC, CP, and Platin (Pt) electrodes as well as Cr-Au electrodes. Riboflavin was polymerized only at GC and CP electrodes since a high potential is required to cause oxidation of riboflavin. All electropolymerizations were performed in a one compartment cell as depicted in **Figure 11**.
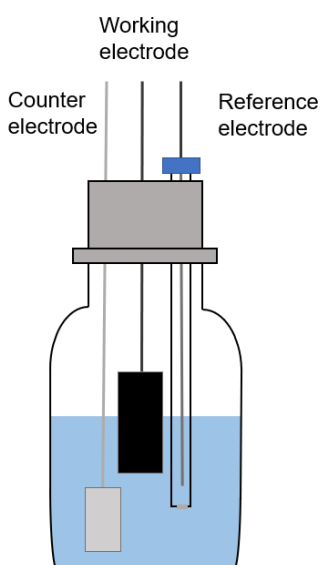
Figure 11. Setup for electropolymerization in a one-compartment cell.

The optimisation of the electrochemical polymerizations of PAAQ, P15DAAQ and PRF together with their applicability as electrocatalyst for the electrochemical oxygen to hydrogen peroxide reduction is summarized in a journal publication by Kleinbruckner *et al.* and currently under revision. [108]

2.2.1. Electropolymerization of 1-Aminoantraquinone

The electropolymerization of 1-AQQ leading to poly(1-aminoanthraquinone) (PAAQ) was performed following the procedure of Badawy *et al.* [68] Therefore, for the oxidative electropolymerization of 1-AAQ a 5 mM solution of 1-AQQ in 6 M H_2SO_4 was purged for approximately 30 min with N_2. A saturated calomel electrode (SCE) was used as the reference electrode and a platinum foil electrode as the counter electrode. The electrochemical polymerization of 1-AAQ was performed either on GC or CP. Additionally, polymerization on platinum as well as on Cr-Au was carried out in order to characterize the polymer films via FTIR

and Raman spectroscopy. (Compare with Chapter 2.6.). After the polymerization, the modified electrodes with PAAQ were washed with 18 MΩ water. The electrochemical parameter used for the potentiodynamic polymerization are shown in **Table 3**. However, the number of cycles was decreased to 20 cycles for the polymerization on Cr-Au to avoid the oxidation of chromium leading to detachment of gold from the glass substrate. Furthermore, for FTIR and Raman spectroscopy measurements a thinner film is desired.

Table 3. Electrochemical parameter versus SCE for the electropolymerization of 1-AAQ.

1st Potential / V	2nd Potential / V	Scanrate / mV s^{-1}	Current Range / mA	Nr. of Cycles
0	1.3	100	100	40

2.2.2. Electropolymerization of 1,5-Diaminoantraquinone

The electropolymerization of 1,5-DAQQ to obtain poly(1,5-diaminoanthraquinone) (P15DAAQ) was performed nearly analogous to the electropolymerization of 1-AAQ based on the procedure of Badawy *et al.* [68] However, the procedure was slightly modified to suit 1,5-DAQQ. Therefore, for the oxidative electropolymerization of 1,5-DAAQ a 2.5 mM solution of 1,5-DAAQ in 6 M H_2SO_4 was prepared and purged for approximately 30 min with N_2 prior polymerization. An SCE was used as the reference electrode and a platinum foil electrode as the counter electrode. The oxidative electrochemical polymerization of 1,5-DAAQ was performed either on GC or CP as well as on Cr-Au for spectroscopic characterization purposes. Compared to the electrochemical parameters for 1-AQQ, the oxidative vertex potential was increased in order to achieve oxidation of 1,5-DAAQ. Afterwards the obtained P15DAAQ film was washed with 18 MΩ water. The exact electrochemical parameters used for the polymerization are shown in **Table 4**. Regarding the polymerization of P15DAAQ on Cr-Au, the number of cycles was again decreased to 20 cycles.

Table 4. Electrochemical parameter versus SCE for the electropolymerization of 1-AAQ.

1st Potential / V	2nd Potential / V	Scanrate / mV s^{-1}	Current Range / mA	Nr. of Cycles
0	1.6	50	100	40

2.2.3. Electropolymerization of riboflavin

The electropolymerization of riboflavin was performed according to Ivanova *et al.* [83] and Radzevic *et al.* [84] and further optimized. The synthesis was performed in a 0.1 M H_2SO_4 solution containing 1 mM of riboflavin. Prior to the polymerization the cell was purged for approximately 30 min with N_2. An Ag/AgCl (3M KCl) was used as the reference electrode and a platinum foil

electrode as the counter electrode. As a working electrode GC or CP was used. Afterwards, the obtained polyriboflavin film was washed with 18 MΩ water. The used electrochemical parameters for the polymerization are listed in **Table 5**.

Table 5. Electrochemical parameter versus SHE for the electropolymerization of riboflavin.

1st Potential / V	2nd Potential / V	Scanrate / mV s^{-1}	Current Range / mA	Nr. of Cycles
-0.55	1.95	50	100	60

2.3. Synthesis of chemically synthesized polymers

2.3.1. Synthesis of P14AQ

The synthesis of poly-(1,4-anthraquinone) (P14AQ) was performed according to Wielend *et al.* [58], originally reported by Yamamoto *et al.* [109] and further optimized by Song *et al.* [110] To produce P14AQ by organometallic condensation reaction, 1,4-dichloroanthraquinone (0.9 mmol, 1 eq.) was weighed in a round flask and flushed with N_2. The flask was transferred into a glovebox, where 6 mL DMF are added and the mixture is stirred for approximately 2h. Subsequently, under inert atmosphere bis(1,5-cyclooctadiene)nickel(0) (1.2 mmol, 1.3 eq.), 2,2´-bipyridine (1.2 mmol, 1.3 eq.) and cyclooctadiene (0.9 mmol, 1eq.) are weighed into a separate flask and dissolved in 9 mL DMF. The previously prepared 1,4-dichloroanthraquinone solution was added to the reaction mixture and sealed. Under argon, the mixture was heated to 60 °C under stirring. After the reaction time of 48 h the solution was cooled to room temperature and neutralized with HCl (30 mL, 0.5M), resulting in the precipitation of the polymer. The precipitate was filtered off and washed with DMF, HCl and subsequently with 18 MΩ water and finally with methanol. The washed product was dried overnight. The polymer was dissolved in chloroform and again precipitated with methanol (15 mL) followed by filtration under vacuum and washing with methanol. The final purified polymer was dried under vacuum at room temperature. The reaction scheme is depicted in **Figure 12** where 1,4-Dichloroanthraquinone reacts via organometallic condensation to P14AQ.
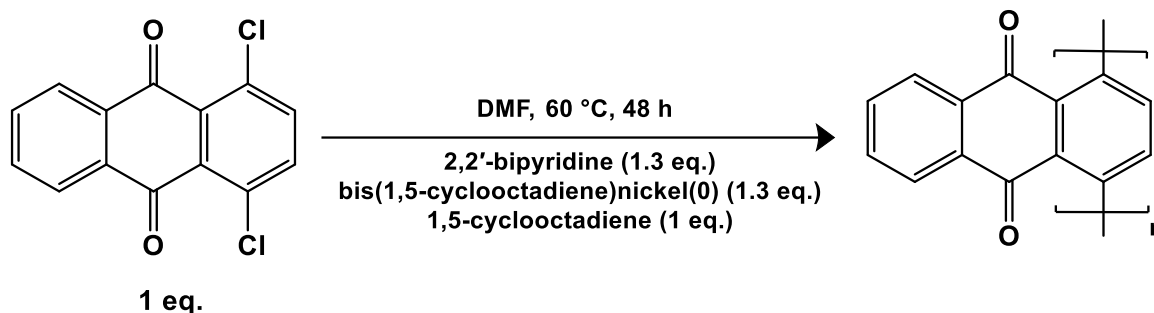
Figure 12. Reaction Scheme of the synthesis of P14AQ.

^{1}H-NMR (300 MHz, CDCl$_3$, δ/ppm): 8.31 (br,1H), 8.11 (br,1H), 7.92 (br,2H), 7.73 (br,2H).

2.3.2. Synthesis of PDDA-FMN

The synthesis of poly(diallyldimethyl ammonium flavin mono nucleotid) (PDDA-FMN) was performed according to a reported procedure for an analogous polymer. [111] For the synthesis, a 50 mM solution of FMN was prepared by dissolving 1.25 mmol of FMN (0.846 g, 76%) in 25 mL 18 MΩ water. Subsequently, 500 µL solution of poly(diallydimethylammonium chloride) (PDADMAC, 0.062 mmol, 20 wt% in H$_2$O, 200 000-350 000 g mol^{-1}) was diluted with 500 µL 18 MΩ water to receive a 10 wt% solution. Over a period of 20 min the aqueous FMN solution was added dropwise under vigorous stirring. During the anion exchange, the soluble PDADMAC is transformed into insoluble PDAA-FMN. The solution was stirred overnight and let sit for another 3h to complete the reaction. The precipitated polymer was filtered off, washed with 18 MΩ water and dried at room temperature overnight. The reaction scheme is depicted in **Figure 13**, where FMN reacts with PDADMAC resulting in the ionic polymer PDDA-FMN.
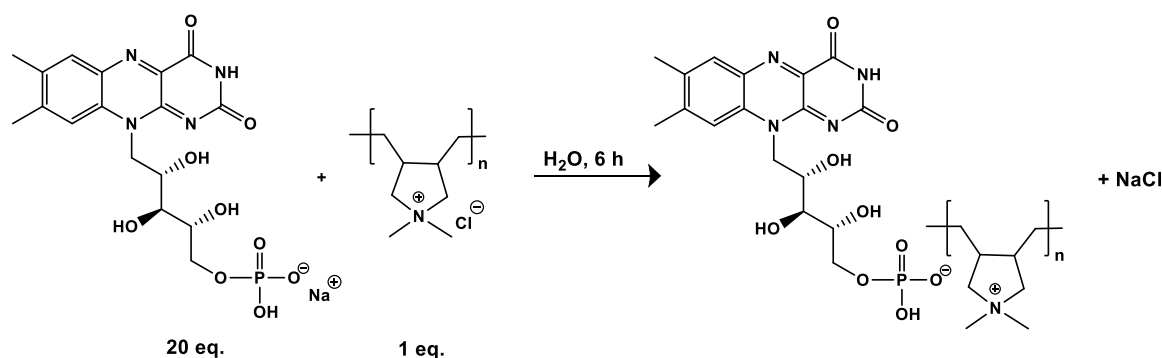
Figure 13. Reaction Scheme of PDDA-FMN.

2.3.3. Synthesis of Polyallylamine-anthraquinone (PAA-AQ)

The synthesis of poly-allylamine-anthraquinone (PAA-AQ) was performed according to the procedure reported by Oka *et al.* [65] Therefore, 2-bromoanthraquinone (1.3 mmol) was added to a polyallylamine solution (0.65 mmol, 20 wt% in H_2O, ρ = 1.02 g mL^{-1}, 17 000 g mol^{-1}) in a flask and flushed with N_2. Subsequently, the reaction mixture was transferred into a glove box, where 10 mL DMF were added and the mixture is stirred for 30 min. Under argon, the mixture was heated to 100 °C under stirring, resulting in a violet solution. With increasing reaction time, a colour change to bright red was observed. After a reaction time of 6h, the solution was cooled to room temperature, resulting in the precipitation of the polymer which was further promoted through addition of diethyl ether. The polymer was filtered of under vacuum, washed with acetone and diethyl ether and dried under vacuum at room temperature for 6h. The reaction scheme of the synthesis of PAA-AQ is depicted in **Figure 14**.
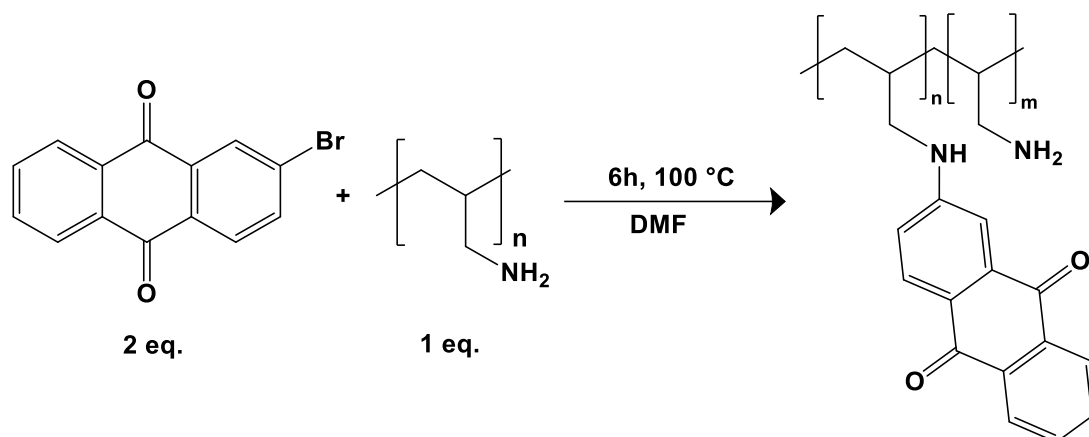
Figure 14. Reaction scheme of the synthesis of PAA-AQ.

2.4. Electrochemical Characterization

For electrochemical characterization in aqueous solution a one compartment cell was used as presented in **Figure 11**, where the WE was either the modified GC plate, CP or GC disc. As CE a Pt plate and as RE a commercial Ag/AgCl (3M KCl) was employed. Prior each CV measurement the cell was purged for 1h with N_2 to obtain an oxygen free environment. For CO_2 capture and release experiments the cell was purged for 30 min with CO_2 and subsequently the cell was purged with N_2 for 2h to remove the dissolved CO_2 to investigate the CO_2 release.

The CV measurements were performed with a scanrate of 50 mV s^{-1} in a potential range of approximately -1200 mV to 1000 mV adjusted to the pH value of the used electrolyte for 2 – 5 cycles. As electrolyte phosphate buffers were used at the pH values 2, 7 and 12. Additional, CV was conducted in 0.1 M NaOH at pH 13. Besides aqueous electrolyte solutions, ionic liquids were

used either pure or as a 5mol% solution with 18 MΩ water. Furthermore, a 1 M NaCl in 0.1 M NaOH electrolyte solution was prepared to investigate the influence of a higher ionic strength.

Prior using ILs as an electrolyte, the electrochemical window of the ILs was determined under inert conditions in a glove box. A three-electrode setup was employed, where a commercial Ag/AgCl electrode (3M KCl) was used as the RE, a platinum plate served as the CE and a glassy carbon disc was utilized as the WE.

CV measurements in pure ionic liquids were performed in a one-compartment cell inside a glove box purged with N_2. Before each measurement the solution was stirred for 2h to ensure efficient ion exchange and transfer between electrolyte and electrode. For capture and release experiments the electrolyte solution was purged with CO_2 for 15 min and subsequently with N_2 for a period of 2h to remove the dissolved CO_2 again.

For electrochemical characterization of the chemically synthesized polymer PAA-AQ and PDDA-FMN, 10 mg polymer was suspended in 1 mL DMSO and DMF, respectively and of this suspension 5 µL were drop casted onto a GC disc. In the case of P14AQ the polymer was dissolved in chloroform as a 10 mg mL^{-1} solution and drop casted onto a GC disc.

Additional electrolysis was performed to investigate the CO_2 reduction ability in aqueous solution to CO of the modified electrodes. Therefore, a two-compartment setup separated by a nafion membrane (117) as presented in **Figure 15** was used. The modified GC or CP electrodes were used as the working electrode, which were situated in the same compartment as the Ag/AgCl (3M KCl) reference electrode and was equipped with a stirrer. In the second compartment, a Pt acting as a counter electrode was placed.
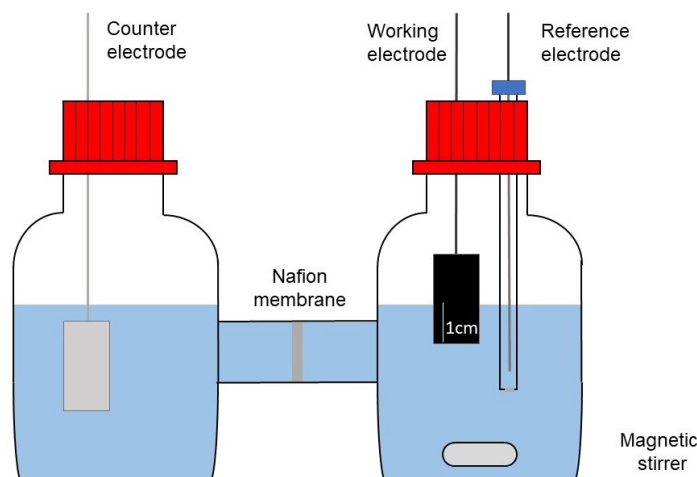
Figure 15. Two compartment cell setup for electrolysis.

2.5. CO_2 capture and release quantification by FTIR spectroscopy

To quantify the amount of CO_2 captured and released by the different polymers a FTIR Bruker VERTEX 80 FTIR spectrometer with an IR gas cell from Thermofisher were used. Before the experiments an external calibration curve was created by injecting with a Hamilton syringe a specific quantity of pure CO_2 (5% in N_2) into the gas cell and measuring the integrated area of the asymmetric stretching band of CO_2, located at 2350 cm^{-1}. The spectrometer chamber was purged with nitrogen during the measurements to prevent interference from atmospheric CO_2. For the CO_2 capture and release experiments, a three-electrode setup in a one compartment cell was used as depicted in **Figure 11**. Prior measurements, the electrochemical cell was again purged with CO_2 for 30 min. For the quantification, CO_2 was captured electrochemically using three CV cycles. After capturing, the cell was purged for 2h with N_2 to get rid of uncaptured CO_2 in the atmosphere as well as solution and subsequently three CV cycles was again performed resulting in the release of the captured CO_2. After the release and stirring the solution, 2 mL headspace gas sample was taken and analysed in the IR gas cell to generate the corresponding IR spectrum of CO_2.

In addition, electro-swing experiments were conducted using P14AQ, where instead of CV a constant potential capture and for release in a time for each purpose was applied.

2.6. Characterization Methods

Spectroscopic characterization of the obtained polymer-coated electrodes was done using attenuated total reflection Fourier transform infrared spectroscopy (ATR-FTIR) and Raman spectroscopy. ATR-FTIR was performed on a Bruker VERTEX 80-ATR spectrometer in the

spectral range of 4000-400 cm^{-1} averaging 64 scans at a resolution of 4 cm^{-1}. Raman spectroscopy was performed on a Bruker MultiRAM using an excitation wavelength of 1064 nm in the spectral shift range between 3600 and 5 cm^{-1}.

The morphology of the prepared electrodes was analyzed by scanning electron microscopy (SEM). A JEOL JSM-6360LV scanning electron microscope was operated under high vacuum settings and an acceleration voltage of 7.0 kV.

^{1}H-NMR spectra were recorded by dissolving the polymer in $CDCl_3$ on a Bruker® Advance 300 spectrometer at 300 MHz.

To analyse CO as reduction product after electrolysis, gas injection chromatography was employed. Therefore, 2 mL of the headspace were injected into a Thermo Scientific Trace GC Ultra with He as carrier gas to detect CO with a thermal conductivity detector (TCD). As column a Restek molecular sieve packed column was used. The applied temperature ramp for the GC is depicted in **Table 6**.

Table 6. Applied temperature ramp.

| Settings	Temperature / °C
Hold for 2 min	30
10 °C / min	30-130
Hold for 10 min	130

The contact angle of electropolymerized polymers on glassy carbon as well as drop-casted polymer films was measured using an Ossila Angle Goniometer. The measurements were conducted at room temperature using 18 MΩ water, and the contact angle was determined using the integrated Ossila Contact Angle v.3.0.4.0 software enabling fitting to accurately determine the contact angle.

3. Results and Discussion

3.1. Poly-(1-Aminoanthraquinone)

3.1.1. Electropolymerization of 1-AQQ

The electropolymerization of 1-AAQ was performed in 6M H_2SO_4, since only via the complete protonation of the amino group, the monomer is dissolved at a concentration of 5 mM. [68] No polymer growth was observed when lower concentrated H_2SO_4 was chosen as the electrolyte. The electropolymerization was performed by sweeping between 0 and +1.3 V. The upper limit was chosen to induce oxidation of the monomer, while the lower limit was selected to avoid reduction of the quinone group. The CV of the electropolymerization of 1-AQQ on a platinum foil electrode is depicted in **Figure 16**.
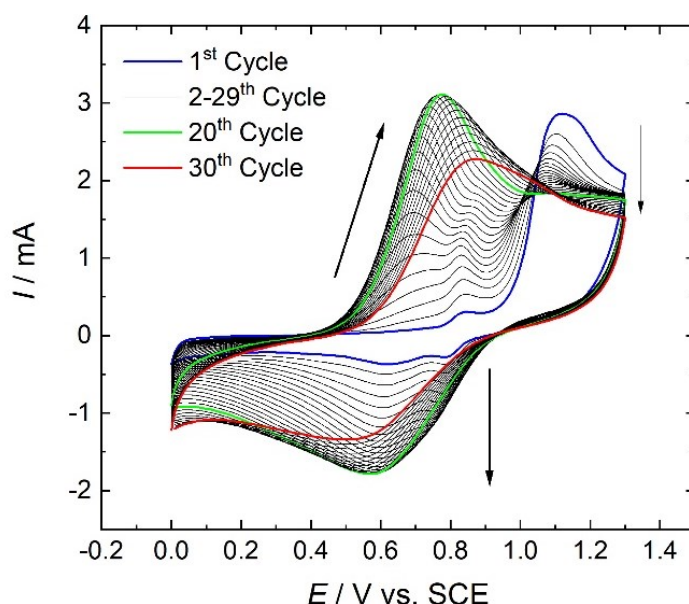
Figure 16. Oxidative polymerization of 5 mM 1-AAQ in 6M H_2SO_4 solution by sweeping between 0.0 V and 1.3 V at a scanrate of 100 mV s^{-1} for 30 cycles on Pt. The first, twentieth and last cycle are highlighted in blue, green and red respectively.

As can be seen in **Figure 16**, the 1-AQQ is irreversibly oxidized at approximately 1.1 V, resulting in a gradual decrease of the anodic peak. This peak can be assigned to the oxidation of the amino side group leading to a radical cation and dication and subsequently to the rapid formation of a polymeric chain. Since no reversible cathodic peak is observed in **Figure 16**, this indicates a subsequent chemical reaction of the electrochemically generated monocation as well as the dication radicals leading to the formation of a polymer film on the corresponding electrode. [68] Furthermore, the increase of the peak current at approximately +0.6 V and +0.75 V is clearly visible with increasing cycle number, which is characteristic for the deposition of electroactive

substance onto the surface of the electrode. However, only an increase until the 20th cycle, highlighted green in **Figure 16**, can be noticed, after that a slight decrease and shift towards more anodic potential is observed of the peaks. Electropolymerization on GC and CP was carried out for electrochemical characterization. Additionally, for enabling IR and Raman measurements, electropolymerization on Cr-Au electrodes were performed. The optical appearance of each electrode can be seen in **Figure 17**.
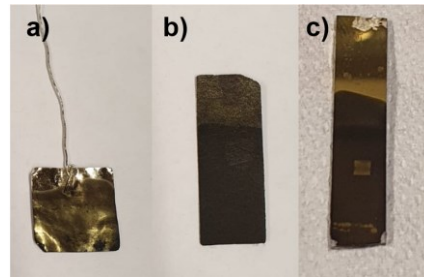
Figure 17. PAAQ film on **a)** Pt foil **b)** CP and **c)** Cr- Au electrodes.

As can be seen in **Figure 17 a**, PAAQ appears on platinum as a greyish golden polymer film, while the polymer film of PAAQ on CP appears nearly in black greyish colour (**Figure 17 b**). Furthermore, the polymerization performed on Cr-Au shows also a brownish-darkish appearance as shown in **Figure 17 c.**

3.1.2. Characterization

In **Figure 18** the IR of the polymer PAAQ is shown in comparison with the monomer AAQ.
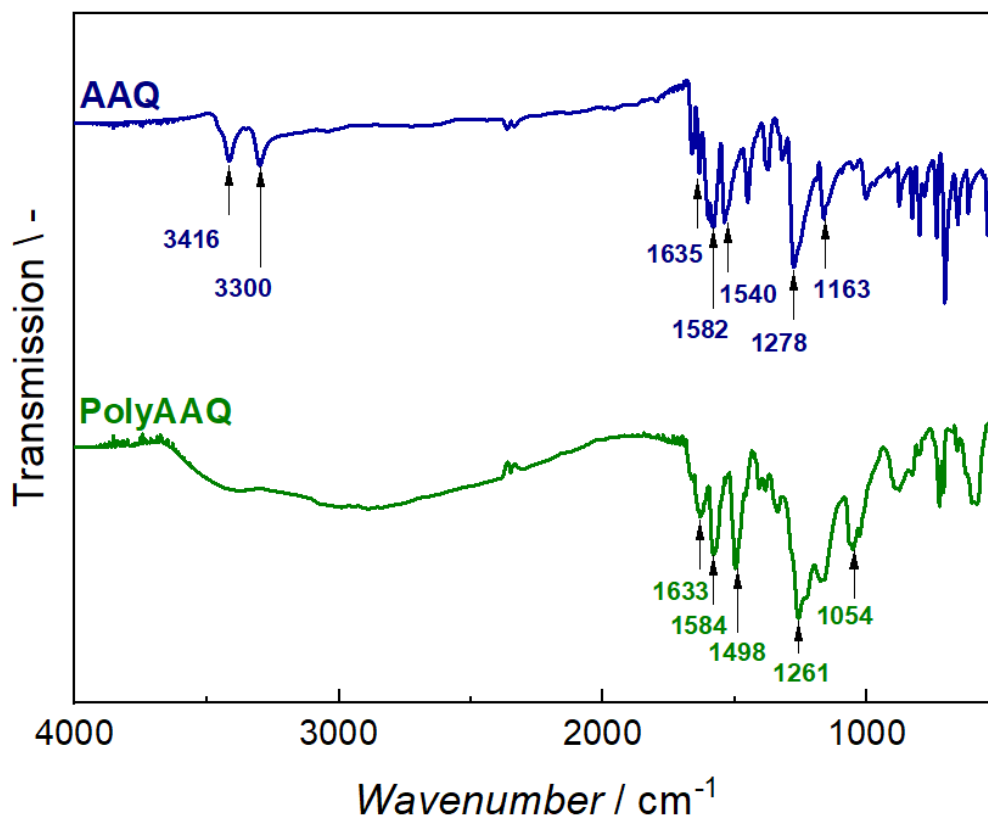
Figure 18. FTIR of the polymer PAAQ and the corresponding monomer AAQ for comparison.

In **Figure 18** can be seen that the monomer shows two peaks at 3416 and 3300 cm^{-1} corresponding to -NH$_2$ group stretching vibration. Comparing the spectrum of the polymer and the monomer, these peaks are disappearing as the -NH$_2$ groups are converted to -NH- groups during the polymerization process resulting in a broad peak as shown in **Figure 18**. In addition, the spectra of the polymer exhibit significantly wider and less distinct peaks compared to those of the monomers, providing additional evidence of a successful polymerization process. Furthermore, a peak can be observed at 1635 cm^{-1} and 1633 cm^{-1} due to C=O stretching vibration of the quinone group, which can be seen in the monomer AAQ as well as in the polymer PAAQ, respectively. The peak assigned to the C=O broadens significantly, as already observed concerning the peak due to -NH- stretching. Furthermore, the peaks at 1584 cm^{-1} and 1498 cm^{-1} in the polymer spectrum can be assigned to stretching of quinoid and benzenoid rings, respectively. The same bands can be observed regarding the monomer at 1582 cm^{-1} and 1540 cm^{-1}. The peak at 1261 cm^{-1} regarding PAAQ and the peak at 1278 cm^{-1} concerning the monomer can be assigned to stretching vibrations of the C-N bond. The FTIR spectrum of PAAQ as well as the monomer AAQ is in accordance to the literature. [59,67,112]

Besides FTIR, Raman spectroscopy was performed as characterization method. The results of the Raman measurements of P15DAAQ and 1,5-DAAQ in comparison are presented in **Figure 19**.
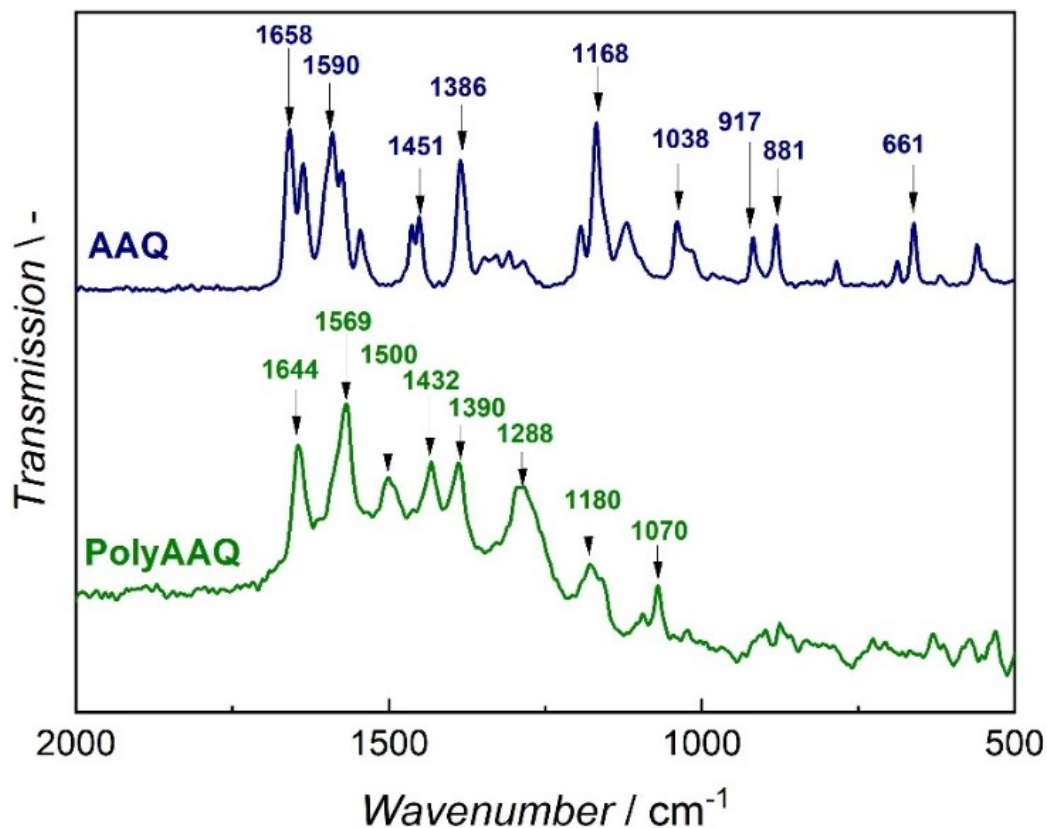
Figure 19. Raman spectroscopy of PAAQ and the corresponding monomer AAQ for comparison.

The vibration peaks at 1644 cm^{-1} regarding PAAQ corresponds to the C=O stretching, which can also be observed for the monomer AAQ with a wavenumber of 1658 cm^{-1}. However, when comparing with the monomer AAQ a bathochromic shift can be observed regarding the C=O vibration of PAAQ due to resonance effects of amines weakening the C=O bond vibration. [113,114] The peak at 1569 cm^{-1} can be assigned to C=C bond stretching vibration, while the peak at 1288 cm^{-1} corresponds to C-N stretching vibrations.

To investigate the morphology of the coated electrodes SEM was performed. In **Figure 20** the SEM images of PAAQ on GC as well as CP in different magnitudes are presented.
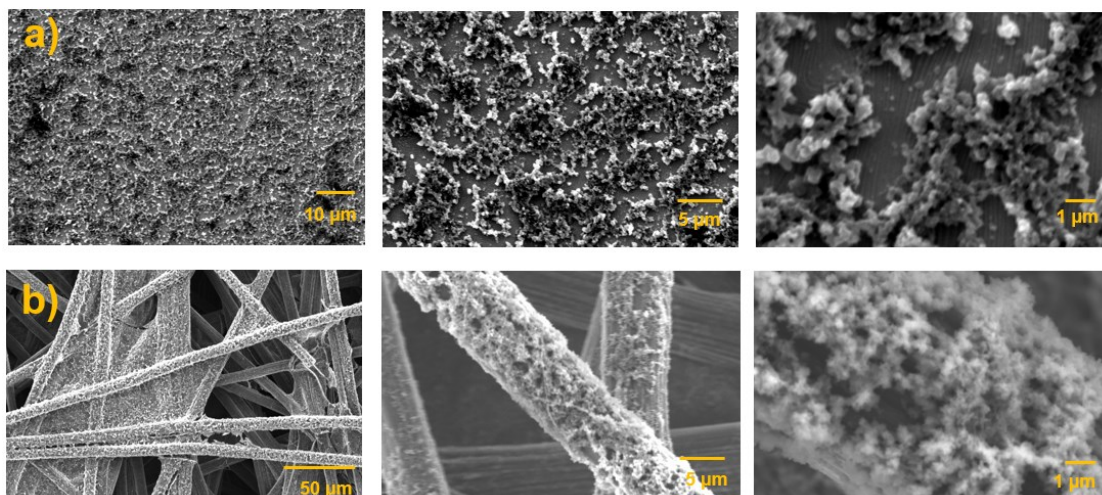
Figure 20. PAAQ on GC **a)** on CP **b)** with increasing magnitudes.

As can be observed in **Figure 20**, PAAQ appears as a sponge-like polymeric film covering the majority of the GC surface. However, comparing PAAQ on CP, better coverage with spongy like structures can be noticed. The structure consists of individual crosslinked fibers, similar to the structure of PANI. [69]

3.1.3. Electrochemical characterization

The capability of PAAQ to capture CO_2 was first examined using polymer-modified GC electrodes and the results are presented in **Figure 21.**
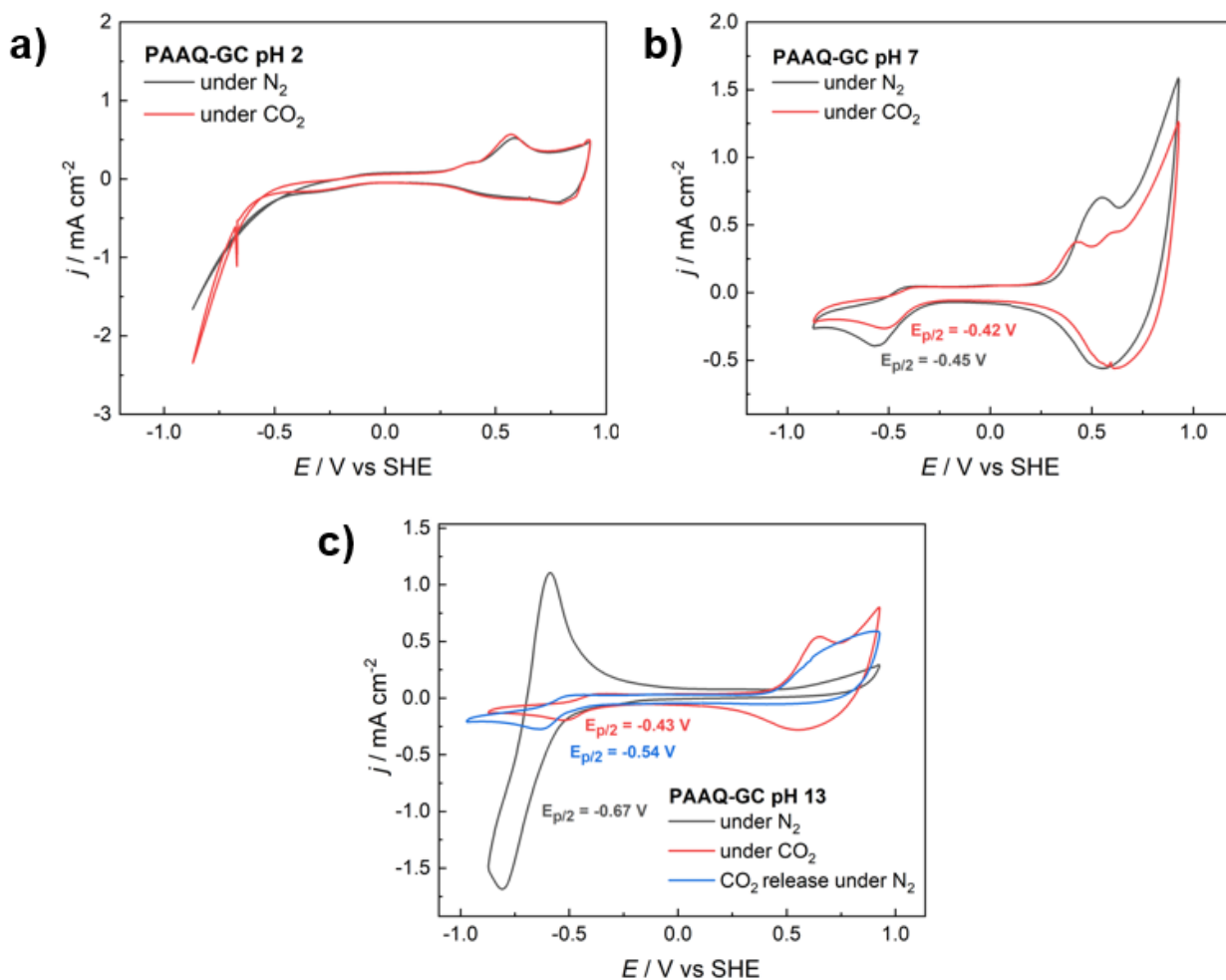
Figure 21. CV of GC coated electrodes with PAAQ in phosphate buffer with pH value of **a)** pH 2 **b)** pH 7 as well as **c)** in 0.1 M NaOH with pH value of 13.

As depicted in **Figure 21 a**, CV measurements conducted in pH 2 reveal that PAAQ shows nearly no current response indicating its limited electrochemical activity under acidic conditions in comparison to other pH levels. Furthermore, at saturated CO_2 conditions no alteration in the CV can be observed indicating no reactivity towards CO_2 at low pH values. However, in pH 7, presented in **Figure 21 b**, the response of PAAQ is more pronounced, displaying a half-potential of -0.45 V. Nevertheless, even in the presence of saturated CO_2 conditions, there is no significant for CO_2 capture.

Notably, at a pH of 13 in **Figure 21 c**, PAAQ demonstrates a distinct peak with the highest current density of 1.75 mA cm^{-2}, characterized by a half-potential of -0.67 V under saturated N_2 conditions. After CO_2 purging, remarkable changes in the cyclic voltammograms can be observed. The current density of the reductive peak shows a significant decline, accompanied by a shift in the half-potential to -0.43 V, alongside the emergence of a reversible oxidative peak at +0.55 V. Upon eliminating the unbound CO_2 through re-purging the system with N_2, a shift towards more cathodic

potentials and the change of the oxidative peak is observable. While these changes and shifts within the CV are suggestive of CO_2 capture, they must be interpreted with caution due to the changes in pH from 13 to approximately 7 resulting from CO_2 purging.

As PAAQ showed promising results in alkaline solution, further experiments with modified CP electrodes were conducted. In addition to measurements in 0.1 M NaOH, CV in phosphate buffer adjusted to pH value 12 in order to avoid fluctuation of the pH value when purging with CO_2. The results of the CV measurements are depicted in **Figure 22**.
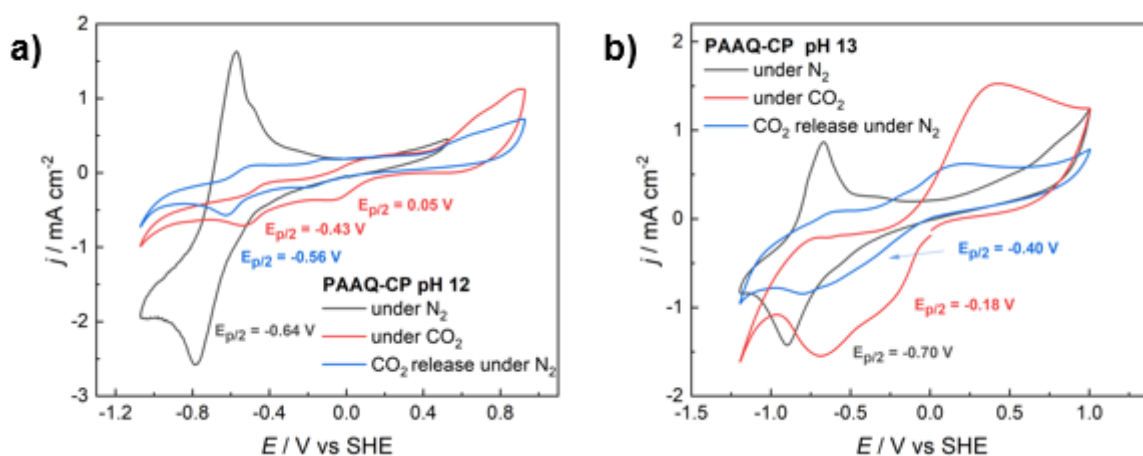

Figure 22. CV of CP coated electrodes with PAAQ in phosphate buffer with pH value of **a)** pH 12 and in **b)** 0.1 M NaOH at pH 13.

As can be seen in **Figure 22** and **Figure 20 c**, consistent half-potential values for PAAQ were obtained across different alkaline solutions, ranging from -0.64 V to -0.70 V operating under saturated N_2 conditions. However, an intriguing observation emerges with respect to measurements performed in pH 12 wherein a larger current density was obtained for the reductive peak characterized by a half-potential of -0.64 V.

Upon closer examination of the pH 13 conditions with PAAQ-CP shown in **Figure 22 b**, quite a difference to the other pH values and electrode material can be observed. Normally, the current declines significantly under CO_2 when CO_2 capture occurs, however in this instance, the current not only exceeds the peak under N_2 but also demonstrates a substantial anodic shift in potential from -0.7 V to -0.18 V. Under saturated N_2 conditions a quasi-reversible reductive peak can be observed, while in the CV under CO_2 the reductive peak and the oxidative peak are highly separated. Upon reversion to N_2 purging, a shift towards more cathodic potential becomes evident, registering a half-potential of -0.40 V. The resulting peaks remains separated and exhibit a lower current density. Although the potential influence of pH fluctuations must not be disregarded, given

the potential drop to approximately pH 7 during CO_2 purging, the magnitude of the observed shift exceeds what can be attributed to pH changes alone.

The CV performed in pH 12 using PAAQ-CP yields similar results akin to those obtained in pH 13 with GC electrodes. However, when subjected to saturated CO_2 conditions a second reductive peak emerges with a half potential of 0.05 V accompanied by an oxidative peak at 0.57 V similar to the results of the CV with GC in pH 13. The current density of this peak decreases upon re-purging with N_2, whereas the current density of the other peak remains nearly unaltered. This observation strongly suggests the release of CO_2.

Additional to measurements in electrolyte with different pH values, the influence of the ionic strength was examined by adding NaCl or an ionic liquid to the 0.1 M NaOH solution. Only EMIM-OTf was investigated since this is the only ionic liquid miscible in this concentration with aqueous solutions. The results in comparison with the CV measured in the pure 0.1 M NaOH are presented in **Figure 23**.
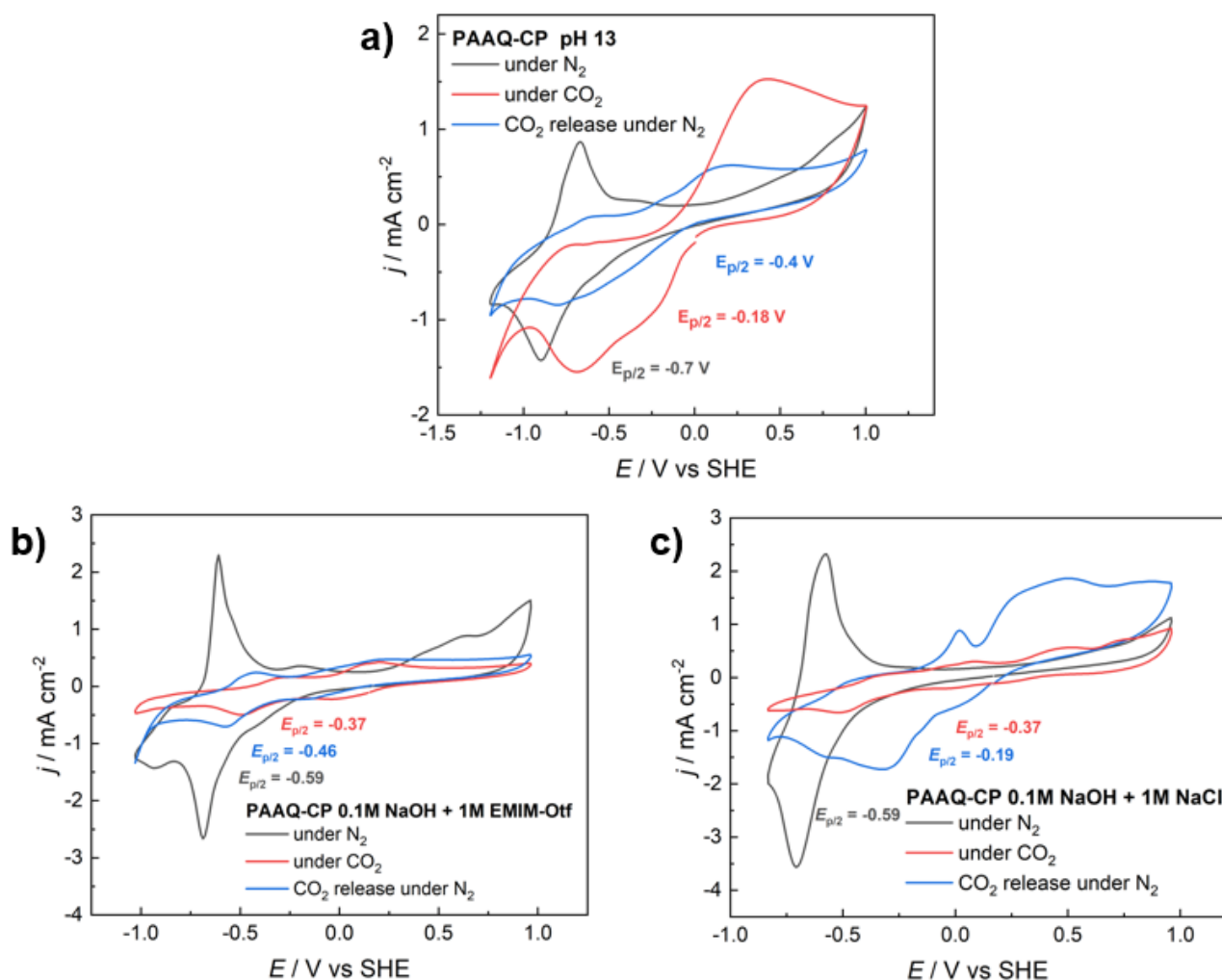
Figure 23. CV measurements of **a)** PAAQ-CP in 0.1 M NaOH as well as addition of **b)** 1 M EMIM-OTf and **c)** 1 M NaCl.

As shown in **Figure 23** both the addition of EMIM-OTf and NaCl resulted in notable enhancements in the current density, whereby the introduction of NaCl improved the response of PAAQ to an even greater extent. Moreover, upon comparing the half-potential of measurements conducted in 0.1 M NaOH with those involving NaCl and EMIM-OTf, a shift towards a more anodic potential becomes evident. However, for both NaCl and EMIM-OTf an identical half potential of -0.59 V under saturated N_2 conditions as well as under saturated CO_2 a half potential of -0.37 V was achieved. However, a notable divergence emerges when examining the CV during the re-purging phase. As the focus of this thesis lies on finding optimum polymers and conditions, mechanistic studies on the origins of these aforementioned differences are subject to further studies.

Besides measurements with the addition of EMIM-OTF to 0.1 M NaOH, experiments in pure ionic liquids were conducted and the results are presented in **Figure 24**.
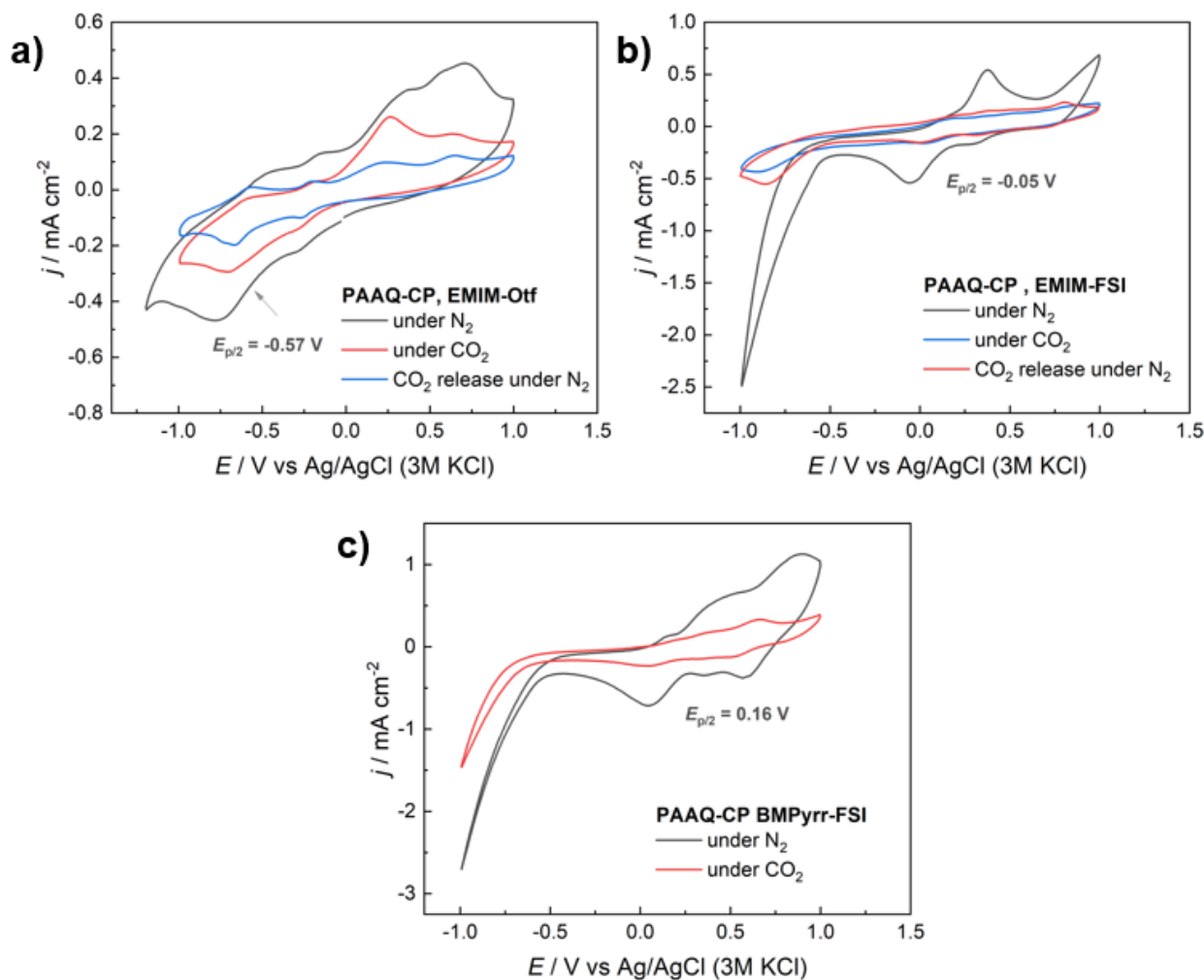
Figure 24. CV measurements of P14AQ on GC disc in pure ionic liquids being **a)** EMIM-OTf **b)** EMIM-FSI as well as **c)** BymPyrr-FSI.

PAAQ on CP, depicted in **Figure 24**, shows electrochemical activity in all ionic liquids, with the most pronounced peaks occurring when using the ionic liquid EMIM-FSI. The half-potential values obtained under N_2 conditions quit vary within the different ionic liquids, ranging from -0.57 V to 0.16 V. However, as depicted in **Figure 24 a**, it becomes evident that the stability of PAAQ is compromised within the ionic liquid as the current density declines significantly over the course of the CV measurements. Furthermore, detachment from the electrode is observed, which can be seen directly by the naked eye.

In the measurements conducted in EMIM-FSI illustrated in **Figure 24 b**, a reduction in current density is evident under saturated CO_2 conditions compared to measurements under N_2. This decline does not exhibit the same rapid progression observed in subsequent CV measurements, as seen with EMIM-OTf. This suggests the potential occurrence of carbon capture, although detachment from the electrode was still observed, it was not as pronounced as in the case of

EMIM-OTf and BMPyrr-FSI. Nevertheless, to investigate whether this decrease in current density results from carbon capture effects or the instability of the polymer in the ionic liquid, further experiments are necessary.

Regarding the measurements conducted in BMPyrr-FSI, as illustrated in **Figure 24 c**, clear detachment of the electrode, visible to the naked eye was observed. Consequently, no additional CV measurements were carried out after exposure to CO_2 conditions.

3.2. Poly-(1,5-Diaminoanthraquinone)

3.2.1. Electropolymerization of 1,5-DAAQ

In analogy to the electropolymerization of 1-AAQ, also a 6 M H_2SO_4 solution was used as an electrolyte solution to ensure the dissolution of 1,5-DAQQ. However, only 2.5 mM of 1,5-DAAQ could be dissolved instead of 5 mM as achieved for 1-AAQ. Compared to the method of electropolymerization of 1-AAQ, the oxidative vertex had to be increased to +1.6 V, otherwise oxidation of the monomer 1,5-DAAQ did not occur. The CV of a representative polymerization of 1,5-DAAQ performed on platinum foil is shown in **Figure 25**.
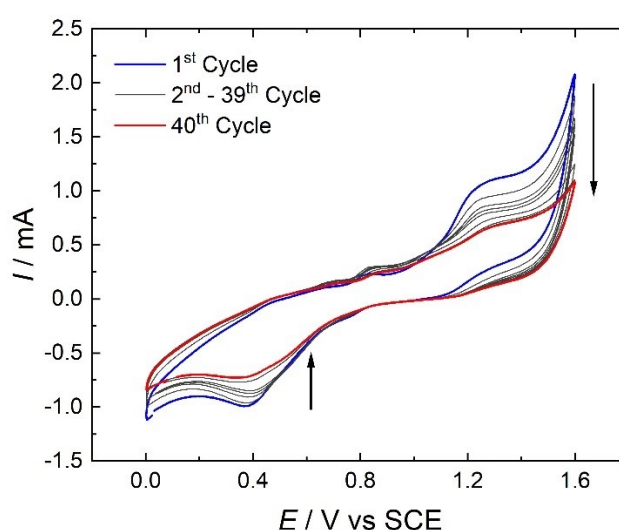
Figure 25. CV of the potentiodynamic oxidative polymerization of 2.5 mM 1,5-DAAQ in 6 M H_2SO_4 in a potential range between 0.0 V and 1.6 V at a scanrate of 50 mV s^{-1} for 40 cycles deposited on Pt.

In **Figure 25** an anodic peak corresponding to the oxidation of to the monomer 1,5-DAAQ can be observed at a potential of approximately +1.4 V, leading to a radical cation and dication and subsequently to the formation of oligomers. Furthermore, it can be seen that the gradual decrease of the peak current with increasing cycles is indicating the polymer growth as the monomer is

oxidized. The electropolymerization of 1,5-DAAQ was also performed on CP, GC and Cr-Au for characterization purposes. The appearance of the different modified electrodes is depicted in **Figure 26**.
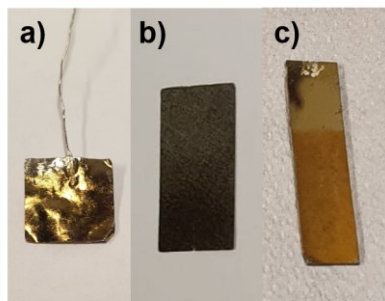
Figure 26. P15DAAQ on **a)** Pt foil **b)** CP and **c)** Cr-Au electrode.

Although no real peak growth is observed in the CV of the electropolymerization in **Figure 25** as compared to the one regarding 1-AAQ, a golden film is clearly visible by the bare eye on the platinum electrode in **Figure 26 a**. On the Cr-Au electrode the P15DAAQ film also appears as a gold yellowish film, while on the carbon paper the polymer appears in dark-greyish colours.

3.2.2. Characterization

To investigate the structure of P15DAAQ, IR spectroscopy was performed and the results of P15DAAQ as well as the monomer DAAQ in comparison are presented in **Figure 27**.
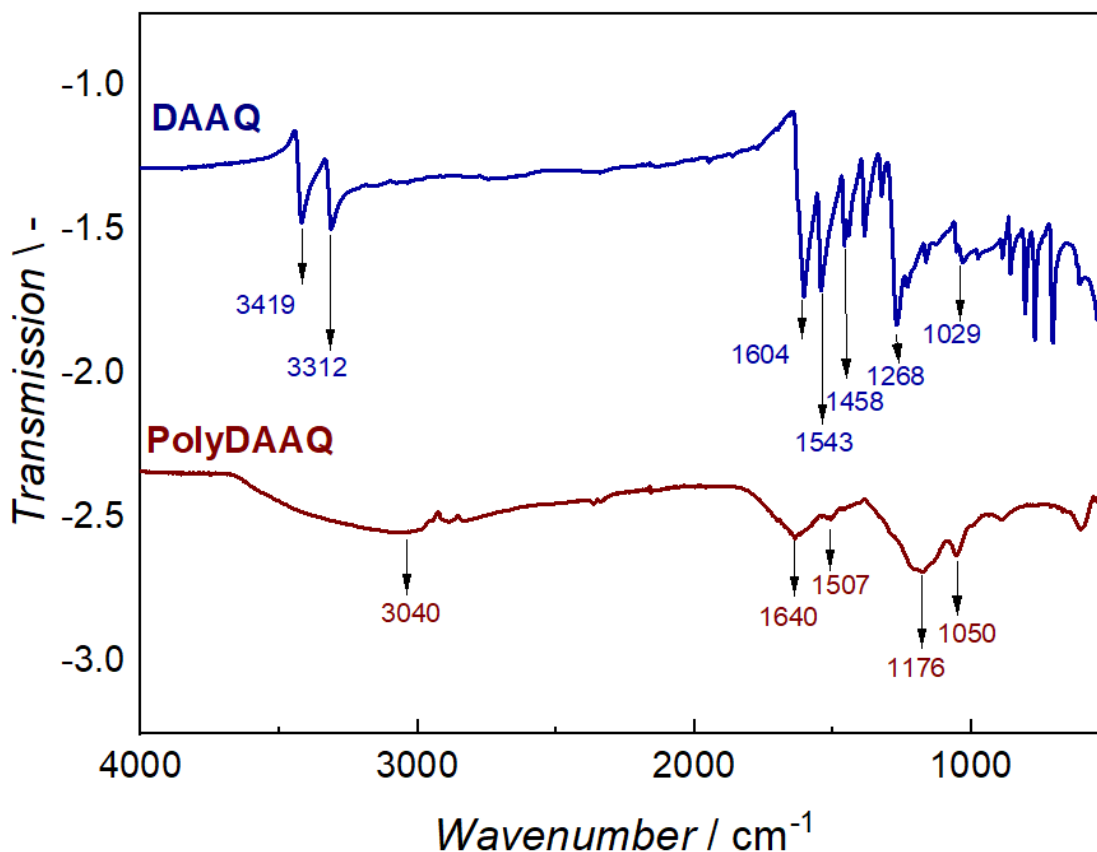
Figure 27. FTIR of the polymer P15DAAQ and the corresponding monomer DAAQ for comparison.

Two bands at 3419 and 3312 cm^{-1} corresponding to -NH$_2$ stretching vibrations of the monomer can be seen in **Figure 27**. These peaks of DAAQ merge into one broad band at approximately 3040 cm^{-1} due to polymerization of P15DAAQ. Bands at 1604 cm^{-1} and 1640 cm^{-1} are corresponding to the C=O stretching vibration of the quinone group for both the monomer and the polymer, respectively. However, a much broader peak is observed for the polymer. In general, the polymer spectra display broader and less well-defined peaks in comparison to the monomer spectra, which serves as further confirmation of a successful polymerization process. The peak observed at 1507 cm^{-1} can be assigned additionally to the quinone group. On the other hand, the absorption band at 1176 cm^{-1} is attributed to the stretching of the C−N bond in aromatic amines. The FTIR spectras are in accordance to examples in literature. [71,112]

To investigate the morphology of DAAQ, SEM measurements were carried out. When DAAQ is polymerised on Pt, a distinct golden film forms, which is easily noticeable without the need for any magnification. Therefore, additional measurements were conducted of Pt coated P15DAAQ plates, where the results can be seen in **Figure 28**.
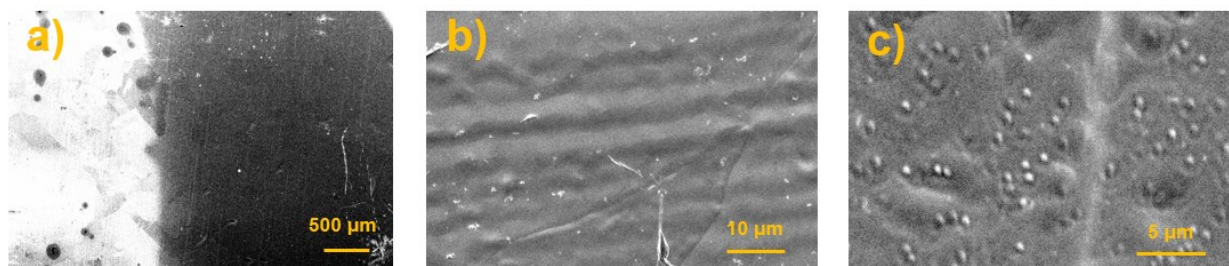
Figure 28. SEM images of P15DAAQ on Pt.

Figure 28 a clearly depicts the interface between pure platinum on the left and its corresponding grain boundaries, while on the right, the platinum surface coated with P15DAAQ can be seen. P15DAAQ appears as a homogeneous film covering the platinum plate fully. Upon further magnification, as shown in **Figure 28 c**, small islands or dots in the polymer are visible.

In addition, SEM of P15DAAQ covered GC and CP as well as blank GC and CP for comparison are presented in **Figure 29**.
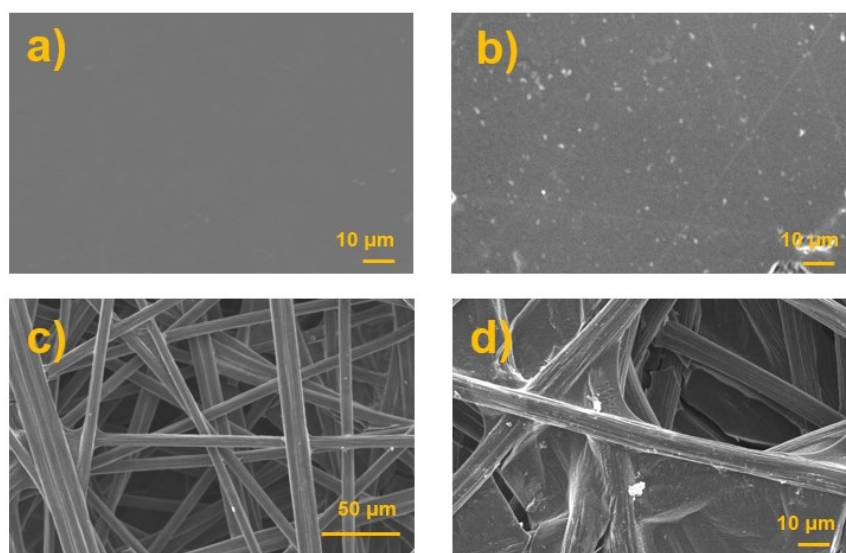
Figure 29. a) Blank GC **b)** GC covered with P15DAAQ **c)** blank CP and **d)** CP covered with P15DAAQ.

In **Figure 29 b)** dots of P15DAAQ are visible on the GC similar to the observation regarding the polymerization of DAAQ on the Pt plate. Comparing **Figure 29** c) to d) only minor differences can be observed, as P15DAAQ is a homogenous and apparently thin film. However, a knob-like structure can be seen.

3.2.3. Electrochemical characterization

CV experiments were performed in phosphate buffers with pH value 2 ,7 as well as in a 0.1 M NaOH solution with a pH value of 13 of coated electrodes with P15DAAQ and the results are presented in **Figure 30**.
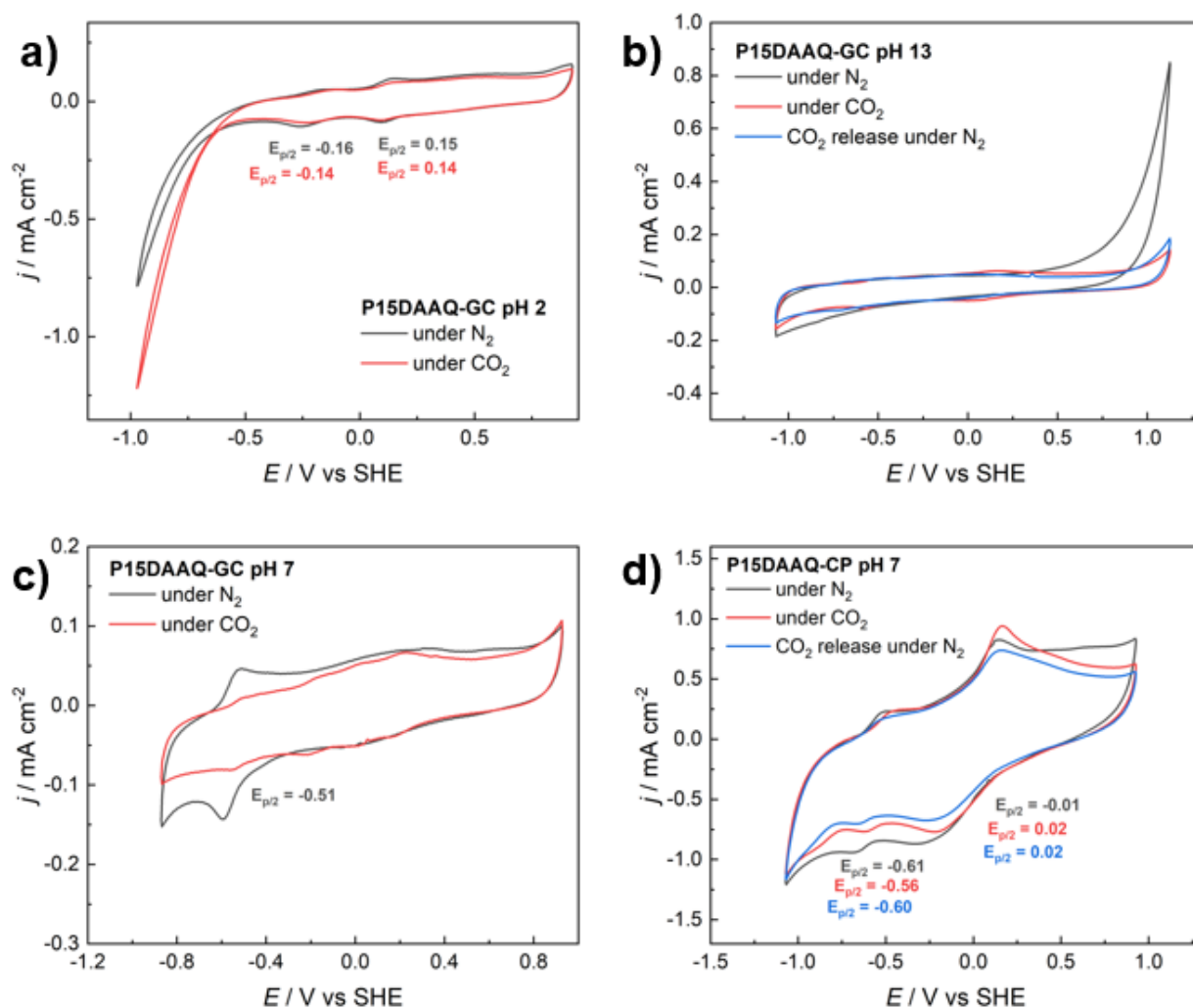
Figure 30. CV of GC coated electrodes with P15DAAQ in phosphate buffer with pH value of **a)** pH 2 **b)** pH 13 **c)** pH 7 as well as **d)** CV of P15DAAQ coated CP electrodes in pH 7.

The capability of P15DAAQ to capture CO_2 was first examined using polymer-modified GC electrodes. As illustrated in **Figure 30 a**, P15DAAQ under N_2 displays two small reversible reductive peaks with a half potential of -0.16 and +0.15. However, when exposed to CO_2 purging, only negligible changes were observed, indicating that there is no tendency for CO_2 capture. Notably, regarding the CV measurement in alkaline solution depicted in **Figure 30 b**, disparities between CV under N_2 and CO_2 can be seen. Nevertheless, these disparities are more likely attributed to pH value changes to a lower pH during CO_2 purging rather than interactions with CO_2.

Furthermore, **Figure 30 c** demonstrates clear discrepancies between N_2 and CO_2 CV results at pH 7. Under N_2, an anodic peak with a half potential of -0.51 is observed. However, similar to polyanthraquinone and the monomer anthraquinone [54], the electrochemical response of this reductive peak of P15DAAQ under CO_2 diminished, resulting in low current density. Consequently,

additional CV experiments were conducted using CP-coated P15DAAQ electrodes, as the electrochemical response of the polymer is typically enhanced and higher currents are obtained with CP as the electrode material, aiming to further investigate its potential for carbon capture in pH 7. However, as illustrated in **Figure 30 d**, only minimal changes in the CV were observed contradicting the results obtained at pH 7 with the GC electrode. To clarify, whether this disappearance of the peak under CO_2 in **Figure 30 c** is attributed to instability of the polymer or inactivation, further investigations are required.

Since no substantial indication of CO_2 capture ability was observed, no further experiments were carried out in other electrolyte media.

3.3. Polyriboflavin

3.3.1. Electropolymerization of riboflavin

The electrochemical polymerization of riboflavin was performed in acidic, basic and neutral conditions, whereby the electropolymerization in acidic medium (0.1 M H_2SO_4) showed the most satisfying results. However, this result is in contradiction to Radzevic *et al.*, where the best polymeric film of polyriboflavin was reported in neutral conditions. [84] Although the synthetic procedure was inspired by previous work by Radzevic *et al*. [84] and Ivanova *et al*. [83] some optimization steps of the electropolymerization were performed. The electropolymerization was only performed on GC and CP, as on Cr-Au the polymerization was not possible due to too high potential for the oxidation of the monomer to enable formation of the polymer. The high potential caused the oxidation of the chromium leading to the detachment of the Au film. The resulting CV of the polymerization of riboflavin on GC can be seen in **Figure 31**. The electropolymerization in neutral and basic conditions are depicted in **Figure 32**.
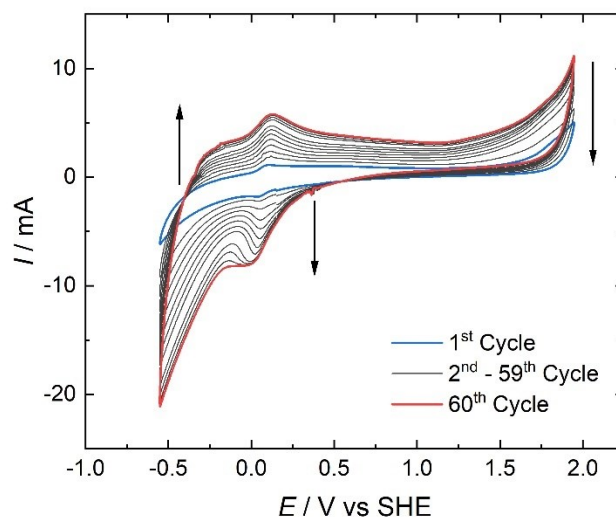
Figure 31. CV of the potentiodynamic oxidative polymerization of 1 mM riboflavin in 0.1 M H_2SO_4 in a potential range between -0.55 V and 1.95 V at a scanrate of 50 mV s^{-1} for 60 cycles deposited on GC. The first and last cycle are highlighted in blue and red respectively.

In 0.1 M H_2SO_4 the riboflavin is fully protonated due to having a pKa of about 10.5 depending on the ionic strength of the solution. [84,115] In **Figure 31**, an anodic peak at 1.9 V can be seen caused by the formation of radicals. The current of the oxidative peak increases with the cycling number.

At 0.13 V and -0.03 V an anodic and cathodic peak can be seen, respectively. The increase of the peak current of these peaks is clearly visible with increasing cycle number, indicating the deposition of polymer onto the surface of the electrode. Furthermore, a current increase at 1.9 V can be observed which was caused by the formation of radicals. [84]

The electropolymerization of riboflavin performed in phosphate buffer adjusted to pH 7 and in a 0.1 M NaOH solution (pH 13) are depicted in **Figure 32**, respectively.
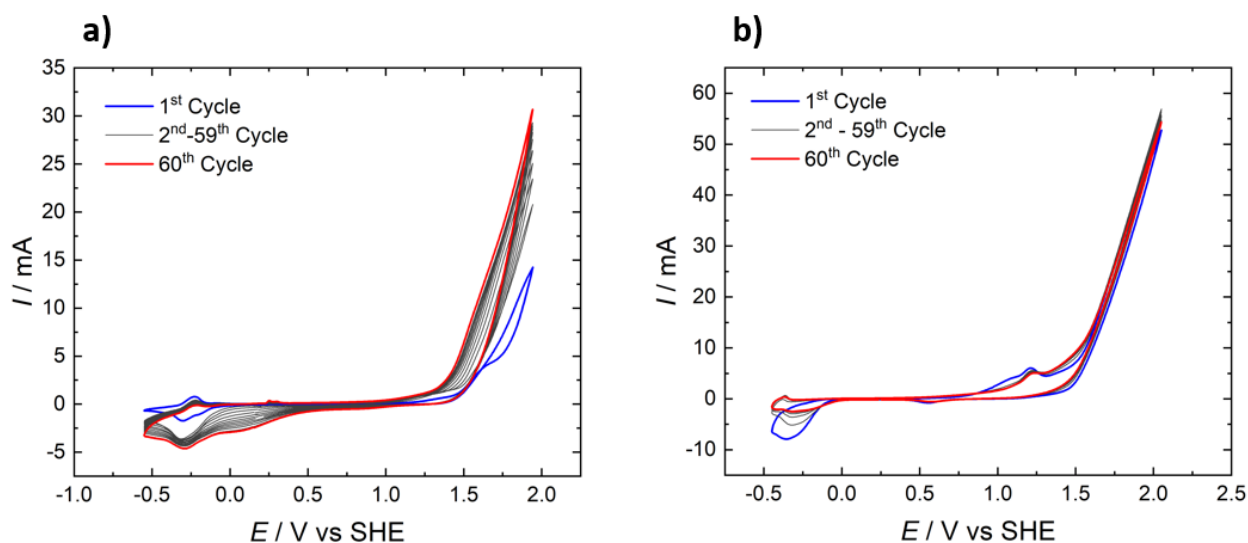
Figure 32. CV of the potentiodynamic oxidative polymerization of 1 mM riboflavin in **a)** 0.1 M phosphate buffer with ph7 and **b)** in 0.1 M NaOH in a potential range between -0.55 V and +1.95 V at a scan rate of 50 mV s^{-1} for 60 cycles deposited on GC. The first and last cycle are highlighted in blue and red respectively.

In **Figure 32 a** an increase of the cathodic peak at -0.3 V can be observed, while for the anodic peak a decrease of -0.2 V can be noticed. Furthermore, an increasing oxidative peak at +1.9 V as already observed for the electropolymerization in acidic conditions can be seen.

As can be seen in **Figure 32 b** no significant current increase indicating the polymer growth can be observed. However, a decrease in current at approximately -0.47 V can be noticed.

In **Figure 33 a** and **b** are the polymeric film of riboflavin on CP and GC depicted, respectively.
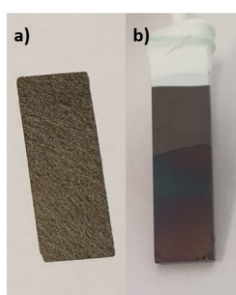
Figure 33. PRF on **a)** CP and **b)** GC polymerized in 0.1 M H_2SO_4.

Polyriboflavin appears on GC as a shimmery film, which can easily be seen by the bare eye. On the contrary, the polymer film of polyriboflavin polymerized on CP is not visible by the bare eye.

3.3.2. Characterization

Unfortunately, as a wide electrochemical range is necessary for the polymerization of PRF, no polymerization occurred on an electrode that was not carbon-based, and consequently, no FTIR or Raman spectra could be measured. Nevertheless, both the visible film formation and the CV results, confirmed successful polymerization which is further discussed in the next chapter. Additionally, SEM images provided further supporting evidence of a successful polymerization and the results can be seen in **Figure 34**.
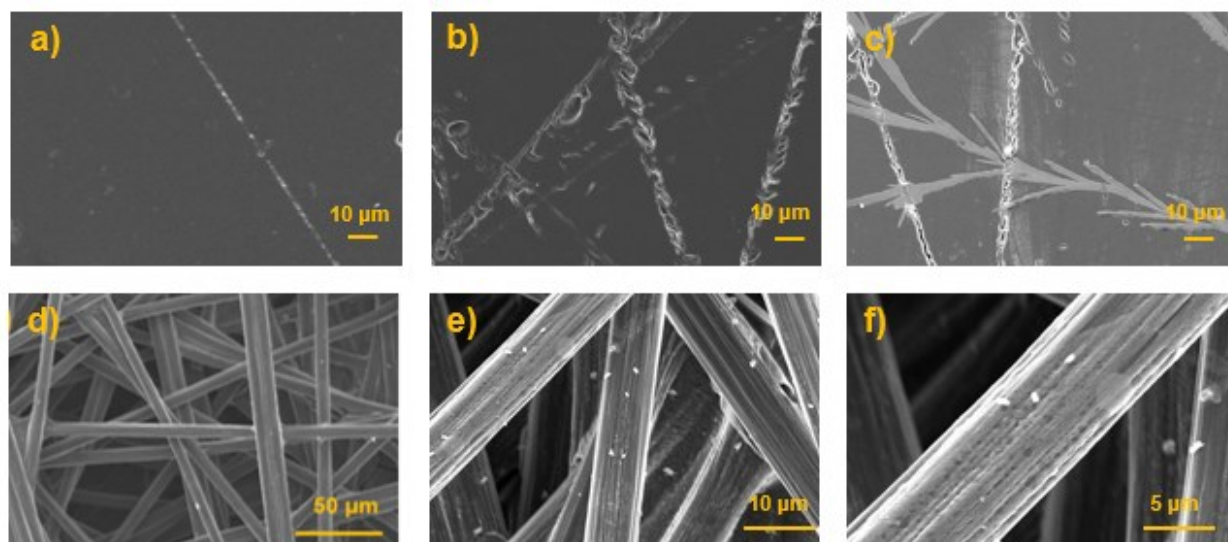
Figure 34. SEM images of **a)** bare GC **b)** PRF on GC **c)** PRF on GC after CV measurements, as well as **d)** bare CP **e)** PRF on CP and **f)** with increased magnitude.

As depicted in the **Figure 34**, while PRF is visible as a reflective thin film on GC when observed with the naked eye, SEM images do not reveal a distinct contrast between bare GC and GC coated with PRF. However, after performing CV measurements, cracks and tendrils become apparent on the PRF thin film, making it distinguishable from the electrode, as illustrated in **Figure 34 c**. In contrast, on CP electrodes, as illustrated in **Figure 34 e,f**, PRF shows the appearance of a knob-like film.

3.3.3. Electrochemical characterization

The capability of PRF to capture CO_2 was first examined using polymer-modified GC electrodes in phosphate buffer with pH value of 7 as well as in 0.1 M NaOH with pH 13 and the results are presented in **Figure 35**.
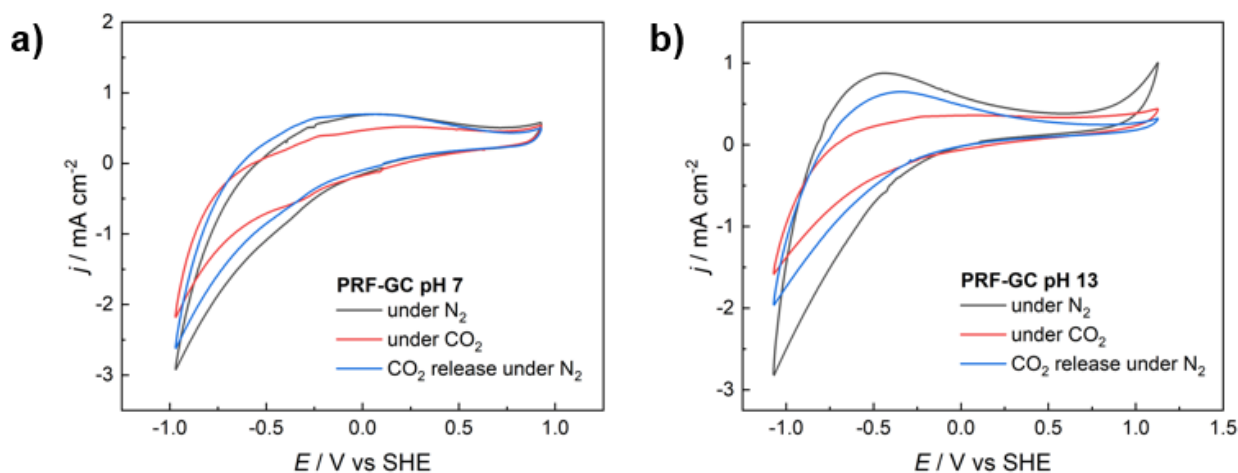
Figure 35. CV of modified GC with PRF performed in phsopahte buffer with pH value **a)** 7 as well as **b)** in 0.1 M NaOH with pH value of 13.

As depicted in **Figure 35** when using the GC electrode material, the response of PRF is rather subtle, particularly evident in measurements conducted at pH 7. However, concerning the results for pH 13, a decrease in current during CO_2 exposure, followed by a subsequent increase upon re-purging with N_2, suggests CO_2 capture and release.

Even though the PRF response on the electrode material GC remains relatively minor, potential indications of CO_2 capture can be observed by a decreased current response under CO_2 which was again rising after N_2 re-purge. To further explore this, measurements were also performed using CP electrodes, and their results are presented in **Figure 36**.
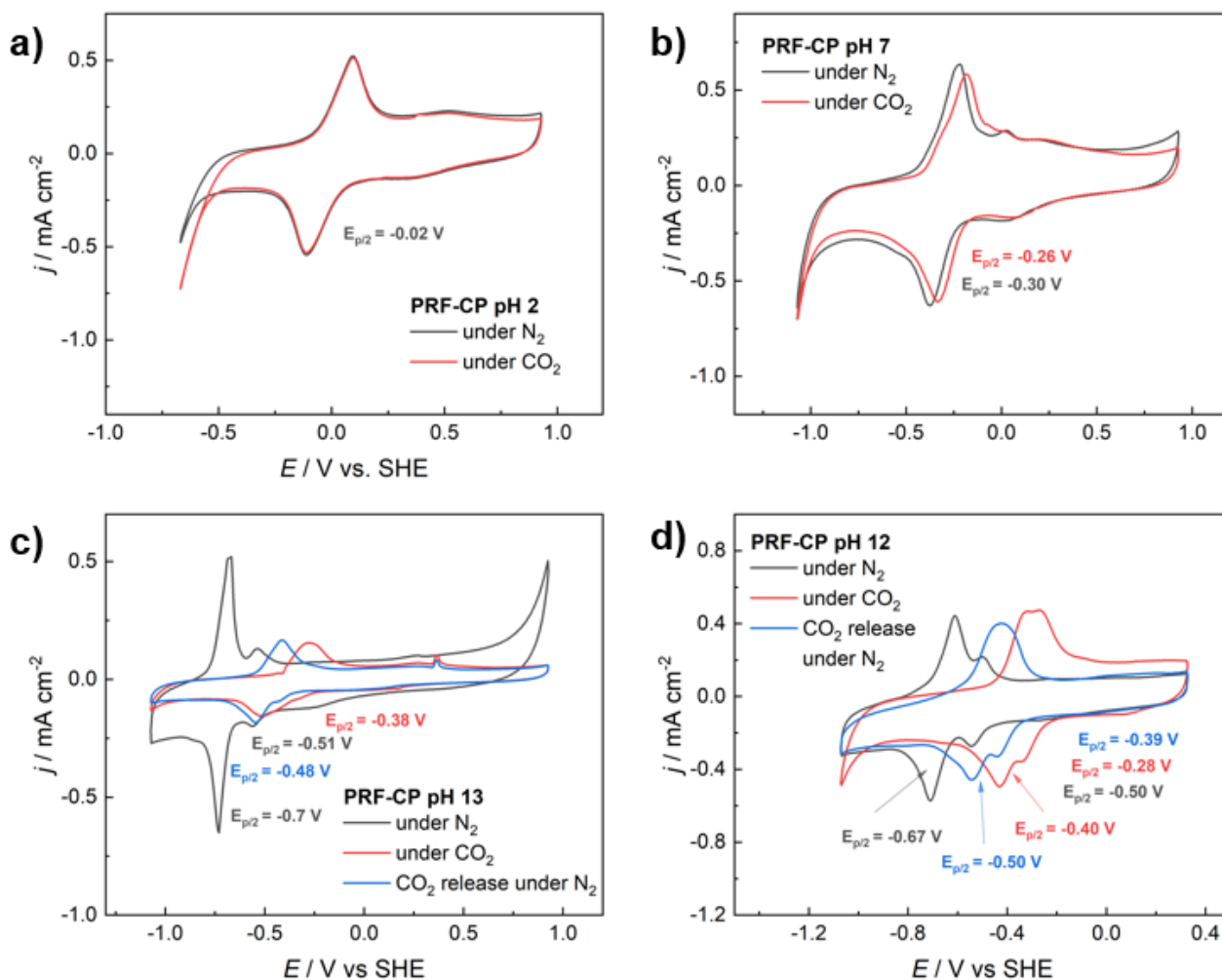
Figure 36. CV of CP coated electrodes with PRF in phosphate buffer with pH value of **a)** pH 2 **b)** pH 7 **d)** pH 12 as well as in **c)** 0.1 M NaOH with pH value of 13.

The electroactivity of PRF is significantly more pronounced when utilizing CP as opposed to GC electrodes. This is particularly evident in the presence of distinct quasi-reversible peaks observed under saturated N_2 conditions at various pH levels. The shape of the CV is in accordance with literature. In **Figure 36 a** the measurement conducted in pH 2 is displayed, where no changes in the CV under saturated CO_2 conditions can be observed. Similarly, **Figure 36 b** representing measurements at pH 7, reveals a comparable behaviour, although with a slight observable shift likely attributable to minor pH fluctuations resulting from CO_2 purging.

When examining **Figure 36 c,** which presents measurements conducted at pH 13, distinct changes in the CV become evident. A noticeable shift occurs, accompanied by a significant reduction in current density under saturated CO_2 conditions. The shift in potential is most likely due to the strong shift in pH upon CO2 saturation, as also previously mentioned for **Figure 21**.

Furthermore, under N_2 saturated conditions the peak respond is very sharp and pronounced with a half potential of -0.7 V and a second small peak can be seen in contrast to the observations at lower pH values. This secondary peak with a half potential of -0.51 V disappears however under saturated CO_2 conditions. Furthermore, the peak separation is more pronounced during CO_2 exposure compared to when re-purging with N_2.

Regarding to measurements performed in pH 12 displayed in **Figure 36 d,** the CV results under saturated N_2 conditions closely resemble those obtained at pH 13. However, upon purging with CO_2 notable differences become apparent. In the case of pH 12, there is no significant reduction in current density, but a substantial shift towards more anodic potential is observed. Moreover, unlike the situation at pH 13, the secondary peak persists upon exposure to CO_2.
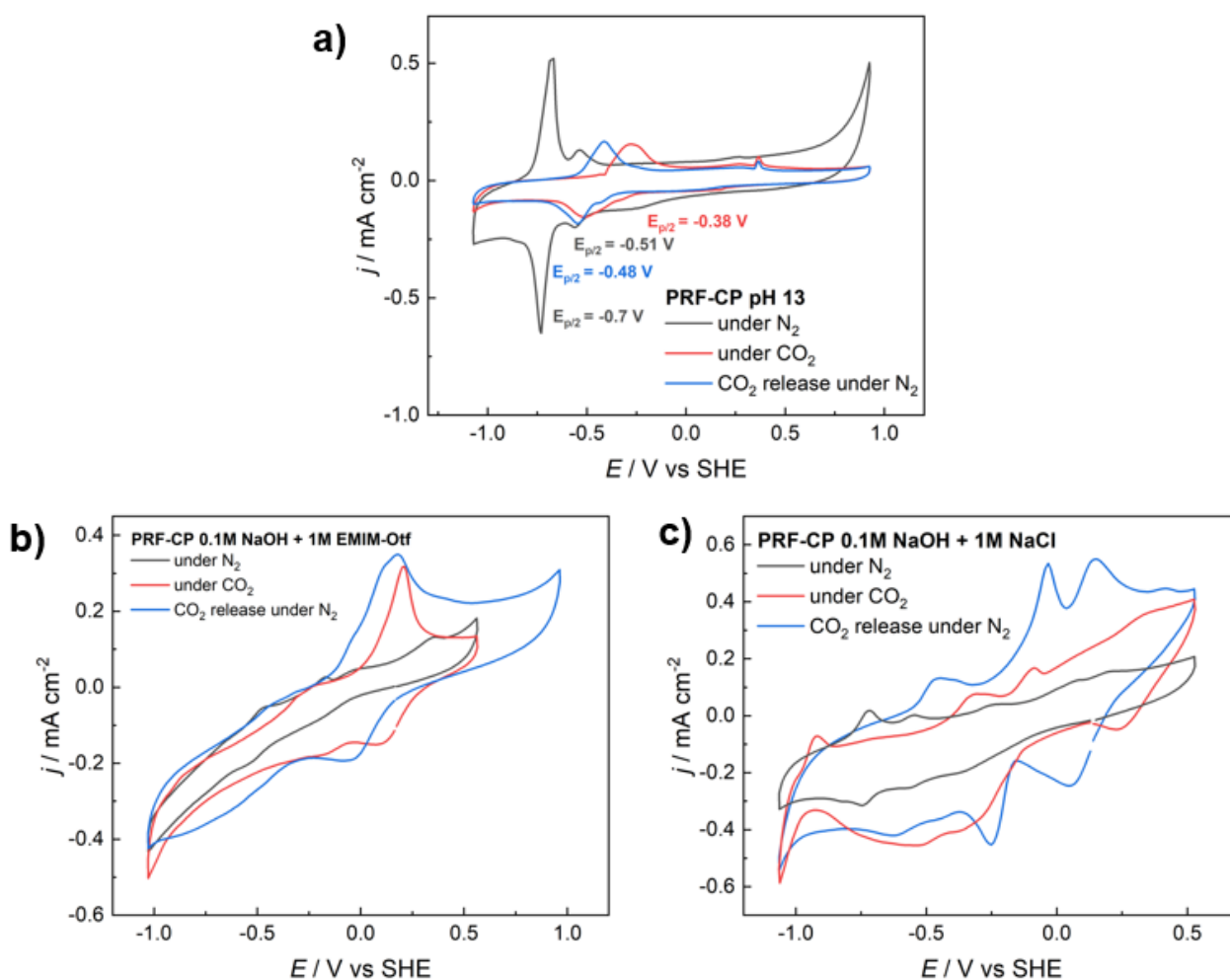
Figure 37. Observation on influence of increase in ionic strength **a)** 0.1 M NaOH without addition of **b)** 1 M EMIM-Otf and **c)** addition of 1 M NaCl.

As observed in **Figure 37**, there is no increase in current density with higher ionic strength, contrary to the typical expectation where higher ionic strength often leads to enhanced electroactivity. Furthermore, a titled CV shape and undefined peak emerges, resulting in the conclusion that the addition of EMIM-Otf or NaCl is not improving the electroactivity of PRF. This might be seen as a hint, that in PRF different redox mechanisms might be present compared to anthraquinone-based polymers, where the justification of this would require further studies.

Additionally, CV measurements in pure ionic liquids were performed and the results are presented in **Figure 38**.
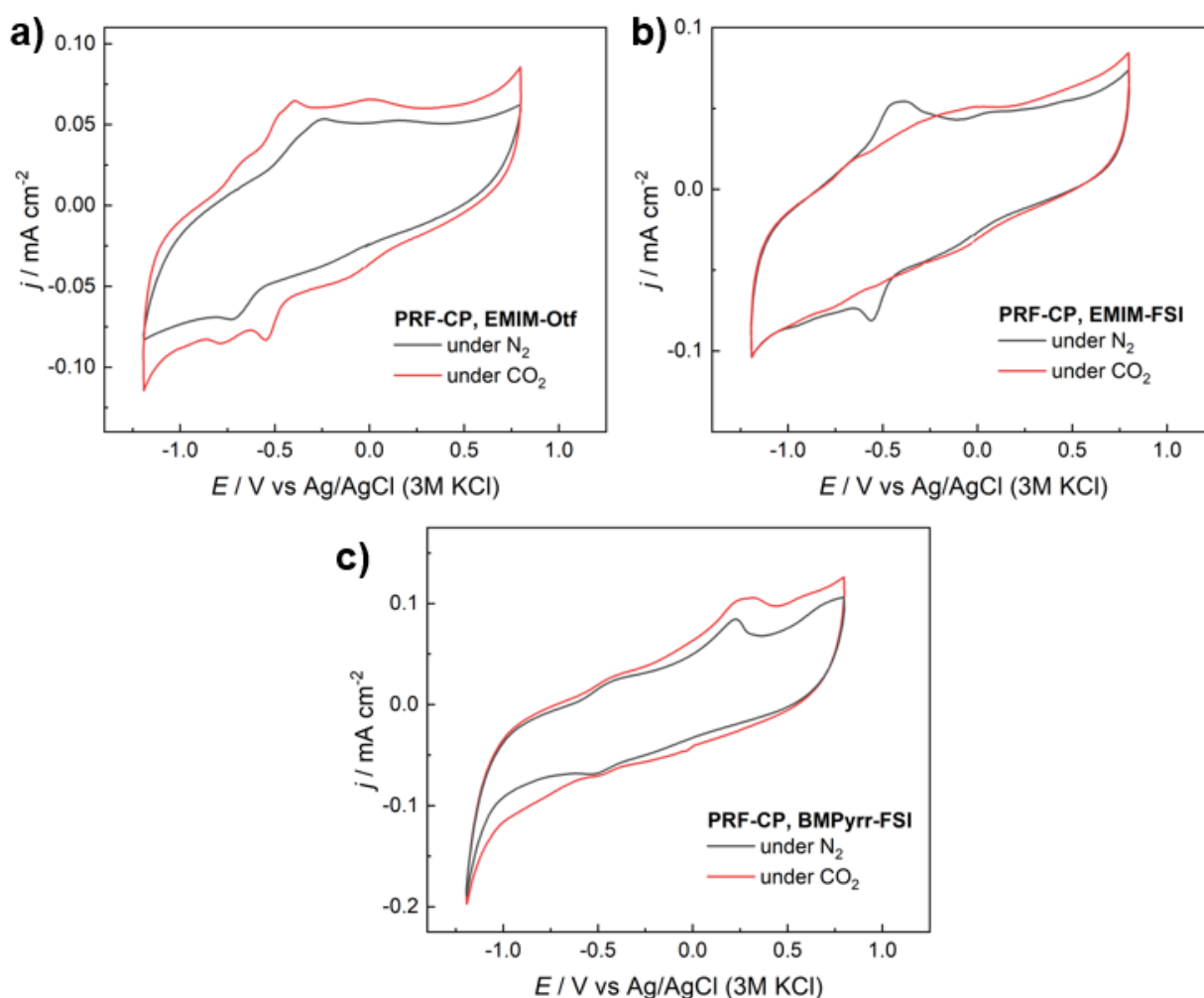
Figure 38. CV measurements of P14AQ on GC disc in pure ionic liquids being **a)** EMIM-OTf **b)** EMIM-FSI as well as **c)** BymPyrr-FSI.

Similar to the results observed for 1 M EMIM-OTF in a 0.1 M NaOH solution, the pure ionic liquids did not enhance the electrochemical response of PRF-CP as can be seen in **Figure 38**. In general,

the peaks are only minimally observable, and there are no significant changes in the CV under saturated CO_2 conditions expect smaller or diminishing peak response.

3.4. Polyallylamine-anthraquinone (PAA-AQ)

PAA-AQ consist of a hydrophilic backbone due to amine group with partially substituted anthraquinone units as presented in **Figure 39**.
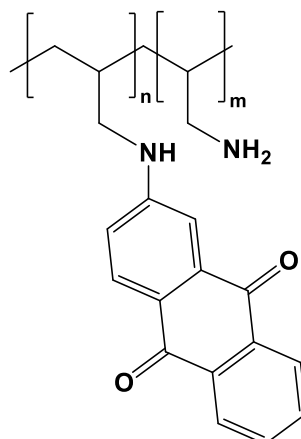
Figure 39. Structure of PAA-AQ.

The synthesis of PAA-AQ through the nucleophilic substitution was performed similiar to Oka *et al.* [65], with small changes in the procedure. The polymer should be dissolved in methanol for work up according to the literature and again be precipitated in diethyl ether, however the product was not soluble in methanol. Therefore, acetone was used for washing to remove unreacted monomer, while the polymer was not dissolved. Furthermore, no NMR in solution could be performed as the polymer was not soluble in DMSO either, although reported in literature. Therefore, only FTIR and SEM were performed as characterization method. Probably, a higher substitution degree was achieved in this work, which decreased the hydrophilicity of the polymer and therefore affecting the solubility. In addition, a polyallylamine with a higher molecular mass was used than in the literature which also contribute to the decreased solubility.

3.4.1. Characterization of the Polymer

To study the structure of PAA-AQ, FTIR measurements of the polymer was performed and the results are depicted in **Figure 40**.
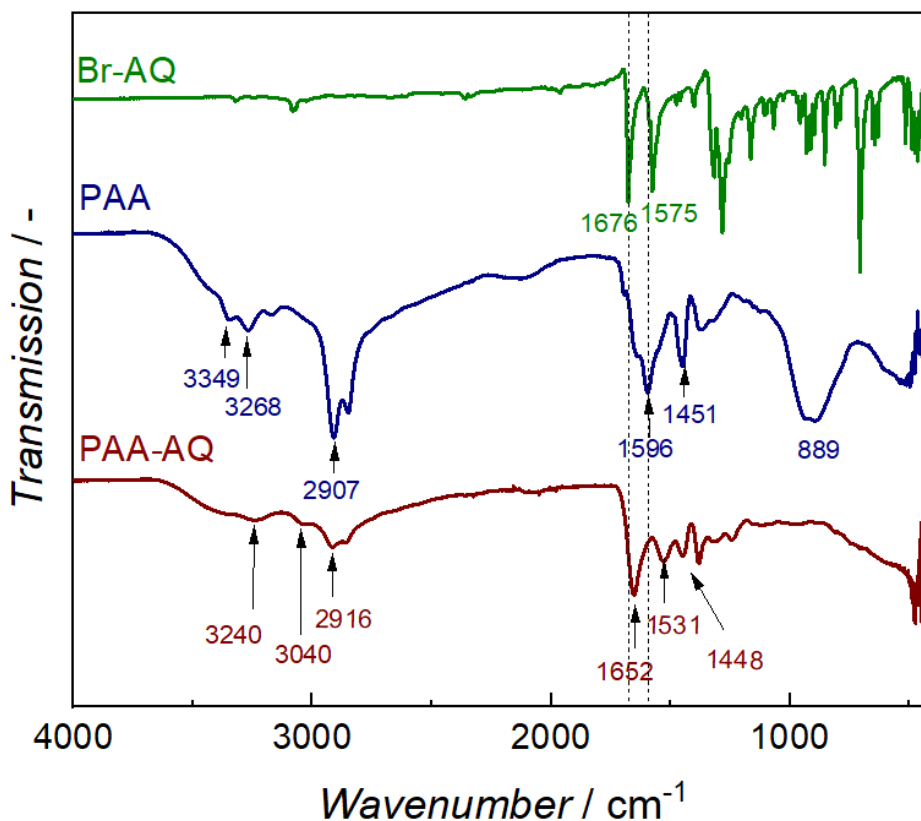
Figure 40. FTIR of 2-bromoanthraquinone, polyallyamine and PAA-AQ in comparison.

In **Figure 40** the FTIR spectra of PAA-AQ in comparison with 2-bromoanthraquinone (Br-AQ) and polyallylamine (PAA) is shown, which are in accordance to literature. [65] In the spectra of PAA the stretching vibrations of the N-H bound can be observed at bands of 3349 cm^{-1} and 3268 cm^{-1}. Regarding PAA-AQ, the band assigned to N-H vibration can be seen at 3240 cm^{-1} in the PAA-AQ spectrum, however compared to PAA the peak is broader and less defined. Furthermore, when comparing the spectra of PAA and PAA-AQ an additional peak at 1652 cm^{-1} is visible corresponding to the carbonyl group of anthraquinone, confirming the successful substitution of anthraquinone into the polymer PAA. However, when comparing the monomer Br-AQ and the polymer PAA-AQ a slight shift of the carbonyl group peaks can be seen. Furthermore, aliphatic C-H stretching vibrations band at 2907 and 2916 cm^{-1} can be observed in PAA as well as in the polymer PAA-AQ, respectively. Additionally, bands at 1596 cm^{-1} and 1531 cm^{-1} attributed to N-H stretching band due amine deformation in PAA as well as PAA-AQ can be observed respectively. Furthermore, the peak at 1448 cm^{-1} can be assigned to stretching vibrations of the C-N bond. Regarding PAA, a broad peak at 889 cm^{-1} can be noticed, which fully disappears in the spectrum of PAA-AQ. [65]

To investigate the morphology and structure of the polymer, SEM measurements were performed of the PAA-AQ drop casted onto to a GC disc presented in **Figure 41**.
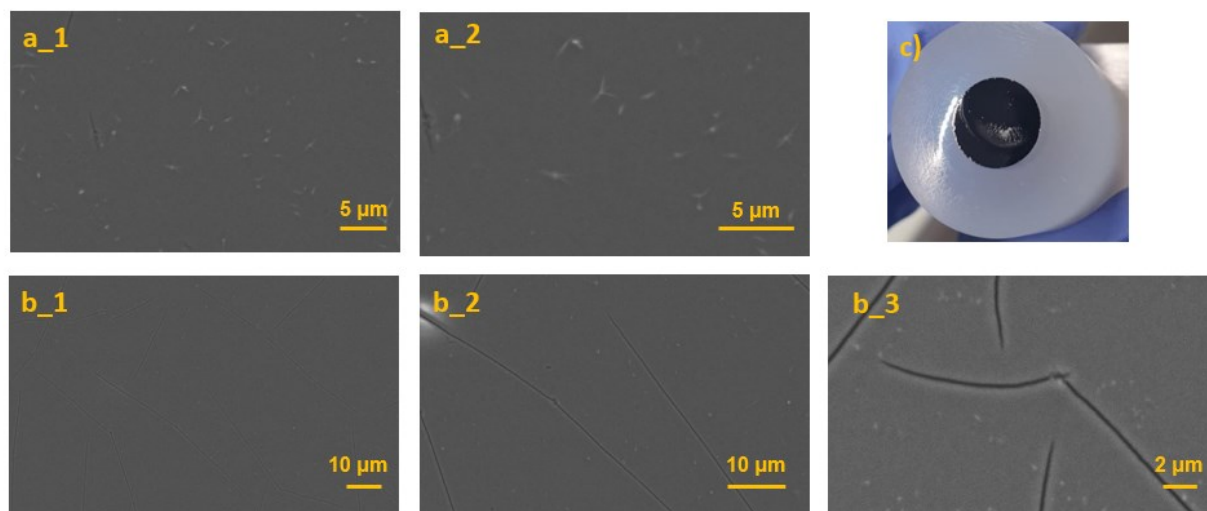
Figure 41. SEM images of different areas **a)** and **b)** of PAA-AQ drop casted onto glassy carbon disc with increasing magnification as well as **c)** an image of the GC disc with PAA-AQ sample used.

Figure 41 depicts two different areas of the measured GC disc with PAA-AQ. In **Figure 41 a** homogeneous thin film with needle-like small island structures is observed. These needle-like structures are likely attributed to the presence of substituted anthraquinone units in PAA-AQ, as the structure bears similarity to evaporated anthraquinone thin films reported in the literature. [54] Additionally, **Figure 41 c** indicates that PAA-AQ can be visually identified as a transparent and uniform thin film. In the SEM images illustrated in **Figure 41 b**, cracks can be observed, which are likely a result of the drying process during drop-casting of the polymer onto the electrode.

3.4.2. Electrochemical characterization

CV were performed in phosphate buffers with pH value of 2,7 and 12, of which the results are presented in **Figure 42**.
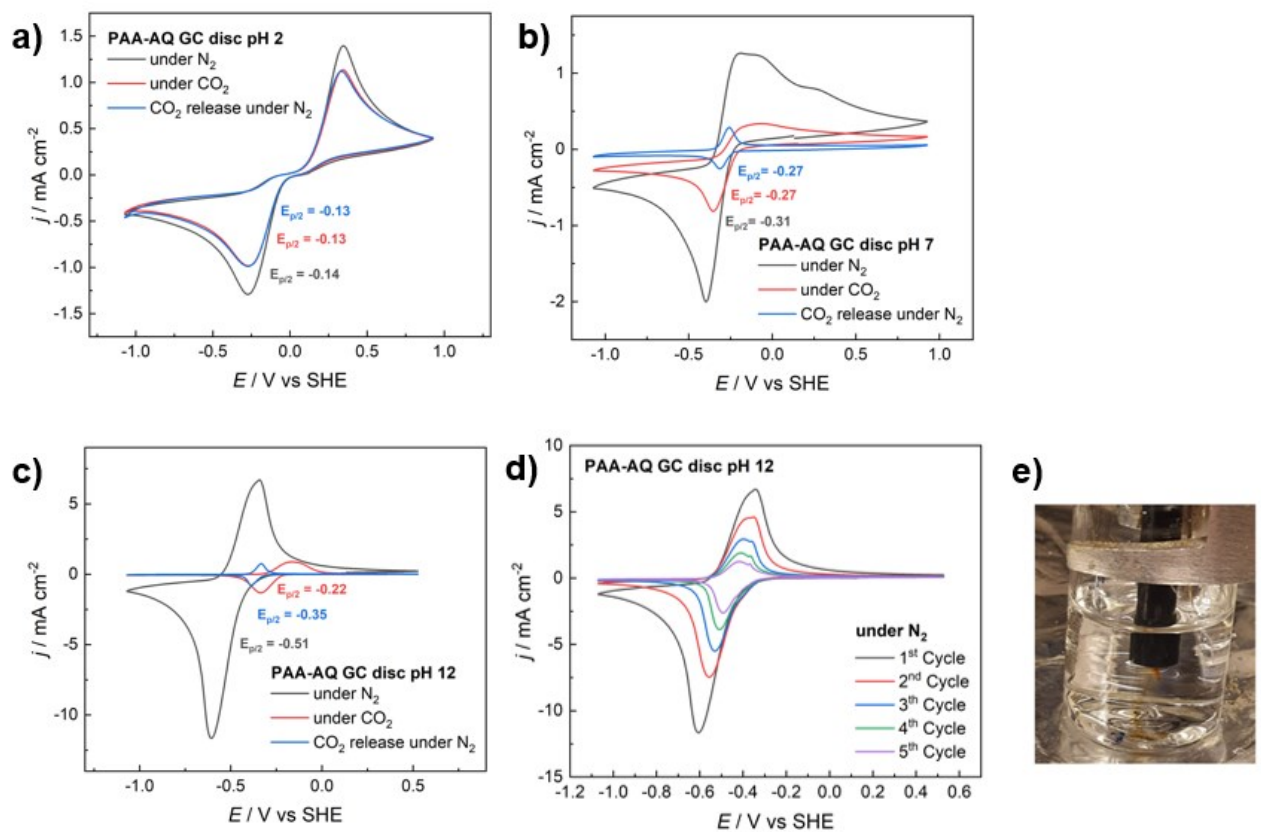
Figure 42. CV von PAA-AQ on GC disc under N_2 and CO_2 in a phosphate buffer with pH value of **a)** 2 **b)** 7 **c)** 12 at scanrate of 50 mV s^{-1}. **d)** 5 cycles of PAA- AQ in pH 12 and **e)** dissolution of PAA-AQ in pH 12.

Under acidic conditions, depicted in **Figure 42 a**, the polymer exhibits distinct and quasi-reversible peaks, with a half potential of -0.14 regarding the reductive peak under N_2. The polymer demonstrates remarkable stability in acidic environments, as evidenced by the absence of any decrease in current density over the course of five CV cycles, which is also in accordance to the literature. [65] However, as the pH value is increased to neutral or alkaline conditions, the stability of the polymer significantly decreases, as clearly shown in **Figure 42 b** and **Figure 42 c**, respectively. Half potentials under N_2 of -0.31 and -0.51 were obtained for pH 7 and pH 12, respectively. The instability of the polymer in alkaline solutions is particularly evident in **Figure 42 d**, where a rapid decrease in current is observed within five cycles under N_2. Notably, even though the polymer is unstable at pH 12, it exhibits the highest current density of approximately 12 mA cm^{-1}. However, visible dissolution of the polymer into the electrolyte solution, as illustrated in **Figure 42 e,** is observed. Furthermore, a slight shift in the half potential can be observed at pH 12 being a potential sign for capturing CO_2, however it is more likely to be attributed to changes in the pH value when purging the solution with CO_2. Unfortunately, no indication of carbon capture behaviour is observed, despite the great stability of the polymer in acidic conditions.

In general, due to the lack of signs for the ability of carbon capture and the instability of the polymer in neutral and alkaline solutions, no further cyclic voltammetry experiments were conducted in other electrolyte media.

3.5. Poly(diallyldimethyl flavin mono nucleotid) PDDA-FMN

PDDA-FMN is an ionic polymer consisting of poly(diallydimethyl) and flavin mono nucleotide (FMN), which appears as yellow-brownish flaky powder as presented in **Figure 43**.
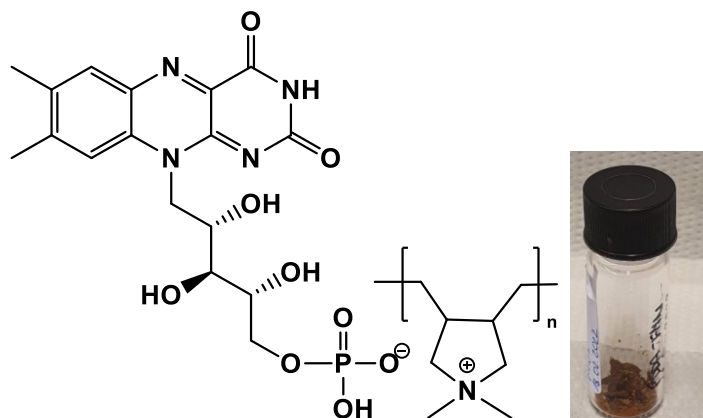
Figure 43. Structure of PDDA-FMN.

3.5.1. Characterization

For characterization FTIR spectroscopy was performed and the results in comparison with the monomer FMN and educt PDAMAC are presented in **Figure 44**.
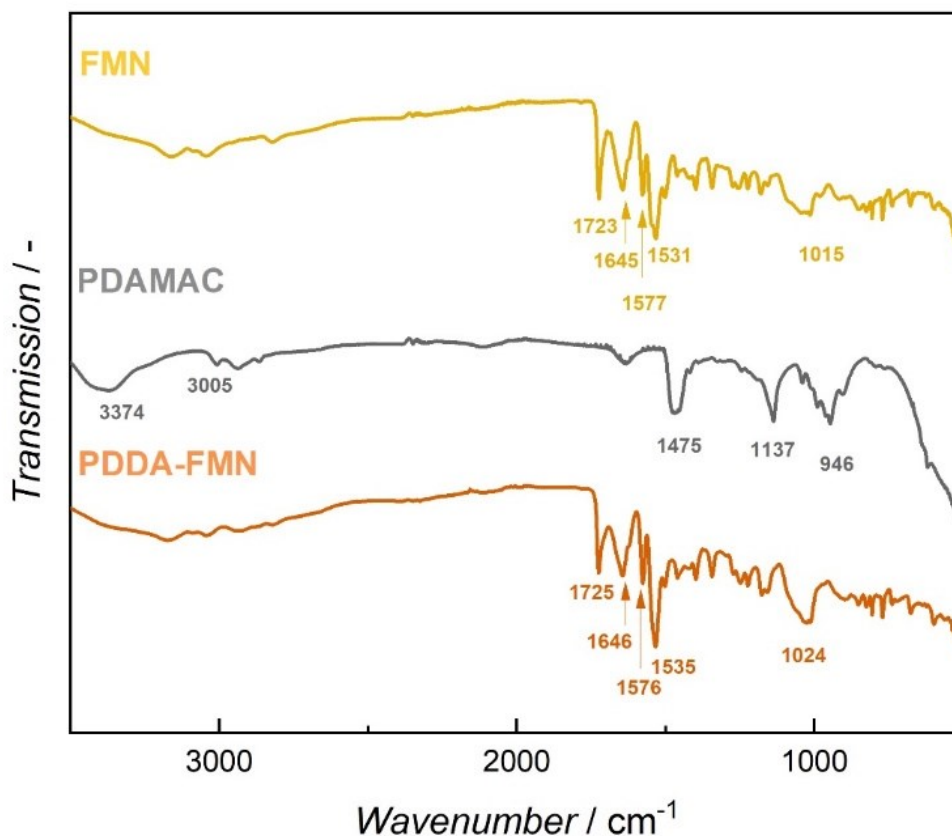
Figure 44. FTIR of PDDA-FMN as well as of the monomers FMN and PDAMAC for comparison.

In FTIR spectra of the monomer FMN, two prominent bands at 1723 cm^{-1} and 1645 cm^{-1} are assigned to the C=O bonds present in the flavin structure. Bands detected at 1577 cm^{-1} and 1531 cm^{-1} correspond to CN and CC stretches and bends within the isoalloxazine ring of FMN. Additionally, a broad band observed at 1015 cm^{-1} can be attributed to the asymmetric phosphate vibrations. [116]

Regarding PDAMAC, characteristic bands of the pyrrolidinium backbone at 1474 cm^{-1} due to the CH_3 bending vibration and 3050 cm^{-1} from the CH_2 stretching vibrations of the pendant methyl units can be observed. Furthermore, the band at 946 cm^{-1} can be assigned to CH_2 bonded to the quaternary ammonium group. [117]

The FTIR spectra of PDAA-FMN is composed of the spectra of the educts FMN and PDAMAC, especially the characteristics-sharp bands of FMN are visible.

To investigate the morphology of PDDA-FMN, SEM images were recorded and the results are presented in **Figure 45**.
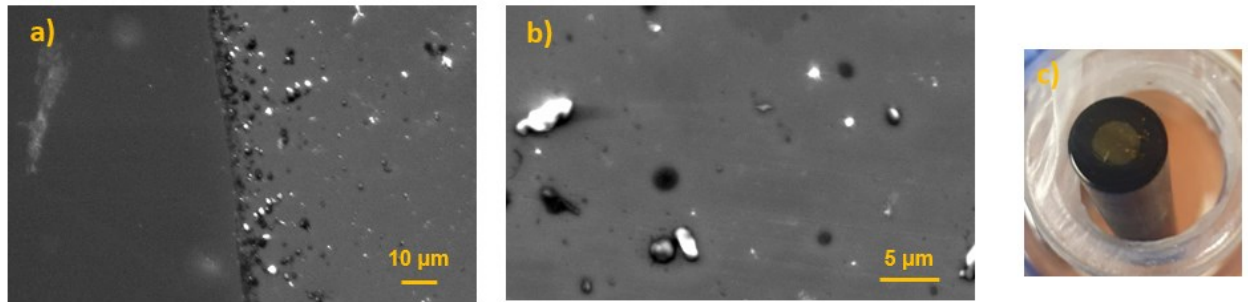
Figure 45. a) and **b)** SEM images of P15DAAQ drop casted on GC disc with different magnitudes as well as **c)** the PDDA-FMN coated GC disc.

In **Figure 45 a** the border between the bare GC disc on the left and the drop casted film of PDDA-FMN is clearly visible. PDDA-FMN seems to form a uniform thin film with small dots, which are most probably not fully dissolved polymer particles. Furthermore, as shown in **Figure 45 b**, the film has a brownish-orange appearance.

3.5.2. Electrochemical characterization of PDDA-FMN

CV experiments were performed in phosphate buffers with pH value 2 ,7 as well as in a 0.1 M NaOH solution with a pH value of 13 of drop casted GC disc electrodes with PDDA-FMN and the results are presented in **Figure 46**.
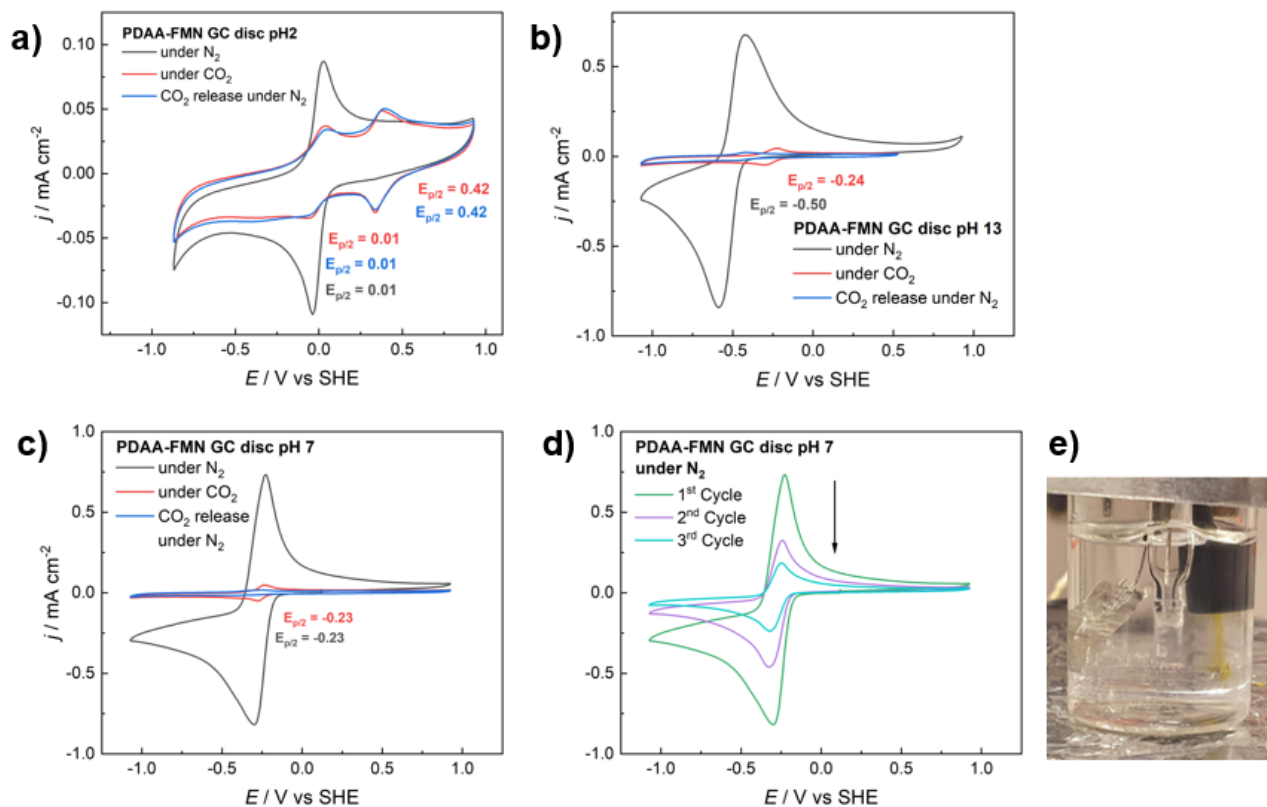
Figure 46. CV of PDDA-FMN AQ on GC disc under N_2 and CO_2 in a phosphate buffer with pH value of **a)** 2 **b)** 13 **c)** 7 at scan rate of 50 mV s^{-1}. **d)** 3 cycles of PDAA- AQ in pH 7 and **e)** dissolution of PAA-AQ in pH 7 into the electrolyte.

Figure 46 presents the CV results obtained at various pH values, presenting distinct reversible redox couples in each CV. However, the polymer exhibits significant instability under N_2 in both neutral and alkaline solutions shown in Figure c and b, respectively. This was also observed for a similar polymer in literature. [58] In **Figure 46 d** and **e**, the instability of PDDA-FMN in pH 7 is further emphasized, as clear indications of a decrease in peak current with increasing cycle number and detachment of the polymer are observed. Similar trends are observed in literature with the analogous polymer PDDA-SAQ, which shows also stability issues in neutral and alkaline solution. [58] In addition, in **Figure 46 b**, a noticeable shift of the half potential from -0.50 under N_2 to -0.23 under CO_2 is observed. However, this change is likely attributed to changes in the pH value from the purging process with CO_2, rather than due to the effects of CO_2 capture as already observed for the other investigated polymers in this work. After the CV, the pH value was found to be significantly reduced to 8, approaching neutral conditions. Moreover, in **Figure 46 b**, the measured half potential under CO_2 of -0.24 V closely resembles the value obtained under CO_2 conditions in **Figure 46 c**, where a potential of -0.23 V was recorded at pH 7. This similarity further reinforces the assumptions that the shift in the electrochemical response is primarily due to pH fluctuations rather than being attributed to CO_2 capture effects.

Examining **Figure 46 a**, where the CV was performed at pH 2, only one peak with a half-potential of 0.01 V under N_2 is observed. Despite observing a decrease in the peak current with increasing cycle number under N_2, similar to pH 7 and pH 13, a clear difference within the results in the other electrolytes can be found. Notably, upon purging the system with CO_2 at pH 2, an additional redox couple appeared, showing a half-potential of +0.42 V. Furthermore, when the electrolyte solution was re-purged with N_2, no changes in the CV were observed. This observation could be attributed to two possible reasons. Firstly, it might be due to CO_2 capture effects, where the CO_2 is strongly bonded to the polymer and not released during N_2 purging or due to the degradation of the polymer. Addressing the questions of possible CO_2 capture and potential polymer degradation requires further investigation.

Due to the polymer's instability, no additional experiments were conducted using ionic liquids, as the increased ionic strength would accelerate the dissolution process even further. Despite obtaining interesting initial results at pH 2 suggesting promising indications for CO_2 capture, it was decided not to pursue additional experiments for quantification of CO_2 capture within the framework of this master's thesis. The primary reason for this decision was the chosen quantification method, which relies on measuring the released CO_2 after the capturing process. Given the suggestion that PDDA-FMN strongly bonds with CO_2 and no significant release occurs, the selected measurement method would not be suitable for accurately quantifying the captured CO_2.

3.6. Poly-1,4-anthraquinone

Poly-1,4-anthraquoninone (P14AQ) was successfully synthesized by an organometallic polycondensation reaction as depicted in **Figure 12**, confirmed by NMR and FTIR spectroscopy. P14AQ is composed of covalently linked anthraquinone repeating units, as illustrated in **Figure 47**. The resulting polymer was obtained as a yellow powder that demonstrates good solubility in chloroform. Furthermore, upon drying, the polymer forms a self-supporting film with an intense yellow colour.
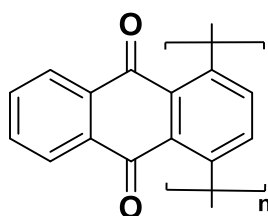
Figure 47. Structure of P14AQ.

3.6.1. Characterization of P14AQ

To investigate the structure of P14AQ ^{1}H-NMR in CDCl$_3$ were recorded. The results of the ^{1}H-NMR of P14AQ are presented in **Figure 48**.
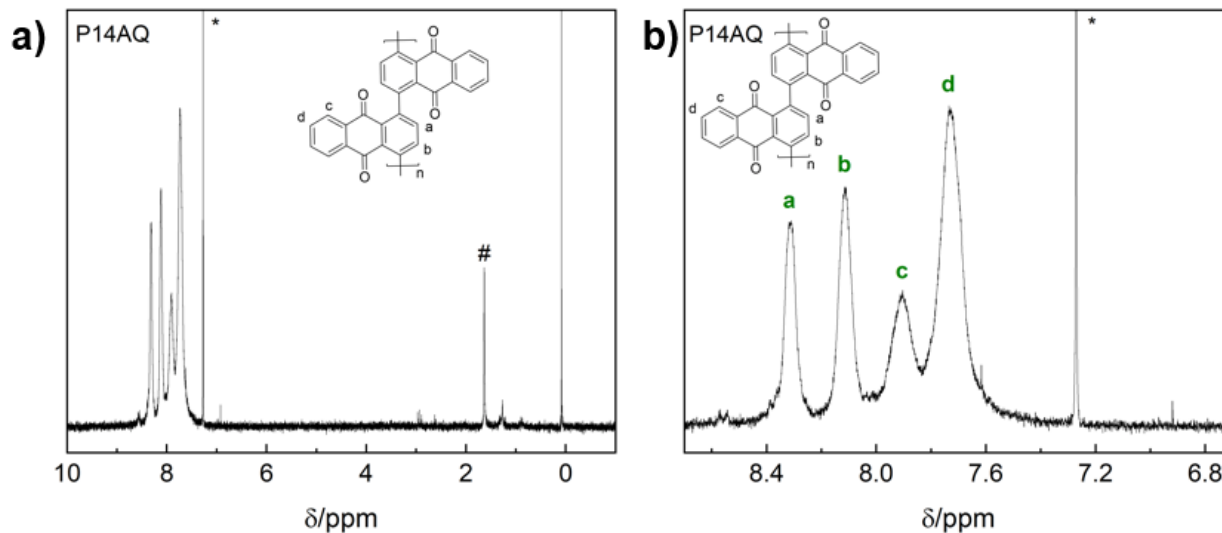
Figure 48. a) ^{1}H-NMR spectrum of P14AQ as well as **b)** a zoomed section recorded in CDCl$_3$. The solvent is marked as * and the occurrence of water is highlighted with #, respectively.

As can be seen in **Figure 48**, the H atoms of anthraquinone are assigned to the corresponding peak in the spectra, which is in accordance to literature. [118] In the spectra of P14AQ, 4 broad singlet peaks can be seen. Broad peaks are usually observed for polymers.

Besides ^{1}H-NMR, FTIR spectroscopy was performed to investigate the structure of P14AQ. The obtained FTIR spectra of P14AQ as well as of the monomer DiCl-AQ for comparison is displayed in **Figure 49**.
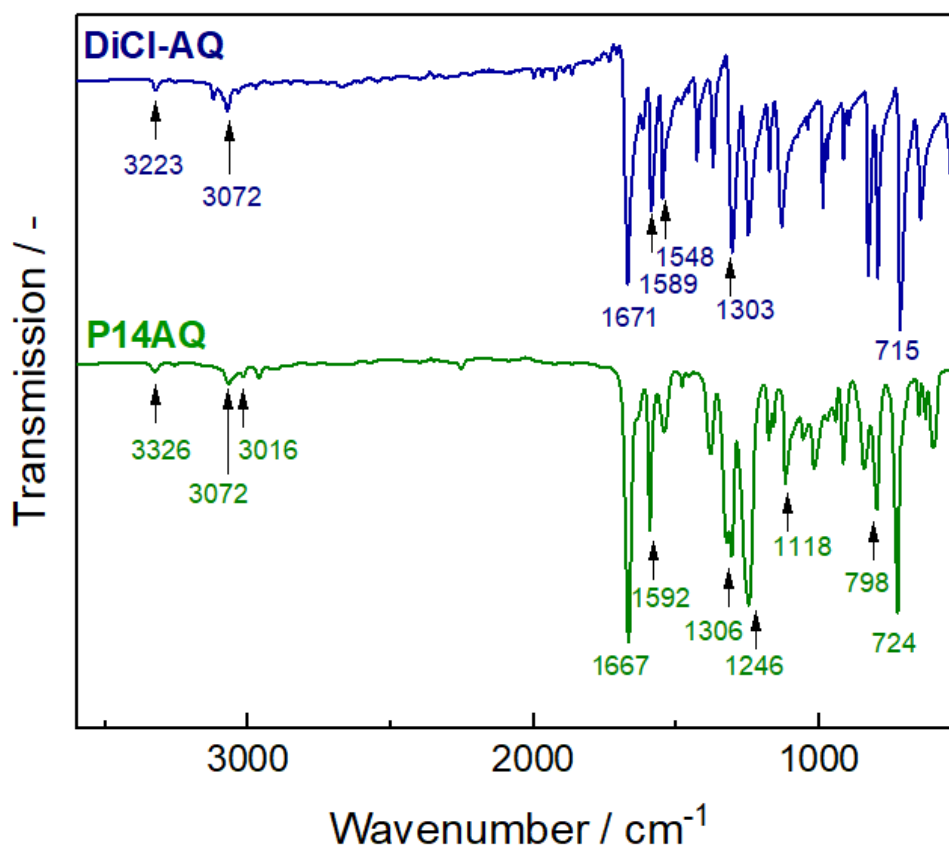
Figure 49. FTIR spectra of the monomer DiCl-AQ and P14AQ in comparison.

The FTIR spectra of P14AQ with the most prominent peaks marked, presented in **Figure 49** is in good accordance to literature. [58,110,118] The strong peaks observed at 1671 cm^{-1} and 1589 cm^{-1} in the spectrum of DiCl-AQ can be assigned to stretching vibrations of the prominent C=O and adjacent aromatic ring C=C bonds, respectively. These peaks are also observed in the spectra of P14AQ at 1667 cm^{-1} and 1592 cm^{-1}, indicating that the anthraquinone rings remain intact after the polymerization process. Generally, the polymer exhibited less, however more uniform and well-defined peaks than the monomer, which aligns with the general trend observed in polymeric structures.

3.6.2. Electrochemical characterization

CV measurements were performed in phosphate buffer with pH value 7 and 12 as well as in 0.1 M NaOH at pH 13. As known from previously reported literature, P14AQ shows no current response in low pH values, therefore measurements in phosphate buffer pH 2 were not performed. [58] The results of the CVs are depicted in **Figure 50.**
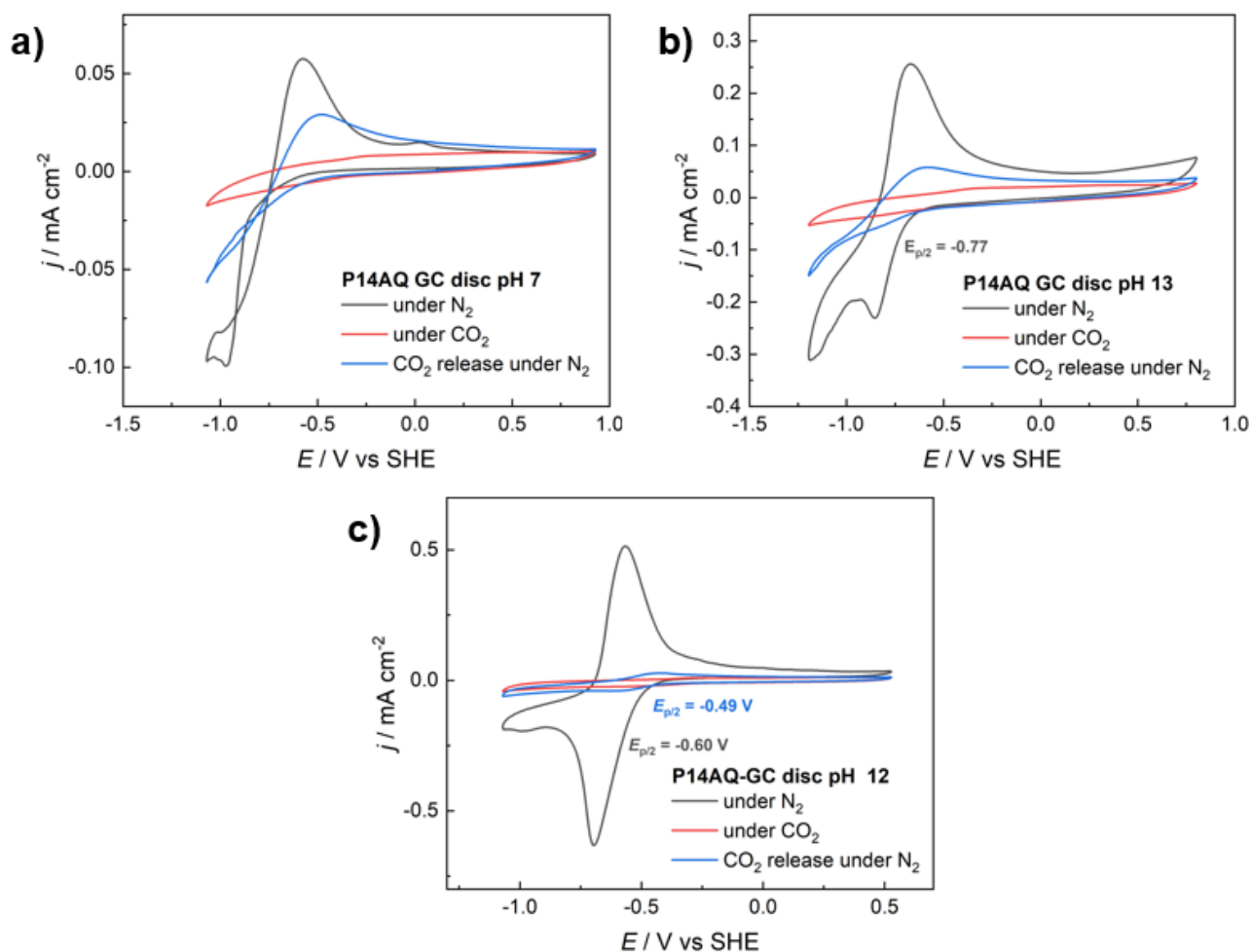
Figure 50. CV of P14AQ on GC disc under N_2 and CO_2 in phosphate buffer with a pH value of **a)** pH 7 **b)** pH 13 and **c)** pH 12.

In **Figure 50** the CV analysis of P14AQ under N_2 saturated conditions intriguing behaviour at different pH values is shown. At pH 13 and pH 12 depicted in **Figure 50 b** and **c**, a quasi-reversible reduction is observed, with half potentials of -0.77 V and -0.6 V, respectively. However, in the case of pH 7 (**Figure 50 a**), small differences become apparent. The quasi-reversible reductive peak is less pronounced, and the peak current response is notably lower compared to pH 12 and pH 13. Upon purging the system with CO_2, the electrochemical response of P14AQ almost vanishes, and only a minimal current is observed during further reduction for all pH conditions. However, upon removing the unbound CO_2 from the solution and saturating it with N_2 again, a small oxidation peak emerges during electrochemical oxidation, which is attributed to the release of CO_2. The phenomenon of reductive peaks vanishing has been already previously reported in literature for evaporated anthraquinone thin films as well as various pigments containing carbonyl groups.[54,55,57]

As promising results for CO_2 capture on GC electrodes was obtained, P14AQ was further drop casted onto CP electrodes and the results are shown **Figure 51**.
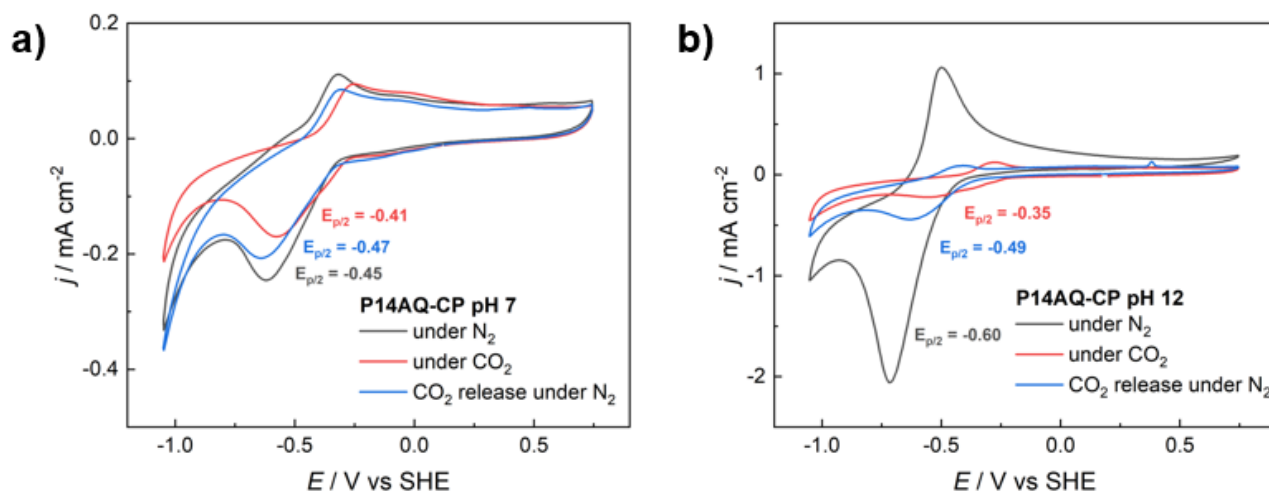
Figure 51. CV of P14AQ on CP in phosphate buffer with pH value **a)** 7 and **b)** 12.

When comparing the results achieved on GC electrode with those on a CP, depicted in **Figure 51 a** at pH 7, it becomes evident that the reductive peak of P14AQ is notably more prominent and well-defined when utilizing the CP electrode as opposed to GC. However, this characteristic peak vanishing trend under saturated conditions with CO_2 is less pronounced compared to using GC as electrode material. Regarding the measurement conducted at pH 12, shown in **Figure 51 b** the same half potential of -0.60 V was obtained using CP, the current density recorded with the CP electrode surpasses that achieved with GC, as is commonly observed. Furthermore, under saturated CO_2 conditions, a substantial decrease in current density, along with an oxidative shift to a more anodic potential, was observed, featuring a half potential of -0.35 V. This aligns with observation by Voskian & Hatton investigating P14AQ in an electrochemical cell with pure ionic liquids. [31] Upon re-saturating the system with N_2, the characteristic peak under N_2 was nearly restored, although with a significantly lower current.

Additional to measurements in electrolyte with different pH values, the influence of the ionic strength was examined by adding NaCl or an ionic liquid to the 0.1 M NaOH solution. Gurkan *et al.* [44] and Lui *et al.* [45] investigated already the addition of different ionic liquids and salts to various quinone for carbon capture, respectively. The results in comparison with the CV measured in the pure 0.1 M NaOH are presented in **Figure 52**.
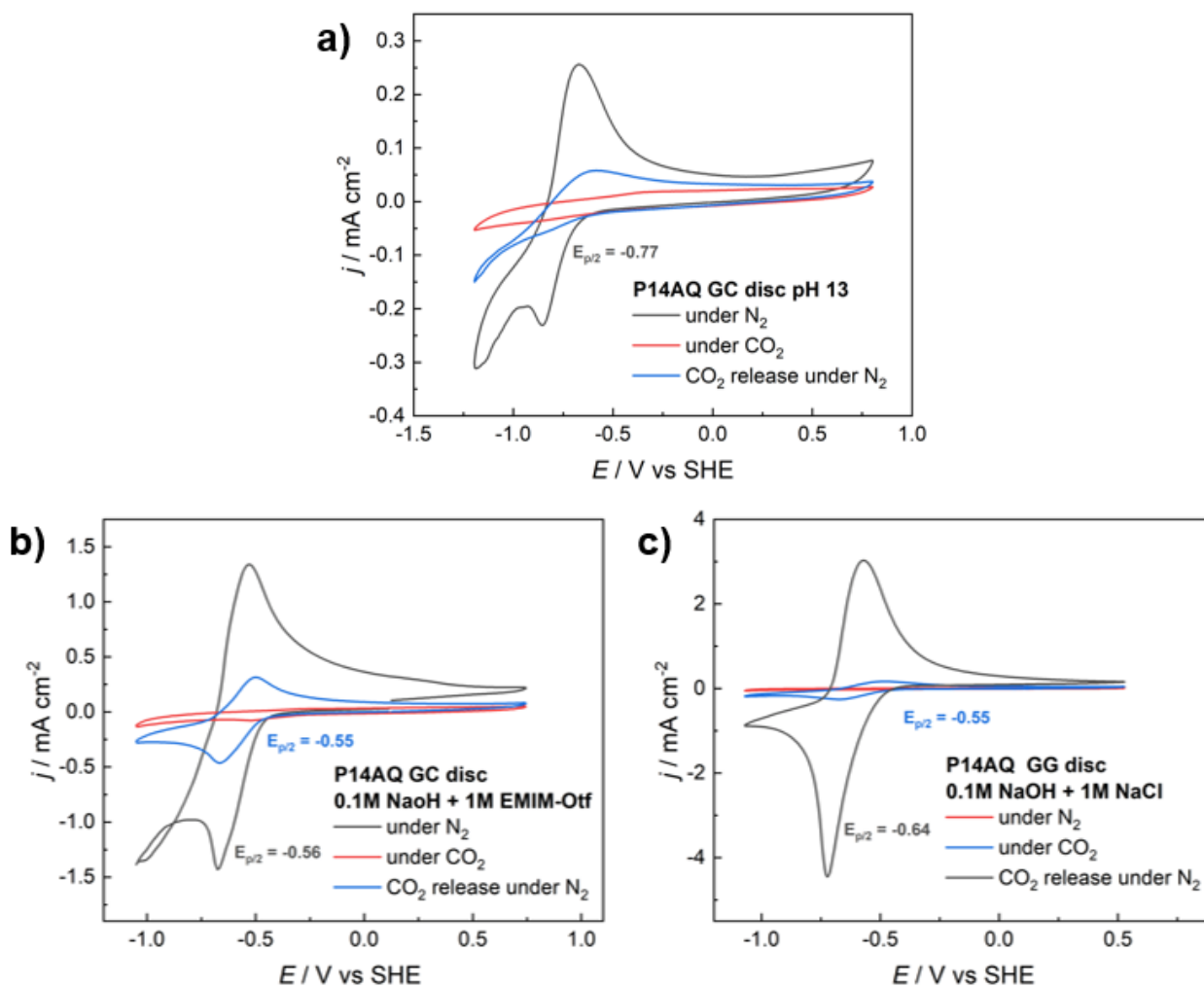
Figure 52. Observation on influence of increase in ionic strength **a)** 0.1 M NaOH without addition as well as with the addition of **b)** 1 M EMIM-Otf and **c)** of 1 M NaCl.

As illustrated in **Figure 52**, the addition of both EMIM-OTF, as well as NaCl, significantly enhanced the electrochemical response of P14AQ compared to a 0.1 M NaOH, resulting in more prominent and sharp peaks. Specifically, when EMIM-OTF is introduced, there is an increase of approximately 5 times in current density, while NaCl induces an impressive 15 times magnification. Minor deviations can be observed in the half-potential of the reductive peak, which shifts toward to more anodic potentials under N_2 conditions for both additions when comparing with the pure 0.1 M NaOH. Moreover, in both cases, as already observed for different pH values, a significant decrease the electrochemical response of P14AQ under saturated CO_2 conditions can be seen. Subsequently, after removing the unbound CO_2 from the solution by saturating it with N_2 again and cycling of the system to negative potentials once more partially restores the characteristic quasi-reversible reductive feature of P14AQ. However, as depicted in **Figure 52 b**, the reappearance of

the peak is more pronounced when using EMIM-OTF as an additive compared to addition of NaCl into 0.1 M NaOH.

Besides measurements with the addition of EMIM-OTF to 0.1 M NaOH, experiments in pure ionic liquids were conducted and the results are presented in **Figure 53**.
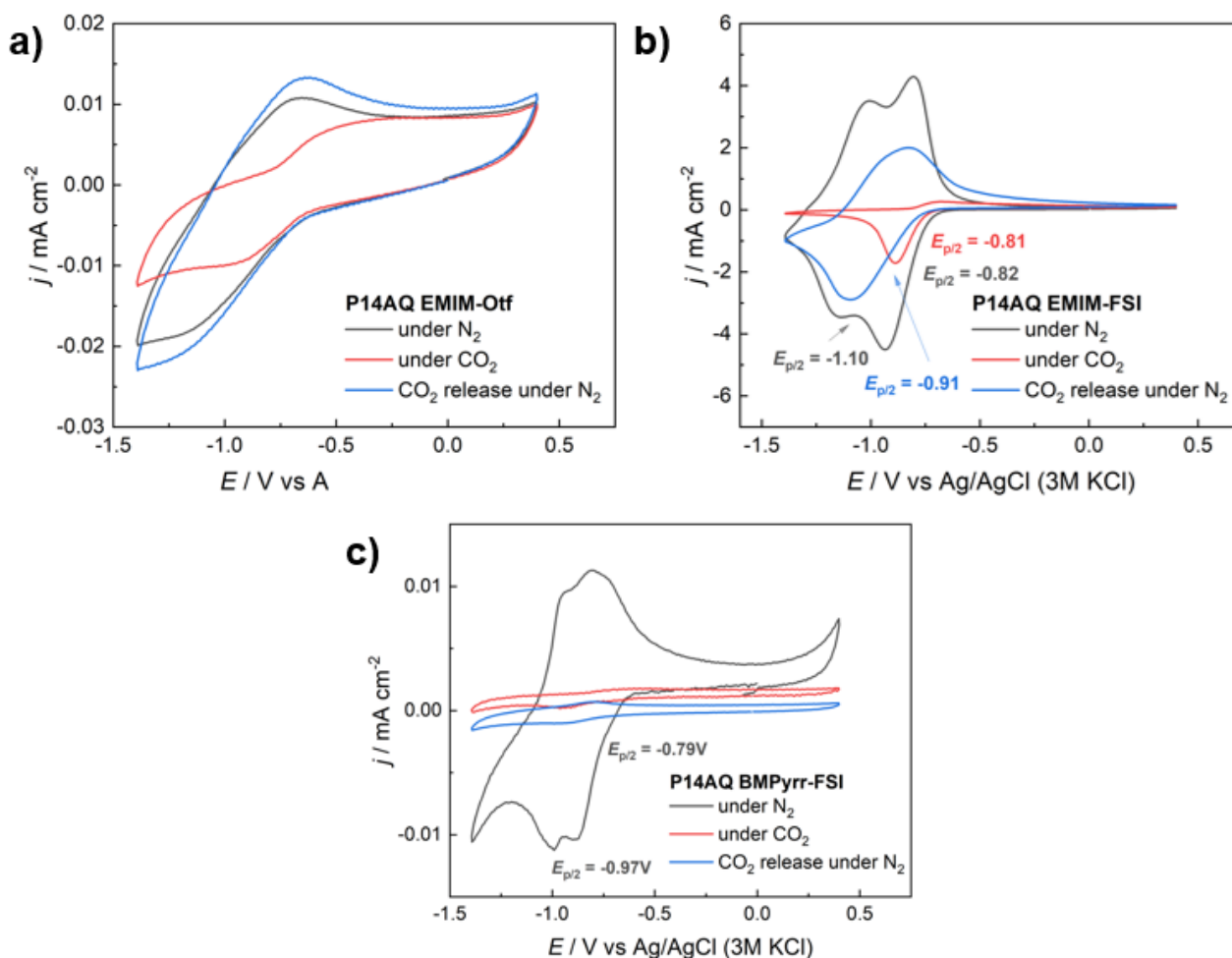
Figure 53. CV measurements of P14AQ on GC disc in pure ionic liquids being **a)** EMIM-Otf **b)** EMIM-FSI as well as **c)** BymPyrr-FSI.

Interestingly, when EMIM-Otf is used as additive in an aqueous solution, there is a significant enhancement in the electrochemical response of P14AQ as shown in **Figure 51 a**. However, in contrast, when pure EMIM-OTF is employed depicted in **Figure 53 a**, the opposite effect is observed. The electroactivity of P14AQ is even supressed. This reduction in electroactivity is likely attributed to inefficient mass transfer between the electrode and electrolyte, despite the electrode being immersed in the ionic liquid for 2 hours prior the measurement to ensure efficient mass transfer.

When using pure EMIM-FSI as an electrolyte depicted in **Figure 53 b**, the current density of P14AQ is significantly enhanced compared to measurements conducted in an aqueous solution. Under an N_2 atmosphere, two distinct reductive peaks with half potentials of -1.10 V and -0.82 V are observed. This is in contrast to measurements in aqueous solution, where only a single reductive peak is observed as in aqueous solution the two-electron quinone reduction occurs in a concerted manner. Upon saturating the system with CO_2, the current density decreases significantly, and the two redox couples merge into one, featuring a potential of -0.81 V, which matches the first reductive peak observed under N_2. Additionally, the current density of the oxidative peak almost disappears. When the system is again saturated with N_2, the peak characteristic is nearly fully restored, although with a potential shift. Only one redox couple can be observed, with a potential of -0.91 V, which is in between the first and the second reductive peak observed under N_2.

In **Figure 53 c**, the CV measurement conducted in BMPyrr-FSi is presented. Similar to the observations made for EMIM-Otf, it is evident that the electrochemical response of P14AQ is comparatively lower to CV conducted in aqueous solution. Nonetheless, a distinct peak with a shoulder, featuring a half potential of -0.97 V, can be observed. Upon saturation of the system with CO_2, there is a further reduction in current density, leading to the disappearance of the characteristic peaks, a phenomenon already observed with prior measurements. However, upon re-saturation of the system with N_2, the reappearance of the P14AQ peaks does not occur, inconsistent with observations in other electrolyte media. In general, P14AQ exhibits the lowest electroactivity in BMPyrr-FSI, likely due to the high viscosity of BMPyrr-FSI. High viscosity is an unfavourable property for the carbon capture application investigated by Gurkan *et al.*, who screened various ionic liquids for carbon capture using different quinones. [44]

Overall, CV measurements conducted in pure EMIM-FSI received the best results.

3.7. Determination of electrochemical window ionic liquids

The determination of the electrochemical window of ionic liquids is a crucial factor for use in electrochemical applications, as it defines the operational range where the electrolyte remains unaffected by oxidation or reduction processes. Prior to determination, a specific level of current density referred to as the cut-off current needs to be selected. This cut-off current is essential for assessing the potentials at which oxidation and reduction processes occur. The range within which the electrochemical window is defined relies on the cathodic limiting potential (E_{CL}) and the anodic limiting potential (E_{AL}), which are influenced by the selection of the cut-off current density. Typically, within the realm of various research studies, this cut-off current density is commonly set

within the range of 0.1 to 1.0 mA cm⁻². [95,119] In the context of this thesis, a cut-off current of 0.5 mA cm^{-2} was selected to define the electrochemical window. This determination was accomplished through cyclic voltammetry using GC disc as WE, as illustrated in **Figure 54** and the results are summarized in **Table 7**.
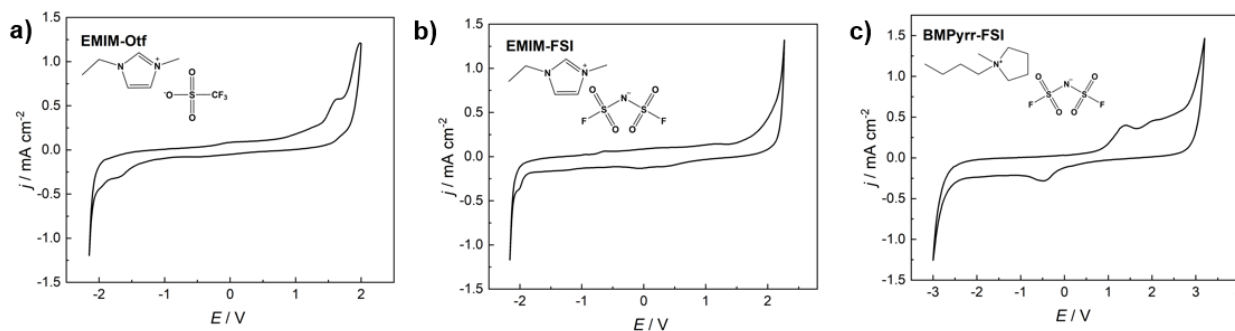
Figure 54. CV of **a)** EMIM-Otf **b)** EMIM-FSI and **c)** BMPyrr-FSI.

As depicted in **Figure 54**, a comparison between EMIM-OTf and EMIM-FSI reveals a similar reduction potential of approximately 2.1 V but different oxidative limits, supporting the hypothesis that altering the anion does have more impact on the oxidative limit. This observation is consistent with previous research, which proposes that the observed cathodic and anodic limits in ionic liquids is due to the oxidation of anions and the reduction of cations, respectively. [119] Interestingly, considering BMPyrr-FSI, despite employing the same anion as EMIM-FSI, the oxidative limit remains higher. Remarkably, BMPyrr-FSI exhibits the most substantial electrochemical window, spanning almost 5.4 V. However, minor peaks are observed in the cyclic voltammograms of the assessed electrochemical windows, but these peaks are neglected due to their currents falling below the predetermined cut-off current density of 0.5 mA cm⁻². These peaks may be attributed to processes such as double layer charging or the presence of impurities within the ionic liquids.[119,120]

Table 7. Electrochemical window (EW), as well as cathodic limiting potential and anodic limiting potential of each IL.

Ionic Liquid	E_{CL} / V	E_{AL} / V	EW / V
EMIM-Otf	-2.05	1.71	3.76
EMIM-FSI	-2.10	2.06	4.16
BMPyrr-FSI	-2.75	2.62	5.37

3.8. Contact angle measurements

Contact angle measurements were conducted to provide additional information about surface properties of the polymer film atop a GC electrode. The chemically synthesized polymers P14AQ, PAA-AQ as well as PDDA-FMN were drop casted onto a GC plate and their contact angles with 18 MΩ water drops were examined. These measurements were then compared to those of the bare GC surface, and the results are presented in **Figure 55**.
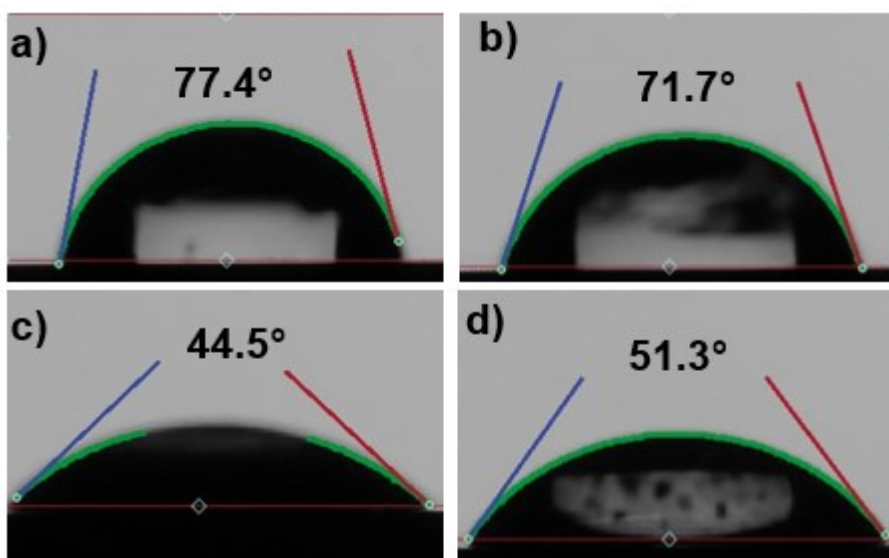
Figure 55. Contact angle measurements using 18 MΩ water droplet on **a)** bare GC, **b)** P14AQ **c)** PAA-AQ, and **d)** PDDA-FMN.

The contact angle of the uncoated GC surface shown in **Figure 55 a** was relatively high, with 77.4° which is in accordance with literature. [58,121] P14AQ exhibits a slightly reduced hydrophobicity, measuring at 71.7°, in comparison to the uncoated GC surface. However, when compared to PAA-AQ and PDDA-FMN, P14AQ emerges as the most hydrophobic polymer. In contrast, PDDA-FMN demonstrates a relatively hydrophilic character with a contact angle of 51.3°, similar to its analogous PDDA-SAQ. [58] Furthermore, PAA-AQ displays the highest level of hydrophilicity with a measured angle of 44.5° due to its hydrophilic backbone featuring amine groups and incomplete substitution of anthraquinone units.

Furthermore, contact angle measurements were performed using GC electrodes coated with electrochemically polymerized PAAQ, P15DAAQ as well as PRF. As the GC electrode prior electropolymerization is activated, the activated bare GC serve as comparison and the results are presented in **Figure 56**.
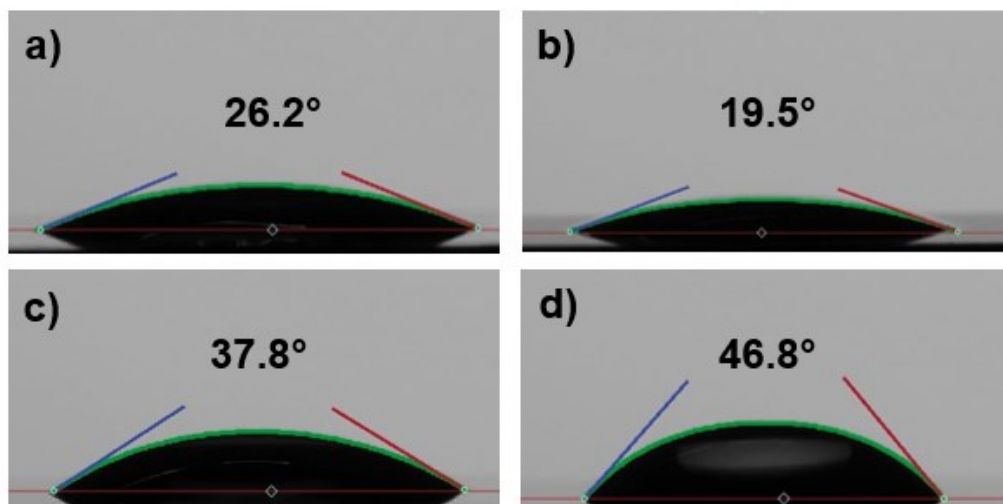
Figure 56. Contact angle measurements using 18 MΩ water droplet on **a)** bare activated GC, **b)** PAAQ **c)** P15DAAQ, and **d)** PRF.

As depicted in **Figure 56 a**, the bare activated GC surface demonstrates a remarkably high level of hydrophilicity, with a contact angle measuring 26.2° attributed to the electrochemical activation process, in contrast to the untreated GC in **Figure 55 a**. Interestingly, PAAQ displays an even elevated hydrophilicity compared to the bare GC, registering a contact angle of 19.5°. This low contact angle could also be related due to the uneven sponge-like structure of PAAQ. In contrast, P15AAQ exhibits lower hydrophilicity compared to PAAQ, with a contact angle of 33.4°. In comparison PRF demonstrate the highest hydrophobicity among the electropolymerized polymers with a contact angle of 46.8°, close the other flavin analogue of PDDA-FMN in **Figure 55 d**. Overall P14AQ is the most hydrophobic polymer and PAAQ the most hydrophilic.

3.9. CO_2 reduction experiments

To investigate if the captured CO_2 is reduced to CO, electrolysis and subsequent GC analysis were performed using CP electrodes coated with PAAQ and PRF. For the investigation a certain potential for 1 or 2h in a two-compartment electrochemical cell as illustrated in **Figure 15** was applied and subsequently 2 mL from the gas headspace was analysed. The exact parameters used during the electrolysis as well as the amount of CO measured using GC are presented in **Table 8**.

Table 8. Potentials vs Ag/AgCl (3M KCl) and time applied during electrolysis as well as the measured CO amount.

Polymer	*E* / V	*t* / h	CO / µL
PAAQ	-0.6	1	0.0
	-0.7	2	0.0
PRF	-0.2	2	0.0
	-0.3	2	0.0
	-0.4	2	0.0

As can be seen in **Table 8**, no amount of CO could be detected using PAAQ and PRF coated CP electrodes with GC analysis.

3.10. CO$_2$ capture and release experiments

In addition to conducting experiments involving the capture and release of CO$_2$ using only CV, experiments were performed involving an additional constant potential was applied for a specific duration to initiate the release of CO$_2$, utilizing P14AQ. Before each experiment, standard CV measurements were carried out under both N$_2$ and CO$_2$ conditions followed by oxidative chronoamperometry. The objective in employing chronoamperometry was to assess whether it could induce the CO$_2$ release process, which was evaluated by a third CV measurement under saturated N$_2$ conditions after the constant positive potential was applied. For these investigations, P14AQ drop-casted onto a GC disc was used, as this specific polymer demonstrated the most promising results in terms of CO$_2$ capture and release.

In order to systematically study this oxidative release, firstly the influence of the applied potential was investigated for 15 minutes and the results are depicted in **Figure 57.**
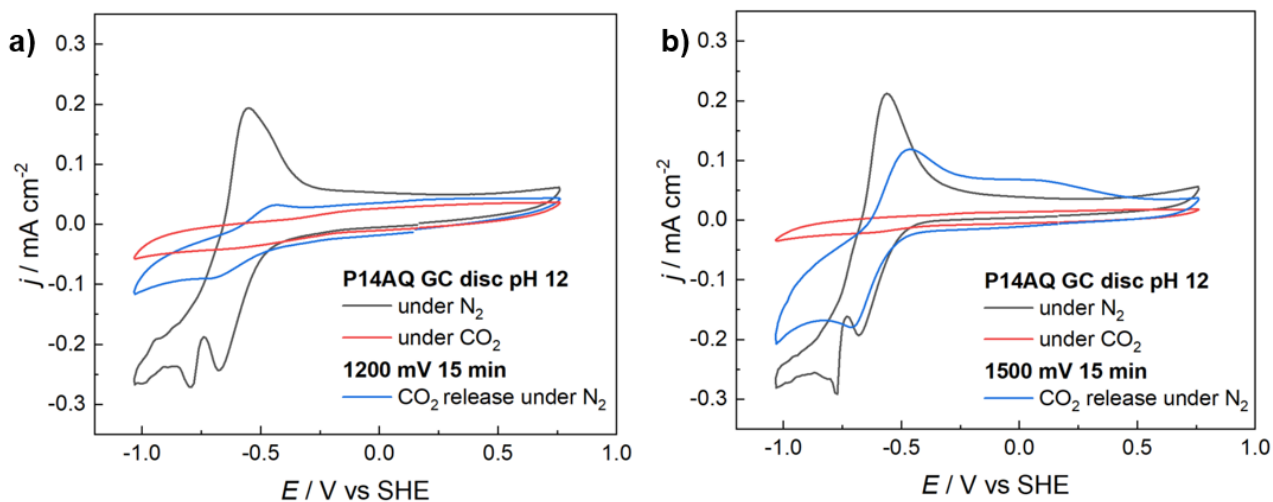
Figure 57. Investigation on influence of potential by applying a constant potential for 15 minutes of **a)** 1200 mV and **b)** 1500 mV.

As can be seen in **Figure 57**, applying of a constant potential of 1500 mV notably enhances the CO_2 release. Moreover, a potential of 1200 mV also demonstrates an improvement in release compared to solely relying on CV measurements in **Figure 51**. However, the impact is significantly greater when a potential of 1500 mV is applied where after the release process nearly the initial peak current density was achieved.

Besides the applied potential, also the influence of time was investigated and the results are presented in **Figure 58**.
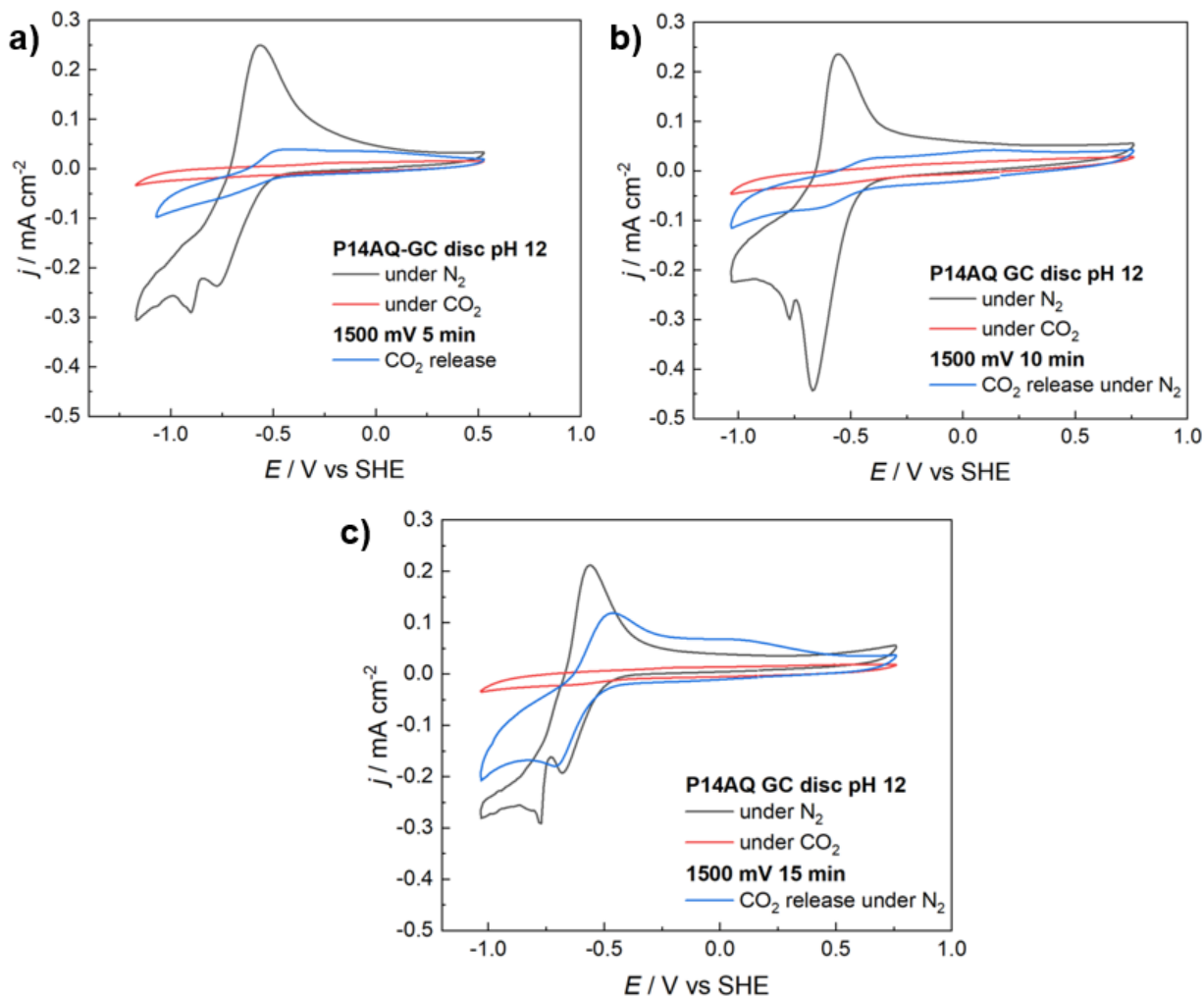
Figure 58. Investigation on influence of time by applying a constant potential of 1500 mV for **a)** 5 min, **b)** 10 min and **c)** 15 min.

As can be seen in **Figure 58**, the current density of P14AQ after CO_2 release initiated by chronoamperometry under N_2 displays a notable increase as the duration of time increases. Consequently, the most favourable results were achieved when applying a potential of 1500 mV for 15 minutes.

To quantify the released CO_2, FTIR measurements were conducted. The procedure involved standard CV experiments conducted under N_2 and CO_2 conditions, followed by a third CV under saturated N_2. Subsequently, 2 mL of the headspace were extracted and injected into an FTIR gas cell for analysis. For this experiment, PAAQ, PRF, and P14AQ were used, as they had previously shown major indications of carbon capture and release, as evaluated in prior chapters. Furthermore, it has to be mentioned that with this quantification method only the released CO_2 can be measured instead of the captured CO_2 itself. In addition, only CP electrodes were used to

increase the electrode surface in order to enhance the CO_2 release. Moreover, only experiments were conducted in aqueous solution as this method relies on quantifying the released CO_2 in the headspace. In ionic liquids, CO_2 tends to be highly soluble, making it even more challenging to detect in the headspace.

Prior measurements a calibration curve with known amount of CO_2 in a N_2 atmosphere was performed and the results are depicted in **Figure 59**.
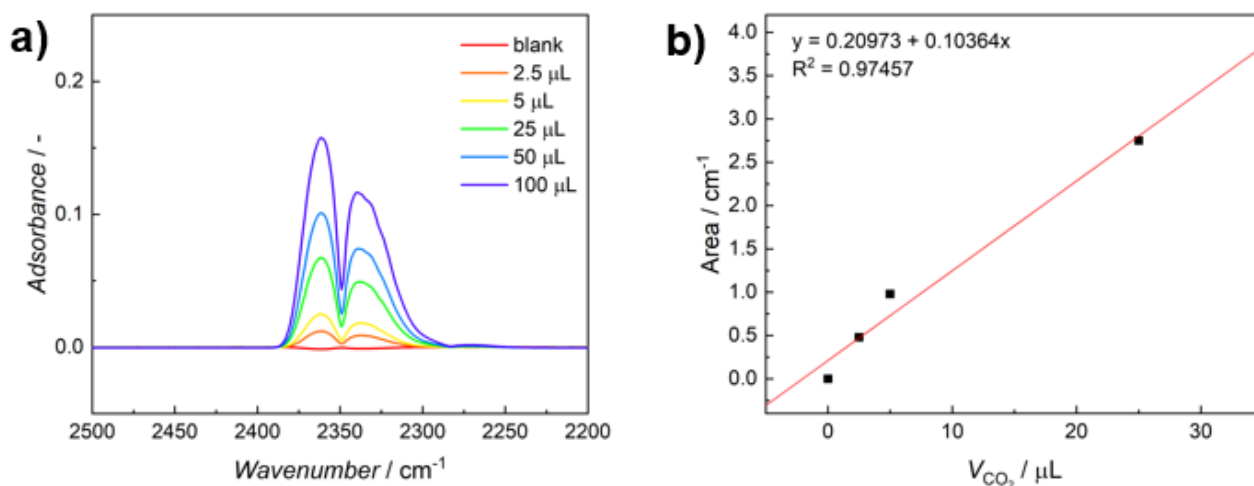
Figure 59. a) IR Spectra of calibration of CO_2 as well as **b)** calibration curve.

In addition to conducting a standard CV, an electro swing experiments were performed utilizing P14AQ. This involved applying -1 V for a duration of 15 minutes to induce carbon capture, followed by a subsequent application of +1.5 V for 15 minutes in N_2 atmosphere to trigger the release of CO_2.

The results of the FTIR measurements showing the characteristic peak of CO_2 are presented in **Figure 60.**
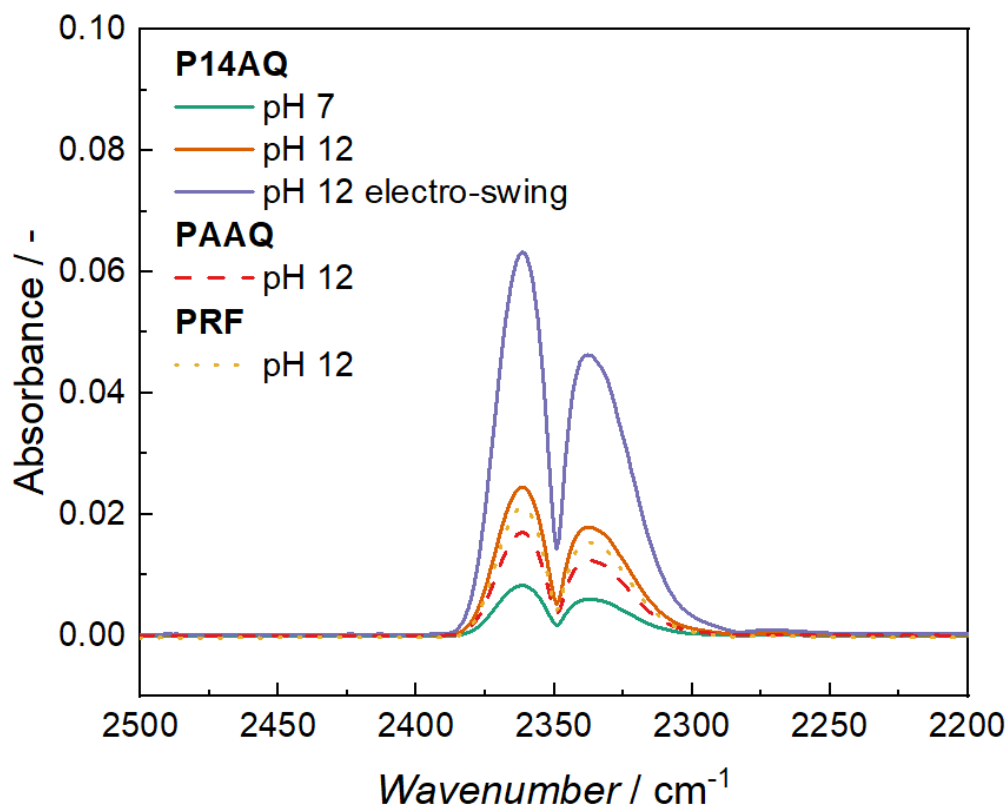
Figure 60. CO_2 release quantified by FTIR.

As depicted in **Figure 60**, measurable quantities of released CO_2 were observed for all polymers. Notably, P14AQ exhibited the highest release of CO_2, particularly at pH 12, surpassing the quantities released by PAAQ and PRF.

Furthermore, conducting CV experiments in an alkaline environment (pH 12) regarding P14AQ led to a notable improvement in the release of CO_2 compared to experiments conducted at pH 7. Additionally, substituting the standard CV with electrochemical swing techniques further enhanced the release of CO_2.

Despite the calibration curve not showing perfect linearity, an estimation of the quantity CO_2 released was calculated and the results are presented in **Table 9** regarding the experiments using CV and **Table 10** concerning the electro swing measurement utilizing P14AQ.

Table 9. Calculated quantities during CO_2 release by CV.

Polymer	Condition	$CO_{2\ released}$ / µL	$CO_{2\ released}$ / µmol	e^- / µmol	$\frac{n(CO_2)}{n(e^-)}$ / %
P14AQ	pH 7	1.34	0.060	0.111	54
	pH 12	1.71	0.077	0.204	38
PAAQ	pH 12	1.54	0.069	0.148	46
PRF	pH 12	1.62	0.072	0.082	88

As shown in **Table 9** , the detected CO_2 release quantities ranged from 1.3 to 1.7 µL. The ratio between moles of CO_2 and moles of electrons was calculated to represent the efficiency of moles CO_2 released per mol electron, where PRF obtained the most promising results with 88 %.

Based on the assumption that 2 moles of CO_2 are captured per mole of repeating unit anthraquinone and the use of 0.5 mg P14AQ corresponding to a value of 2.5 µmol, the theoretical uptake was calculated to be 5 µmol CO_2 per 0.5 mg of P14AQ.

Table 10. Calculated quantities during CO_2 release by electro swing.

Polymer	Condition	$CO_{2\ released}$ / µL	$CO_{2\ released}$ / µmol	e^- / µmol	$\frac{n(CO_2)}{n(e^-)}$ / %
P14AQ	Capture	-	-	16.8	-
	Release	2.63	0.117	262.3	0.04

As observed in **Table 10**, a higher quantity of released CO_2 was detected in comparison to experiments utilizing standard CV in **Table 9**. Nonetheless, a substantial larger amount of electrons was detected compared to the moles of CO_2 and P14AQ, suggesting the possibility of various side reactions taking place during the release process. This is particularly evident given the significantly higher amount of electrons involved in the oxidative release process. However, it should be noted that further investigations are required to substantiate these assumptions.

Overall, despite the considerable errors resulting from measuring released CO_2 in the headspace above an aqueous solution and from the calibration curve, these results are clear evidence of capture and release of CO_2 including qualitative trends when using the polymers P14AQ, PAAQ and PRF.

4. Conclusion

In summary, in this thesis six polymers were successfully synthesised electrochemically or chemically and comprehensively characterized, offering valuable insights into their electrochemical behaviour and their potential use in CO_2 capture applications. For characterization a range of analytical techniques, such as ATR-FTIR, Raman spectroscopy, SEM, NMR and contact angle measurements was employed, except for PRF only SEM and contact angle characterizations were possible due to being unable to polymerize the polymer onto a material suitable for spectroscopy measurements.

Furthermore, of all polymers the electrochemical behaviour was investigated under saturated N_2 as well as CO_2 conditions using CV measurements in aqueous solutions with different pH values. Significantly, P14AQ, PRF, and PAAQ have shown notable CO_2 capture and release capabilities during CV measurements in aqueous solutions, especially in alkaline solutions. Furthermore, the ionic polymer PDDA-FMN showed as well possible signs of carbon capture, however further experiments are necessary to evaluate this assumption. Therefore, for further experiments only PRF, PAAQ and P14AQ were used.

Additional to measurements in electrolyte with different pH values, the influence of the ionic strength was examined by adding NaCl or an ionic liquid to the 0.1 M NaOH solution. Regarding the polymer PAAQ, both additives enhanced the current density, with NaCl showing a more significant improvement. However, during the re-purging phase, differences in cyclic voltammetry emerged, suggesting that further mechanistic studies are required to understand these variations. Contrary to results of PAAQ, higher ionic strength did not lead to increased electroactivity of PRF and an unusual CV shape appeared. Moreover, the addition of EMIM-OTF and NaCl significantly enhanced the electrochemical response of P14AQ compared to a 0.1 M NaOH reference. EMIM-OTF increased the current density by approximately 5 times, while NaCl induced a remarkable 15-fold rise. There were minor shifts in the half-potential of the reductive peak, particularly under N_2 conditions, and a significant decrease in electrochemical response under saturated CO_2 conditions as already observed in other electrolytes. Cycling the system and removing unbound CO_2 partially restored the characteristic reductive feature of P14AQ, with EMIM-OTF being more effective in this regard than NaCl when added to 0.1 M NaOH.

The electrochemical window of the selected ionic liquids was successfully determined, yielding values of 3.8 V for EMIM-OTf and 4.2 V for EMIM-FSI. BMPyrr-FSI, exhibits a significantly higher oxidative limit and an impressive electrochemical window extending almost 5.4 V. EMIM-OTf and EMIM-FSI demonstrates a similar reduction potential at around 2.1 V but differing oxidative limits,

suggesting that changing the anion does indeed influence the oxidative limit, in line with prior research findings.

When subjected to CV measurements in pure ionic liquids, the electrochemical behaviour of PAAQ, RRF and P14AQ exhibited interesting variations. PAAQ displayed electrochemical activity in all ionic liquids, with the most pronounced peaks observed in EMIM-FSI. However, the stability of PAAQ within these ionic liquids was compromised, leading to a significant decline in current density and visible detachment from the electrode. Regarding PRF, only minor electrochemical responses of the polymer can be seen within in the pure ionic liquids, whereas in EMIM-Otf the best result were obtained. Particularly, P14AQ demonstrated enhanced electroactivity when used in combination with the ionic liquid EMIM-FSI. Pure EMIM-FSI as an electrolyte significantly enhanced electrochemical response of P14AQ, with distinct reductive peaks, and the response changed upon CO_2 saturation. BMPyrr-FSI showed comparatively lower electroactivity for P14AQ, attributed to its high viscosity. Interestingly, using pure EMIM-OTF suppressed the electroactivity of P14AQ, whereas EMIM-OTf in an aqueous solution did enhance the electroactivity likely due to inefficient mass transfer. Overall, P14AQ in pure EMIM-FSI yielded the most promising results among the tested conditions.

Additionally, the assessment of potential CO_2 reduction performance of PRF and PAAQ via gas chromatography yielded no detectable CO production, suggesting that CO_2 was not reduced to CO in the examined conditions. To check whether other reduction products were formed, further measurements are required, as our analysis only focused on CO detection using GC.

To quantify the released CO_2, FTIR measurements were conducted. For this experiment, PAAQ, PRF, and P14AQ were used, as they had shown indications of carbon capture and release. Despite the considerable error resulting from the calibration curve, this could be interpreted as evidence supporting the capture and release of CO_2 when using the polymers P14AQ, PAAQ and PRF. However, using this quantification method only the released CO_2 can be measured instead of the captured CO_2 itself.

In conclusion, this thesis has presented an investigation into the electrochemical properties and CO_2 capture abilities of six synthesized polymers. The findings reveal promising potential for P14AQ, PRF, and PAAQ in the realm of CO_2 capture and release, although the specific mechanisms require further elucidation. Future research should focus on investigating the electrochemical CO_2 capture processes of the polymers and optimizing the quantification of captured CO_2.

5. References

1. Campbell-Lendrum, D., Corvalán, C. Neira, M. Global climate change: implications for international public health policy. *Bulletin of the World Health Organization* **85** (2007).

2. Boot-Handford, M. E. *et al.* Carbon capture and storage update. *Energy Environ. Sci.* **7**, 130–189 (2014).

3. Ghiat, I., Al-Ansari, T. A review of carbon capture and utilisation as a CO_2 abatement opportunity within the EWF nexus. *Journal of CO2 Utilization* **45,** 235-237 (2021).

4. Nanda, S., Reddy, S. N., Mitra, S. K., Kozinski, J. A. The progressive routes for carbon capture and sequestration. *Energy Science and Engineering* **4**, 99–122 (2016).

5. Bronselaer, B., Winton, M., Griffies, S., Hurlin, W., Rodgers, K., Sergienko, O., Stouffer R., Russell, J. Change in future climate due to Antarctic meltwater. *Nature* **564**, 53–58 (2018).

6. Rackley, S. A. Introduction in *Carbon Capture and Storage* 3-21, 2nd Edition, (Elsevier, 2017).

7. Rheinhardt, J. H., Singh, P., Tarakeshwar, P., Buttry, D. A. Electrochemical capture and release of carbon dioxide. *ACS Energy Letters* **2**, 454–461 (2017).

8. Millar, R. J., Allen, M. R. Understanding the Role of CCS Deployment in Meeting Ambitious Climate Goals. in *Carbon Capture and Storage* 8–35, 1st Edition (The Royal Society of Chemistry, 2019).

9. Gibbins, J., Chalmers, H. Carbon capture and storage. *Energy Policy* **36**, 4317–4322 (2008).

10. Al-Mamoori, A., Krishnamurthy, A., Rownaghi, A. A., Rezaei, F. Carbon Capture and Utilization Update. *Energy Technology* **5,** 834–849 (2017).

11. Sanz-Pérez, E. S., Murdock, C. R., Didas, S. A., Jones, C. W. Direct Capture of CO_2 from Ambient Air. *Chemical Reviews* **116**, 11840–11876 (2016).

12. Kang, J. S., Kim, S., Hatton, T. A. Redox-responsive sorbents and mediators for electrochemically based CO_2 capture. *Current Opinion in Green and Sustainable Chemistry* **31**, 100504 (2021).

13. Rochelle, G. T. Amine Scrubbing for CO_2 Capture. *Science* **325**, 1652–1654 (2009).

14. Rochelle, G. T. Conventional amine scrubbing for CO_2 capture. in *Absorption-Based Post-Combustion Capture of Carbon Dioxide* 35–67, 1st Edition (Elsevier, 2016).

15. Torralba-Calleja, E., Skinner, J., Gutiérrez-Tauste, D. CO_2 capture in ionic liquids: A review of solubilities and experimental methods. *J Chem,* 473584 (2013).

16. Zito, A. M., Clarke, L. E., Barlow, J. M., Bím, D., Zhang, Z., Ripley, K. M., Li, C. J., Kummeth, A., Leonard, M. E., Alexandrova, A. N., Brushett, F. R., Yang J. Y. Electrochemical Carbon Dioxide Capture and Concentration. *Chem Rev* **123**, 8069-8098 (2023).

17. Puxty, G., Rowland, R., Allport, A., Yang, Q., Bown, M., Burns, R., Maeder, M., Attalla, M. Carbon dioxide postcombustion capture: A novel screening study of the carbon dioxide absorption performance of 76 amines. *Environ Sci Technol* **43**, 6427–6433 (2009).

18. Veltman, K., Singh, B., Hertwich, E. G. Human and environmental impact assessment of postcombustion CO_2 capture focusing on emissions from amine-based scrubbing solvents to air. *Environ Sci Technol* **44**, 1496–1502 (2010).

19. Li, X., Wang, S., Chen, C. Experimental study of energy requirement of CO_2 desorption from rich solvent. *Energy Procedia* **37**, 1836–1843 (2013).

20. Hack, J., Maeda, N., Meier, D. M. Review on CO_2 Capture Using Amine-Functionalized Materials. *ACS Omega* **7**, 39520–39530 (2022).

21. Choi, G. H., Song, H., Lee, S., Kim, J., Moon, M., Yoo, P. Electrochemical direct CO_2 capture technology using redox-active organic molecules to achieve carbon-neutrality. *Nano Energy* **112**, 108512 (2023).

22. Sharifian, R., Wagterveld, R. M., Digdaya, I. A., Xiang, C., Vermaas, D. A. Electrochemical carbon dioxide capture to close the carbon cycle. *Energy and Environ Sci* **14**, 781–814 (2021).

23. Apaydin, D. H., Schlager, S., Portenkirchner, E., Sariciftci, N. S. Organic, Organometallic and Bioorganic Catalysts for Electrochemical Reduction of CO_2. *ChemPhysChem* **18**, 3094–3116 (2017).

24. Baena-Moreno, F. M., Rodríguez-Galán, M., Vega, F., Alonso-Fariñas, B., Vilches Arenas, L. F., Navarrete, B. Carbon capture and utilization technologies: a literature review and recent advances. *Energy Sources, Part A: Recovery, Utilization and Environmental Effects* **41**,1403–1433 (2019).

25. Al-Mamoori, A., Krishnamurthy, A., Rownaghi, A. A., Rezaei, F. Carbon Capture and Utilization Update. *Energy Technology* **5**, 834–849 (2017).

26. Hu, B., Guild, C., Suib, S. L. Thermal, electrochemical, and photochemical conversion of CO_2 to fuels and value-added products. *Journal of CO_2 Utilization* **1**,18–27 (2013).

27. Aresta, M., Dibenedetto, A., Angelini, A. Catalysis for the valorization of exhaust carbon: From CO_2 to chemicals, materials, and fuels. technological use of CO_2. *Chemical Reviews* **114**,1709–1742 (2014).

28. Wang, M., Herzog, H. J., Hatton, T. A. CO_2 Capture Using Electrochemically Mediated Amine Regeneration. *Ind Eng Chem Res* **59**, 7087–7096 (2020).

29. Renfrew, S. E., Starr, D. E., Strasser, P. Electrochemical Approaches toward CO_2 Capture and Concentration. *ACS Catal* **10**, 13058–13074 (2020).

30. Rahimi, M., Khurram, A., Hatton, T. A., Gallant, B. Electrochemical carbon capture processes for mitigation of CO_2 emissions. *Chemical Society Reviews* **51**, 8676–8695 (2022).

31. Voskian, S., Hatton, T. A. Faradaic electro-swing reactive adsorption for CO_2 capture. *Energy Environ Sci* **12**, 3530–3547 (2019).

32. Xu, Y., Zheng, M., Musgrave, C., Zhang, L., Goddard, W., Bukowski, B., Liu, Y. Assessing the Kinetics of Quinone-CO_2 Adduct Formation for Electrochemically Mediated Carbon Capture. *ACS Sustain Chem Eng* **11***,* 11333-11341 (2023) .

33. Stern, M. C., Simeon, F., Herzog, H., Hatton, T. A. Post-combustion carbon dioxide capture using electrochemically mediated amine regeneration. *Energy Environ Sci* **6**, 2505 (2013).

34. Seo, H., Hatton, T. A. Electrochemical direct air capture of CO2 using neutral red as reversible redox-active material. *Nat Commun* **14**, 313 (2023).

35. Jin, S., Wu, M., Jing, Y., Gordon, R. G., Aziz, M. J. Low energy carbon capture via electrochemically induced pH swing with electrochemical rebalancing. *Nat Commun* **13**, 2140 (2022).

36. Jin, S., Wu, M., Gordon, R. G., Aziz, M. J., Kwabi, D. G. PH swing cycle for CO_2 capture electrochemically driven through proton-coupled electron transfer. *Energy Environ Sci* **13**, 3706–3722 (2020).

37. Yan, Z., Hitt, J. L., Zeng, Z., Hickner, M. A., Mallouk, T. E. Improving the efficiency of CO_2 electrolysis by using a bipolar membrane with a weak-acid cation exchange layer. *Nat Chem* **13**, 33–40 (2021).

38. Smith, K. *et al.* Demonstration of a concentrated potassium carbonate process for CO_2 capture. *Energy and Fuels* **28**, 299–306 (2014).

39. Huynh, M. H. V., Meyer, T. J. Proton-coupled electron transfer. *Chemical Reviews* **107**, 5004–5064 (2007).

40. Xie, H. Jiang, W., Liu, T., Wu, Y., Wang, Y., Chen, B., Niu, D., Liang, B. Low-Energy Electrochemical Carbon Dioxide Capture Based on a Biological Redox Proton Carrier. *Cell Rep Phys Sci* **1**, 100046 (2020).

41. Huang, C., Liu, C., Wu, K., Yue, H., Tang, S., Lu. H., Liang, B. CO_2 Capture from Flue Gas Using an Electrochemically Reversible Hydroquinone/Quinone Solution. *Energy and Fuels* **33**, 3380–3389 (2019).

42. Watkins, J. D., Siefert, N. S., Zhou, X., Myers, C. R., Kitchin J. R., Hopkinson, D. P., Nulwala H. B. Redox-Mediated Separation of Carbon Dioxide from Flue Gas. *Energy and Fuels* **29**, 7508–7515 (2015).

43. Mizen, M. B., Wrighton, M. S. Reductive Addition of CO_2 to 9,10-Phenanthrenequinone. *J Electrochem Soc* **136**, 941–946 (1989).

44. Gurkan, B., Simeon, F., Hatton, T. A. Quinone Reduction in Ionic Liquids for Electrochemical CO_2 Separation. *ACS Sustain Chem Eng* **3**, 1394–1405 (2015).

45. Liu, Y., Ye, H.-Z., Diederichsen, K. M., Van Voorhis, T., Hatton, T. A. Electrochemically mediated carbon dioxide separation with quinone chemistry in salt-concentrated aqueous media. *Nat Commun* **11**, 2278 (2020).

46. Hemmatifar, A., Kang, J. S., Ozbek, N., Tan, K. J., Hatton, T. A. Electrochemically Mediated Direct CO_2 Capture by a Stackable Bipolar Cell. *ChemSusChem* **15**, e202102533 (2022).

47. Barlow, J. M., Yang, J. Y. Oxygen-Stable Electrochemical CO_2 Capture and Concentration with Quinones Using Alcohol Additives. *J Am Chem Soc* **144**, 14161–14169 (2022).

48. Comeau Simpson, T., Durand, R. R. Reactivity of carbon dioxide with quinones. *Electrochim Acta* **35**, 1399–1403 (1990).

49.	Scovazzo, P., Poshusta, J., DuBois, D., Koval, C., Noble, R. Electrochemical Separation and Concentration of <1% Carbon Dioxide from Nitrogen. *J Electrochem Soc* **150**, D91-D98 (2003).

50.	Nagaoka, T., Nishii, N., Fujii, K., Ogura, K. Mechanisms of reductive addition of CO_2 to quinones in acetonitrile. *Journal of Electroanalytical Chemistry* **322**, 383–389 (1992).

51.	Simeon, F., Stern M.C., Diederichsen, K. M., Liu, Y., Herzog, H. J., Hatton T. A. Electrochemical and Molecular Assessment of Quinones as CO2-Binding Redox Molecules for Carbon Capture. *Journal of Physical Chemistry C* **126**, 1389–1399 (2022).

52.	Schimanofsky, C., Wielend, D., Kröll, S., Lerch, S., Werner, D., Gallmetzer, J. M., Mayr, F., Neugebauer, H., Irimia-Vladu, M., Portenkirchner, E., Hofer T. S., Sariciftci N. S. Direct Electrochemical CO_2 Capture Using Substituted Anthraquinones in Homogeneous Solutions: A Joint Experimental and Theoretical Study. *Journal of Physical Chemistry C* **126**, 14138–14154 (2022).

53.	Iida, H., Kondou, S., Tsuzuki, S., Tashiro, M., Shida, N., Motokura, K., Dokko, K., Watanabe, M., Ueno, K. Imidazolium-Functionalized Anthraquinone for High-Capacity Electrochemical CO2 Capture. *Journal of Physical Chemistry C* **127**, 10077–10086 (2023).

54.	Wielend, D., Apaydin, D. H., Sariciftci, N. S. Anthraquinone thin-film electrodes for reversible CO2 capture and release. *J Mater Chem A* **6**, 15095–15101 (2018).

55.	Apaydin, D. H., Głowacki, E. D., Portenkirchner, E., Sariciftci, N. S. Direct electrochemical capture and release of carbon dioxide using an industrial organic pigment: Quinacridone. *Angewandte Chemie - International Edition* **53**, 6819–6822 (2014).

56.	Kerschbaumer, A., Wielend, D., Leeb, E., Schimanofsky, C., Kleinbruckner, N., Neugebauer, H., Irimia-Vladu, M., Sariciftci, N. S. How to use a rotating ring-disc electrode (RRDE) subtraction method to investigate the electrocatalytic oxygen reduction reaction? *Catal Sci Technol* **13**, 834-843 (2023).

57.	Apaydin, D. H., Gora, M., Portenkirchner, E., Oppelt, K., Neugebauer, H., Jakesova, M., Głowacki, E. D., Kunze-Liebhäuser, J., Zagorska, M., Mieczkowski, J., Sariciftci, N.S. Electrochemical Capture and Release of CO_2 in Aqueous Electrolytes Using an Organic Semiconductor Electrode. *ACS Appl Mater Interfaces* **9**, 12919–12923 (2017).

58. Wielend, D., Salinas, Y., Mayr, F., Bechmann, M., Yumusak, C., Neugebauer, H., Brüggemann, O., Sariciftci, N. S. Immobilized Poly(anthraquinones) for Electrochemical Energy Storage Applications: Structure-Property Relations. *ChemElectroChem* **8**, 4360–4370 (2021).

59. Li, X. G., Li, H., Huang, M. R., Moloney, M. G. Synthesis and multifunctionality of self-stabilized poly(aminoanthraquinone) nanofibrils. *Journal of Physical Chemistry C* **115**, 9486–9497 (2011).

60. Wielend, D., Vera-Hidalgo, M., Seelajaroen, H., Sariciftci, N. S., Pérez, E. M., Whang, D. R. Mechanically Interlocked Carbon Nanotubes as a Stable Electrocatalytic Platform for Oxygen Reduction. *ACS Appl Mater Interfaces* **12**, 32615–32621 (2020).

61. Nellaiappan, S., Kumar, A. S. Selective flow injection analysis of iodate in iodized table salts by riboflavin immobilized multiwalled carbon nanotubes chemically modified electrode. *Electrochim Acta* **109**, 59–66 (2013).

62. Reynolds, J.R, Thompson, B. C., Skotheim, T. A. *Handbook of Conducting Polymers*, 4th edition, 578 (2019, CRC Press)

63. Shirakawa, H., Louis, E. J., MacDiarmid, A. G., Chiang, C. K., Heeger, A. J. Synthesis of electrically conducting organic polymers: halogen derivatives of polyacetylene, (CH) x. *J Chem Soc Chem Commun* **16,** 578 (1977).

64. MacDiarmid, A. G., Heeger, A. J. Organic metals and semiconductors: The chemistry of polyacetylene, (CH)x, and its derivatives. *Synth Met* **1**, 101–118 (1980).

65. Oka, K., Murao, S., Kataoka, M., Nishide, H., Oyaizu, K. Hydrophilic Anthraquinone-Substituted Polymer: Its Environmentally Friendly Preparation and Efficient Charge/Proton-Storage Capability for Polymer-Air Secondary Batteries. *Macromolecules* **54**, 4854–4859 (2021).

66. Zarren, G., Nisar, B., Sher, F. Synthesis of anthraquinone-based electroactive polymers: a critical review. *Materials Today Sustainability* **5**, 100019 (2019).

67. Ismail, K. M., Khalifa, Z. M., Azzem, A., Badawy, W. A. Electrochemical preparation and characterization of poly(1-amino-9,10-anthraquinone) films. *Electrochim Acta* **47**, 1867-1873 (2002)

68. Badawy, W. A., Ismail, K. M., Medany, S. S. Optimization of the electropolymerization of 1-amino-9,10-anthraquinone conducting films from aqueous media. *Electrochim Acta* **51**, 6353–6360 (2006).

69. Rabl, H., Wielend, D., Tekoglu, S., Seelajaroen, H., Neugebauer, H., Heitzmann, N., Apaydin, D., Scharber, M.C., Sariciftci, N. S. Are polyaniline and polypyrrole electrocatalysts for oxygen (O_2) reduction to hydrogen peroxide (H_2O_2)? *ACS Appl Energy Mater* **3**, 10611–10618 (2020).

70. Naoi, K., Suematsu, S., Manago, A. Electrochemistry of Poly(1,5-diaminoanthraquinone) and Its Application in Electrochemical Capacitor Materials. *Journal of The Electrochemical Society* **147**, 420 (2000).

71. Gao, M., Yang, F., Wang, X., Zhang, G., Liu, L. Electrochemical characteristics and stability of poly(1,5-diaminoanthraquinone) in acidic aqueous solution. *Journal of Physical Chemistry C* **111**, 17268–17274 (2007).

72. Ding, Y., Ren, X., Chen, D., Wen, F., Li, T., Xu, F. Poly(1,5-diaminoanthraquinone) as a High-Capacity Bipolar Cathode for Rechargeable Magnesium Batteries. *ACS Appl Energy Mater* **5**, 3004–3012 (2022).

73. Troiani, E. D. P., Faria, R. C. Cathodically pretreated poly(1-aminoanthraquinone)-modified electrode for determination of ascorbic acid, dopamine, and uric acid. *J Appl Electrochem* **43**, 919–926 (2013).

74. Pinto, J. T., Zempleni, J. Riboflavin. *Advances in Nutrition* **7**, 973–975 (2016).

75. Singh, R., Rathore, D., Pandey, C. M., Srivastava, R. Electrochemical and Spectroscopic Studies of Riboflavin. *Analytical Chemistry Letters* **8**, 653–664 (2018).

76. Roushani, M., Abdi, Z. Novel electrochemical sensor based on graphene quantum dots/riboflavin nanocomposite for the detection of persulfate. *Sens Actuators B Chem* **201**, 503–510 (2014).

77. Lan, Y., Yuan, F., Fereja, T., Wang, C., Lou, B., Li, J., Xu, G. Chemiluminescence of Lucigenin/Riboflavin and Its Application for Selective and Sensitive Dopamine Detection. *Anal Chem* **91**, 2135–2139 (2019).

78. Zhang, F., Xu, W., Zhang, L., Xi, L., Du, Y., Ma, L., Chen, S., Du, D. Riboflavin as a non-quinone redox mediator for enhanced Cr(VI) removal by Shewanella putrefaciens. *J Mol Liq* **351**, 118622 (2022).

79. Malinauskus, A. Electrochemical study of riboflavin adsorbed on a graphite electrode. *Chemija* **19**, 1-3 (2008)

80. Chen, W., Chen, J., Lu, R., Qian, C., Li, W., Yu, H. Redox reaction characteristics of riboflavin: A fluorescence spectroelectrochemical analysis and density functional theory calculation. *Bioelectrochemistry* **98**, 103–108 (2014).

81. Wang, A., Bonakdarpour, A., Wilkinson, D. P., Gyenge, E. Novel organic redox catalyst for the electroreduction of oxygen to hydrogen peroxide. *Electrochim Acta* **66**, 222–229 (2012).

82. Leeb, E., Wielend, D., Schimanofsky, C., Sariciftci, N. S. Substrate and pH-dependent homogeneous electrocatalysis using riboflavin for oxygen reduction. *Electrochemical Science Advances* **2**, e2100211 (2022).

83. Ivanova, Y. N., Karyakin, A. A. Electropolymerization of flavins and the properties of the resulting electroactive films. *Electrochem commun* **6**, 120–125 (2004).

84. Radzevič, A. Niaura, G., Ignatjev, I., Rakickas T., Celiešiūtė, R., Pauliukaite, R. Electropolymerisation of the natural monomer riboflavin and its characterisation. *Electrochim Acta* **222**, 1818–1830 (2016).

85. d'Souza, E. S., Manjunatha, J. G., Chenthattil, R., Tigari, G., Ravishankar, D. K. Rapid electrochemical monitoring of tyrosine by poly (Riboflavin) modified carbon nanotube paste electrode as a sensitive sensor and its applications in pharmaceutical samples. *Biointerface Res Appl Chem* **11**, 14661–14672 (2021).

86. Krishnan, R. G., Saraswathyamma, B., Raj, T. A., Gopika, M. G. Poly (riboflavin) modified pencil graphite for the simultaneous electrochemical determination of serotonin and dopamine. *AIP Conference Proceedings* **2259**, 02007 (2020).

87. Lei, Z., Chen, B., Koo, Y. M., Macfarlane, D. R. Introduction: Ionic Liquids. *Chemical Reviews* **117**, 6633–6635 (2017).

88. MacFarlane, D. R., Kar, M., Pringle, J. M. An Introduction to Ionic Liquids. *Fundamentals of Ionic Liquids* 1–25 (Wiley-VCH Verlag GmbH & Co. KGaA, 2017).

89. Marsh, K. N., Boxall, J. A., Lichtenthaler, R. Room temperature ionic liquids and their mixtures - A review. *Fluid Phase Equilibria* **219**, 93–98 (2004).

90. Kaur, G., Kumar, H., Singla, M. Diverse applications of ionic liquids: A comprehensive review. *Journal of Molecular Liquids* **351**, (2022).

91. Tiago, G. A. O., Matias, I. A. S., Ribeiro, A. P. C., Martins, L. M. D. R. S. Application of Ionic Liquids in Electrochemistry-Recent Advances. *Molecules* **25**, 5812 (2020).

92. Shukla, S. K., Khokarale, S. G., Bui, T. Q., Mikkola, J. P. T. Ionic liquids: Potential materials for carbon dioxide capture and utilization. *Frontiers in Materials* **6**, 00042 (2019).

93. Zheng, J. *et al.* Understanding Thermodynamic and Kinetic Contributions in Expanding the Stability Window of Aqueous Electrolytes. *Chem* **4**, 2872–2882 (2018).

94. Ruch, P. W., Cericola, D., Foelske, A., Kötz, R., Wokaun, A. A comparison of the aging of electrochemical double layer capacitors with acetonitrile and propylene carbonate-based electrolytes at elevated voltages. *Electrochim Acta* **55**, 2352–2357 (2010).

95. Ong, S. P., Andreussi, O., Wu, Y., Marzari, N.,Ceder, G. Electrochemical windows of room-temperature ionic liquids from molecular dynamics and density functional theory calculations. *Chemistry of Materials* **23**, 2979–2986 (2011).

96. Jacquemin, J., Costa Gomes, M. F., Husson, P., Majer, V. Solubility of carbon dioxide, ethane, methane, oxygen, nitrogen, hydrogen, argon, and carbon monoxide in 1-butyl-3-methylimidazolium tetrafluoroborate between temperatures 283 K and 343 K and at pressures close to atmospheric. *Journal of Chemical Thermodynamics* **38**, 490–502 (2006).

97. Krishnan, A., Gopinath, K., Vo D.N, Malolan, R., Nagarajan, V., Arun, J. Ionic liquids, deep eutectic solvents and liquid polymers as green solvents in carbon capture technologies: a review. *Environmental Chemistry Letters* **18**, 2031–2054 (2020).

98. Fu, Y., Yang, Z., Mahurin, S. M., Dai, S. & Jiang, D. Ionic liquids for carbon capture. *MRS Bull* **47**, 395–404 (2022).

99. Orhan, Y. O. Effects of various anions and cations in ionic liquids on CO_2 capture. *Journal of Molecular Liquids* **333**, 115981 (2021).

100. Shama, V. M., Swami, A. R., Aniruddha, R., Sreedhar, I., Reddy, B. M. Process and engineering aspects of carbon capture by ionic liquids. *Journal of CO2 Utilization* **48**, 101507 (2021).

101. Martin, S., Pratt, H. D., Anderson, T. M. Screening for High Conductivity/Low Viscosity Ionic Liquids Using Product Descriptors. *Mol Inform* **36**, 1600125 (2017).

102. Gurkan, B. *et al.* Molecular design of high capacity, low viscosity, chemically tunable ionic liquids for CO2 capture. *Journal of Physical Chemistry Letters* **1**, 3494–3499 (2010).

103. Sequeira, M. C. M., Avelino, H. M. N. T., Caetano, F. J. P., Fareleira, J. M. N. A. Viscosity measurements of 1-ethyl-3-methylimidazolium trifluoromethanesulfonate (EMIM OTf) at high pressures using the vibrating wire technique. *Fluid Phase Equilib* **505**, 112354 (2020).

104. Yambou, E. P., Gorska, B., Béguin, F. Electrical Double-Layer Capacitors Based on a Ternary Ionic Liquid Electrolyte Operating at Low Temperature with Realistic Gravimetric and Volumetric Energy Outputs. *ChemSusChem* **14**, 1196–1208 (2021).

105. Sánchez-Ramírez, N., Assresahegn, B. D., Bélanger, D., Torresi, R. M. A Comparison among Viscosity, Density, Conductivity, and Electrochemical Windows of N-n-Butyl-N-methylpyrrolidinium and Triethyl-n-pentylphosphonium Bis(fluorosulfonyl imide) Ionic Liquids and Their Analogues Containing Bis(trifluoromethylsulfonyl) Imide Anion. *J Chem Eng Data* **62**, 3437–3444 (2017).

106. Weingarth, D., Czekaj, I., Fei, Z., Foelske-Schmitz, A., Dyson, P., Wokaun, A., Kötz, R. Electrochemical Stability of Imidazolium Based Ionic Liquids Containing Cyano Groups in the Anion: A Cyclic Voltammetry, XPS and DFT Study. *J Electrochem Soc* **159**, H611–H615 (2012).

107. Pardal, T. *et al.* Syngas production by electrochemical CO2 reduction in an ionic liquid based-electrolyte. *Journal of CO2 Utilization* **18**, 62–72 (2017).

108. Kleinbruckner, N., Leeb, E., Wielend, D., Kerschbaumer, A., Yumusak, C., Richtar, J., Scharber, M. C., Neugebauer, H., Irimia-Vladu, M., Krajcovic, J., Sariciftci, N. S. Polymerized Riboflavin and Anthraquinone derivatives for Oxygen Reduction Reaction. *Under Revision*.

109. Yamamoto, T., Etori, H. Poly(anthraquinone)s Having a-Conjugation System along the Main Chain. Synthesis by Organometallic Polycondensation, Redox Behavior, and Optical Properties. *Macromolecules* **28**, 3371-3379 (1995).

110. Song, Z. *et al.* Polyanthraquinone as a Reliable Organic Electrode for Stable and Fast Lithium Storage. *Angewandte Chemie* **127**, 14153–14157 (2015).

111. Hernández, G. *et al.* Redox-active poly(ionic liquid)s as active materials for energy storage applications. *J Mater Chem A Mater* **5**, 16231–16240 (2017).

112. Ding, Y. *et al.* Poly(1,5-diaminoanthraquinone) as a High-Capacity Bipolar Cathode for Rechargeable Magnesium Batteries. *ACS Appl Energy Mater* **5**, 3004–3012 (2022).

113. Jae Lee, C., Soo Kang, J., Park, Y.-T., Mohammad Rezaul, K., Sang Lee, M. Study of Substitution Effect of Anthraquinone by SERS Spectroscopy. *Bull. Korean Chem. Soc* **25**, 1779-1783 (2004).

114. Wagner, M., Rębiš, T., Inganäs, O. Enhancing charge storage of conjugated polymer electrodes with phenolic acids. *J Power Sources* **302**, 324–330 (2016).

115. Ghasemi, J., Ghobadi, S., Abbasi. B., Kubista, M., Spectrophotometric Determination of Acidity Constants of Group B Vitamins in Different Ionic Strengths at 25±0.1 °C. *Journal of 'the Korean Chemical Society* **49**, 269-277 (2005).

116. Spexard, M., Immeln, D., Thöing, C., Kottke, T. Infrared spectrum and absorption coefficient of the cofactor flavin in water. *Vib Spectrosc* **57**, 282–287 (2011).

117. Padhye, L. *et al.* PolyDADMAC and dimethylamine as precursors of N - nitrosodimethylamine during ozonation: Reaction kinetics and mechanisms. *Environ Sci Technol* **45**, 4353–4359 (2011).

118. Li, Y. *et al.* Rechargeable Aqueous Polymer-Air Batteries Based on Polyanthraquinone Anode. *Chem* **5**, 2159–2170 (2019).

119. Hayyan, M., Mjalli, F. S., Hashim, M. A., AlNashef, I. M., Mei, T. X. Investigating the electrochemical windows of ionic liquids. *Journal of Industrial and Engineering Chemistry* **19**, 106–112 (2013).

120. Randström, S., Appetecchi, G. B., Lagergren, C., Moreno, A., Passerini, S. The influence of air and its components on the cathodic stability of N-butyl-N-methylpyrrolidinium bis(trifluoromethanesulfonyl)imide. *Electrochim Acta* **53**, 1837–1842 (2007).

121. Zou, Y., Walton, A. S., Kinloch, I. A., Dryfe, R. A. W. Investigation of the Differential Capacitance of Highly Ordered Pyrolytic Graphite as a Model Material of Graphene. *Langmuir* **32**, 11448–11455 (2016).